

HIGH GRADIENT MAGNETIC SEPARATION OF
HEMATITE FROM LEAD SULPHATE AND
SILVER IN THE RESIDUE OF
THE SULPHATION ROAST-
LEACH-ELECTROWIN
PROCESS.

by



Rodolfo Espinosa-Gomez

A Thesis Submitted to the
Faculty of Graduate Studies and Research,
in Partial Fulfillment of the Requirements for the Degree of
Master of Engineering:

Department of Mining and Metallurgical Engineering
McGill University
Montreal, Canada

December 1981

To my parents, brothers and Rosaura for their
encouragement, support and love.

Rodolfo

Para mis padres, hermanos y Rosaura por su
motivación, apoyo y amor.

Rodolfo

ABSTRACT

High gradient magnetic separation (HGMS) of hematite to produce a lead/silver concentrate from the residue of the sulphation roast-leach-electrowin (SRLE) process was investigated. Neutral and hot acid leach residues (NALR and HALR) were generated from calcine of Brunswick Mining bulk concentrate provided by the New Brunswick Research and Productivity Council. The calcine assayed 28% Zn, 6% Pb, 16% Fe and 120 ppm Ag.

The major phases in the calcine, NALR and HALR were identified by a combination of X-ray diffraction, optical and electron microscopy and phase isolation on the Frantz isodynamic separator (Frantz). Both residues were fine, 100% $-25 \mu\text{m}$ and well liberated. From analysis of the magnetic profile, generated on the Frantz, the HALR was selected as the best candidate for HGMS. This was mainly to avoid zinc reporting to both mags (as ferrite) and non-mags (as marmatite). The HALR was about 38% Fe (as hematite), 24% Pb (as lead sulphate) and 10% quartz.

The HALR was vigorously dispersed with calgon in an ultrasound bath. Operating conditions for HGMS were selected using a recovery model. Experiments were conducted with flow velocities of 7-14 cm/s and field strengths of 13,800 to 21,400 Oe.

Lead/silver concentrates were produced ranging from 48% Pb at 74% recovery to 34% Pb at 95% recovery with 450-550 ppm silver

at recoveries of 60-85%. Analysis of the products by scanning electron microscopy revealed ultra-fine hematite particles ($< 1 \mu\text{m}$) in the lead concentrate (the non-mags) and 0.5 to 3 μm lead sulphate particles in the mags, which is the finer end of the lead distribution. The fine hematite in the non-mags is a result of too low a magnetic trapping force; a possible explanation of the lead loss is due to aggregation with fine hematite rendering the smallest lead sulphate particles susceptible to magnetic capture.

The separation is judged to be technically quite successful.

RESUME

Des recherches furent entreprises sur la séparation magnétique à haut gradient (SMHG) de l'hématite, afin de produire un concentré plomb/argent à partir des résidus du procédé "grillage sulfatant-lixiviation-électrolyse". Des résidus de lixiviation neutre et acide à température élevée (RLN et RLATE) furent produits à partir des grillages de concentré global de Brunswick Mining mis à notre disposition par le New-Brunswick Research and Productivity Council. Les essais des grillages donnèrent 28% Zn, 6% Pb, 16% Fe et 120 ppm d'Ag.

Les phases majeures rencontrées dans le grillage, le RLN et le RLATE furent identifiées à l'aide d'une combinaison de diffraction Rayons-X, de microscope optique et électronique et, d'isolation de phase grâce au séparateur isodynamique Frantz (Frantz). Les deux résidus sont très fins, 100% - 25 µm et bien libérés. Des analyses des profils magnétiques, obtenus grâce au Frantz, le RLATE fut retenu comme étant le meilleur candidat pour une SMHG. Ce choix fut fait principalement pour éviter d'avoir des apports de zinc côté magnétique (sous forme de ferrites) et de non magnétique (sous forme de marmatite). L'analyse du RLATE donna 38% Fe (sous forme d'hématite), 24% Pb (sous forme de sulfate de plomb) et 10% de quartz.

Les RLATE furent vigoureusement dispersés, à l'aide d'une solution de calgon, dans un bain à ultra-sons. Les conditions

de fonctionnement du SMHG furent choisies en se basant sur un modèle de récupération. Diverses expériences furent conduites, variant le débit de 7 à 14 cm/sec et l'intensité du champ de 13,800 à 21,400 Oe. Des concentrés de plomb/argent furent produits donnant des essais variant de 48% Pb avec une récupération de 74% à 34% Pb avec 95% de récupération et des analyses d'Ag de 450-550 ppm avec une récupération de 60 à 85%. L'analyse des produits à l'aide d'un microscope électronique à balayage révéla la présence de particules d'hématite ultra-fines ($< 1 \mu\text{m}$) dans le concentré de plomb (portion non-magnétique) et des particules de sulfate de plomb de 0.5 à 3 μm dans la portion magnétique, ce qui représente la partie la plus fine de la distribution granulométrique du plomb. La présence de fines particules d'hématite dans les non-magnétiques fut le résultat de forces magnétiques trop faibles; l'explication à la perte de plomb serait l'agglomération avec de fines particules d'hématite, rendant ainsi les plus petites particules de sulfate de plomb susceptibles à une séparation magnétique.

La séparation, techniquement parlant, fut qualifiée de succès.

RESUMEN

Separación magnética con altos gradientes (HGMS) en hematita, para producir un concentrado plomo/plata de los residuos del proceso, tostación sulfatante-lixiviación-electrodeposición (SRLE) fue investigada. Residuos de lixiviación neutral y de lixiviación caliente (NALR y HALR) fueron generados de el producto de tostación sulfatante (calcinado) de un concentrado de flotación de la compañía Brunswick Mining and Smelting conteniendo todos los sulfuros valubles. El calcinado fue proporcionado por New Brunswick Research and Productivity Council. El análisis químico del calcinado fue 28% Zn, 6% Pb, 16% Fe y 120 ppm de Ag.

Las principales fases mineralógicas de el calcinado, NALR y HALR fueron identificadas empleando una combinación de difracción de rayos X, microscopios oculares y microscopía electrónica. Aislamiento de las fases mineralógicas fue realizado mediante un separador isodinámico Frantz (Frantz). Ambos residuos fueron de tamaños muy finos, 100% - 25 μ m, y las fases estaban bien liberadas. Partiendo de un análisis sobre el comportamiento bajo separación magnética, generado por el Frantz, el HALR fue seleccionado como mejor candidato para HGMS. Ello fue principalmente para evitar que el zinc se presentara en los 2 productos de separación magnética, en los magnéticos (mags) como

ferrita y en los no magnéticos (non-mags) como marmatita. El HALR analizo 38% Fe (como hematita), 24% Pb (como sulfato de plomo) y 10% de cuarzo.

El HALR fue vigorosamente dispersando con calgon en un baño ultrasónico. Las condiciones de operación en HGMS fueron seleccionadas utilizando un modelo de recuperación magnética. Los experimentos fueron conducidos con velocidades de flujo que variaron de 7-14 cm/s e intensidades magnéticas de 13,800 a 21,400 Oe.

Concentrados plomo/plata fueron producidos, variando desde 48% Pb con 74% de recuperación, hasta 34% Pb con 95% de recuperación; la plata analizó de 450-550 ppm con recuperaciones de 60-85%. Un examen de los productos empleando microscopía electrónica reveló la existencia de partículas ultrafinas de hematita ($< 1 \mu\text{m}$) en el concentrado de plomo (non-mags) y partículas de sulfato de plomo entre 0.5-3 μm (rango más fino en el cual se encuentra distribuido el sulfato de plomo) en los magnéticos (mags). La presencia de partículas tan finas de hematita en los non-mags, es el resultado de una baja atracción magnética a tales tamaños; una posible explicación de las pérdidas en plomo, es la aglomeración de estas, con partículas pequeñas de hematita, transformando a las partículas de sulfato de plomo, susceptibles de ser atrapadas magnéticamente.

La separación es juzgada desde el punto de vista técnico, como todo un éxito.

ACKNOWLEDGEMENTS

The author wishes to express his gratitude and appreciation to Dr. J.A. Finch for his constant help and enthusiasm during the investigation and for his orientation and critical comments in the preparation of this thesis.

Thanks are also due to fellow graduate students and technicians of the Department of Mining and Metallurgical Engineering for their help on many occasions.

Special appreciation is extended to Dr. N. Rowlands (Mining, McGill) for help in the scanning electron microscopy examination. Thanks are also extended to Dr. M. Mackinnon (Geology, McGill) for help in the microprobe examination and to Mr. P. Moloughney (CANMET) for the silver assays.

The use of the HGMS at CANMET is gratefully appreciated.

Finally, financial support from the Mexican Government through CONACYT is gratefully acknowledged.

TABLE OF CONTENTS

	<u>Page</u>
ABSTRACT	i
RESUME	iii
RESUMEN	v
ACKNOWLEDGEMENTS	vii
TABLE OF CONTENTS	viii
LIST OF FIGURES	xii
LIST OF TABLES	xvi
1. INTRODUCTION	1
1.1 Treatment of Complex Sulphide Ores	1
1.1.1 Background	1
1.1.2 Mineralogy	2
1.1.3 Mineral Processing	2
1.1.4 Processing of Bulk Concentrates	18
2. STATEMENT OF PROBLEM	27
2.1 Method of Attack	27
3. THE CHARACTERISTICS OF THE CALCINES AND LEACH RESIDUES	29
3.1 The Calcine	29
3.1.1 Assays of RPC Samples	29
3.1.2 Size and Metal Distribution of Calcine	29
3.1.3 Mineralogical Examination	31
-X-Ray Diffraction (XRD)	31
-Microscope Examination	31
3.2 Characteristics of the Neutral Acid Leach Residue (NALR)	34
3.2.1 Leach Procedure	34
3.2.2 Metal Distribution in NAL	35

3.2.3	Size and Metal Distribution of the NALR	35
3.2.4	Mineralogical Examination	36
	- X-Ray Diffraction (XRD)	36
	- Metallurgical Microscope with Reflected Light	37
	- Vickers Microscope with Reflected Light.	37
	- Carl-Zeiss Microscope with Transmitted Light; Degree of Liberation	40
	- Electron Microprobe	40
	- Scanning Electron Microscopy (SEM)	45
	- Resumé of Mineralogical Examination	45
3.3	Characteristics of the Hot Acid Leach Residue (HALR).	47
3.3.1	Leach Procedure	47
3.3.2	Metal Distribution in Hot Acid Leach (HAL)	48
3.3.3	Size and Metal Distributions	48
3.3.4	Mineralogical Examination of HALR	49
	- X-Ray Diffraction (XRD)	49
	- Metallurgical Microscope with Reflected Light	50
	- Vickers Microscope with Reflected Light.	50
	- Carl-Zeiss Microscope with Transmitted Light; Degree of Liberation	50
	- Electron Microprobe	50
	- Scanning Electron Microscopy (SEM)	53
	- Resumé of Mineralogical Examination	57
4.	ESTIMATING POTENTIAL FOR MAGNETIC SEPARATION	58
4.1	Magnetic Profile Using a Frantz Isodynamic Magnetic Separator	58
4.1.1	Description of the Frantz	58
4.1.2	Frantz Separator on Synthetic Mixtures.	60
4.1.3	Separation of NALR on Frantz	63
4.1.4	Separation of HALR on Frantz	68
4.1.5	Evaluation of Frantz Results	70

	<u>Page</u>
5. DISPERSION	71 .
6. HIGH GRADIENT MAGNETIC SEPARATION (HGMS)	74
6.1 Background	74
6.2 A Recovery Model for HGMS	74
- Particle Parameters	76
- Operating Parameters	77
6.3 Equipment	79
6.4 Conditions of the tests	79
6.5 Results.	79
6.5.1 Results of Test Series 1-13,800 Oe- Matrix A	79
6.5.2 Results of Test Series 2-21,400 Oe - Matrix A	85
6.5.3 Results of Test Series 3-13,800 Oe - Matrix B	88
6.5.4 Graphical Summary of Results	92
6.5.5 Size of the Final Products	96
6.5.6 Scanning Electron Microscopy (SEM) Examination of the Final HGMS Pro- ducts	99
7. DISCUSSION	107
7.1 Mineralogical Identification	107
- Electron Microprobe Examination	107
- Scanning Electron Microscope Ex- amination	107
- Frantz Separator	108
- Degree of Liberation	109
7.2 Magnetic Separation	110
- Estimation of Fluid Velocities, "U _m ", and Magnetic Recoveries, R(%) in HGMS	110
- Physical Trapping in HGMS	110
- Separation Results	112
- General Observation	113
7.3 Assay of the Samples	113

	<u>Page</u>
8. CONCLUSIONS	117
Appendix A X-Ray Identification	120
Appendix B Degree of Liberation	128
Appendix C Dispersion Tests	134
Appendix D SI Units	135
REFERENCES	138

LIST OF FIGURES

<u>Figure Number</u>	<u>Caption</u>	<u>Page</u>
1.	Microphotograph of a complex sulphide ore from Brunswick Mining and Smelting (BMS)	4
2.	Microphotograph of a lead concentrate from BMS	4
3.	Relationship between the physical and chemical properties of fine particles and their behavior in flotation	6
4.	Effect of entrainment of quartz on grade of chalcopyrite concentrate in a typical batch flotation test at pH 11 without collector . .	8
5.	Influence of alumina slimes on the flotation of galena with potassium ethylxanthate (KEX)	11
6.	Flowsheet for a sequential selective flotation	13
7.	Flowsheet for semi-bulk flotation	14
8.	Generalized flowsheet of Brunswick Mining and Smelting (BMS) flotation circuit	15
9.	Sherrit Gordon Pressure Leach Process applied to New Brunswick Ores. Simplified process flow diagram	20
10.	Flowsheet of the Mizoguchi-Habashi Process .	23
11.	The Sulphation Roast-Leach-Electrowinning (RPC or SRLE) Process	25
12.	Microphotograph of a -37 + 25 μ m calcine fraction	33
13.	Microphotograph of a -37 + 25 μ m calcine fraction at 440 magnification with reflected light, under polarized conditions	33

<u>Figure</u>	<u>Page</u>
14. Microphotograph of -37 + 25 μm particles of NALR	38
15. Microphotograph of -25 + 15 μm particles of NALR at 440 magnification with reflected light, under polarized conditions	38
16. Microphotograph of -25 + 15 μm particles of NALR at 620 magnification with reflected light, under polarized conditions	39
17. Microphotograph of -25 + 15 μm particles of NALR under transmitted light	39
18. Microphotograph of mags fraction up to 100 mA on Frantz, of the NALR	43
19. Microphotograph of mags fraction up to 100 mA on Frantz of the NALR.	43
20. Microphotograph of mags 650-850 mA fraction in Frantz, of the NALR.	44
21. Microphotograph of mags 650-850 mA fraction on Frantz, of the NALR	44
22. SEM microphotograph of a floccule of NALR at 10,000 magnification. The size of the floccule is about 8 μm	46
23. SEM microphotograph of some particles in the NALR at 40,000 magnification	46
24. EDAX of the particles from Fig. 23	46
25. Microphotograph of -37 + 25 μm particles of the HALR at 440 magnification with reflected light, under polarized conditions	51
26. Microphotograph of -25 + 15 μm particles of the HALR at 620 magnification with reflected light, under polarized conditions	51
27. Microphotograph of -25 + 15 μm particles of the HALR with transmitted light	52
28. SEM microphotographs of the HALR. Lead particles (anglesite) are differentiated from iron (hematite) with a lead X-ray map (particles showing the white dots), right side picture	55

<u>Figure</u>	<u>Page</u>
29. SEM microphotographs of the HALR. Lead particles (anglesite) are differentiated from iron (hematite) with a lead X-ray map (particles showing the white dots), right side picture	56
30. Photograph of the Frantz Isodynamic Magnetic Separator.	59
31. A force balance of a paramagnetic particle between the pole pieces of the Franz separator	61
32. Profile of magnetic separation of the NALR, by Frantz separator, -25 + 15 μ m fraction	64
33. Microphotograph of mags fraction up to 200 mA in Frantz, of the NALR.	65
34. Microphotograph of the mags fraction at 300 to 350 mA in Frantz, of the NALR.	65
35. Microphotograph of the mags fraction at 850 to 1050 mA in Frantz, of the NALR	66
36. Microphotograph of the non-mags fraction of the NALR at 1050 mA on Frantz.	66
37. Profile of magnetic separation of the HALR, by Frantz separator, -25 + 15 μ m fraction	69
38. Degree of dispersion. Size distribution of the HALR using different dispersion procedures	73
39. Schematic diagram of HGMS.	80
40. A schematic representation of the HGMS flowsheet, followed in Run 1.	82
41. A schematic representation of the HGMS flowsheet, followed in Runs 2 and 3.	83
42. A schematic representation of the HGMS flowsheet, followed in Series 2 and 3	86
43. Lead recovery and grade in the non-mags as a function of the flow velocity	93
44. Lead recovery and grade in the lead concentrate as a function of the flow velocity	94

<u>Figure</u>	<u>Page</u>
45. Grade-recovery relationship for the lead, constructed from the nine runs	95
46. Grade-recovery relationship for the silver	97
47. Particle size of the final products	98
48. SEM microphotographs of the mags showing 2 views of remaining lead. Lead particles are identified with a lead X-ray map (particles showing the white dots), right side pictures	101
49. SEM microphotographs of the mags showing 2 views of remaining lead. Lead particles are identified with a lead X-ray map (particles showing the white dots), right side pictures	102
50. SEM microphotographs of the mids-1. Lead particles are identified with a lead X-ray map (particles showing the white dots), right side pictures	103
51. SEM microphotographs of the non-mags. Lead particles are identified with a lead X-ray map (particles showing the white dots), right side pictures.	104
52. SEM microphotographs of the non-mags. Lead particles are identified with a lead X-ray map (particles showing the white dots), right side pictures.	105
53. SEM microphotographs of the slimes. Lead particles are identified with a lead X-ray map (particles showing the white dots), right side pictures.	106

LIST OF TABLES

<u>Table Number</u>	<u>Page</u>
1. Typical results in grade and recovery of complex sulphide ores.	16
2. Comparison of recoveries obtained by selective and bulk flotation	17
3. Average analyses of New Brunswick concentrates used in Sherritt Gordon process test	21
4. Assay of the New Brunswick bulk concentrate used in the Mizoguchi-Habashi Process	22
5. Operating Conditions in the SRLE Process	26
6. Assay of calcine samples	30
7. Assay of the representative head sample	30
8. Size and metal distribution of the calcine	31
9. Mineralogical composition of the calcine	34
10. Metal distribution in the Neutral Acid Leach (NAL) step.	35
11. Size and metal distribution of NALR	36
12. Degree of liberation in coarser NALR sizes	41
13. Resumé of mineralogical identification of NALR.	47
14. Metal distribution in the Hot Acid Leach (HAL) step.	48
15. Size and metal distribution of HALR	49
16. Degree of liberation in coarser HALR sizes	53
17. Resumé of mineralogical examination of HALR	57
18. Frantz separations upon synthetic mixtures (Fe ₂ O ₃ - Pbs). I = 450 mA	62
19. Frantz separator upon NALR	67

<u>Table</u>	<u>Page</u>
20. Separation of NALR on Frantz at 400 mA	68
21. Separation of HALR at 450 mA	70
22. Summary of the calculations to estimate the re- quired flow velocity	78
23. Conditions of the HGMS tests	81
24. Series 1. Fluid velocities in rougher and scavengers	85
25. HGMS results of series 1, 13,800 Oe- Matrix A.	87
26. Series 2. Fluid velocity in rougher and sca- venger	88
27. HGMS Results of series 2, 21,400 Oe-Matrix A.	89
28. Series 3. Fluid velocity in rougher and sca- venger	90
29. HGMS results of series 3. 13,800 Oe - Matrix B.	91
30. HGMS. Estimation of fluid velocities, U_{50} , and a comparison between the measured and pre- dicted recoveries	111
31. Comparison between assays reported by CANMET and McGill	115
32. Results from runs 2, 5 and 8, using the CANMET reported assays	116
 <u>Appendix</u>	
A - 1 Calcine. Comparison of measured and listed "d" values in XRD	121
A - 2 NALR. Comparison of measured and listed "d" values by XRD	122
A - 3 NALR. Mags fraction at 650 to 850 mA on Frantz. Comparison of measured and listed "d" values by XRD	124
A - 4 HALR. Comparison of measured and listed "d" values by XRD	126

<u>Appendix</u>	<u>Page</u>
B - 1 Error with 95% of confidence, obtained in point counting technique on the NALR and the HALR.	129
B - 2 Record sheet used for particle counting in NALR, to measure degree of liberation, "L" of the anglesite	130
B - 3 Record sheet used for particle counting in HALR, to measure degree of liberation, "L" of the anglesite	132
C - 1 Dispersants tested in NALR and HALR	134
D - 1 Symbols and SI Units	136
D - 2 Summary of the calculations to estimate the required flow velocity in S.I. Units .	137

1. INTRODUCTION

1.1 Treatment of Complex Sulphide Ores

1.1.1 Background

Complex sulphide ores can be defined as intricate associations of chalcopyrite (CuFeS_2), sphalerite (ZnS), galena (PbS) and pyrite (FeS_2) and/or pyrrhotite (Fe_{1-x}S). They present specific and difficult problems during most stages of beneficiation, from mineral processing to extractive metallurgy (1,2).

These ores are important because they represent large resources of non-ferrous and precious metals. For example, it is estimated they represent about 8% of world's reserves of copper. In Canada, the complex sulphides of New Brunswick represent the largest domestic reserves of zinc, lead and silver.

Ore deposits classified as complex sulphide ores are rather numerous and are found in many geological strata of various ages. The size of these deposits ranges from about 200,000 t contained base metals to a few million tonnes (Broken Hill and Mount Isa in Australia, Kimberley and Bathurst in Canada). Typical compositions usually are in the following ranges: Cu, 0.1-3%; Zn, 0.2-10%; Pb, 0.3-3%; Fe, 10-40%; S, 20-50%; Ag, 30-100 g/t and Au, 0-10 g/t.

1.1.2 Mineralogy

Some important mineralogical parameters that influence the processing of complex sulphide ores are:

- (i) The presence of pyrite or pyrrhotite in relatively large quantities: for example, New Brunswick ores (3) contain about 45% pyrite and Iberian Peninsula deposits (4) are about 35% pyrite.
- (ii) The very complex texture: the association of the main minerals is generally extremely intricate, the size of the valuable mineral present ranging from extremely fine (a few micrometres) to fine (a few tens of micrometres), (5-7).
- (iii) The presence of minor minerals: these could be of significant economic importance (e.g. Au and Ag) or could have a deleterious impact on subsequent metallurgical treatment or on the environment (e.g. presence of arsenic (As), antimony (Sb), bismuth (Bi), mercury (Hg), and cadmium (Cd)).
- (iv) The presence of alteration minerals: This is particularly important for copper and non-sulphide minerals (8).

1.1.3 Mineral Processing

a) Problems in Flotation:

The processing of complex sulphide ores to produce separate concentrates for smelting is limited by the selectivity

of the methods that can be used. Because of the nature of complex sulphide ores, they have only been treated by flotation, but with relatively poor results. Flotation problems can be broken down into three main parts:

- 1) liberation
- 2) flotation of extremely fine particles (less than 10 μ m)
- 3) selectivity vs. considerable quantities of pyrite

1) Liberation

A problem encountered in practice during the treatment of complex sulphide ore is related to the extremely fine size of the valuable minerals present and the corresponding fine grinding size that is required for liberation. In addition to this, the minerals themselves have mechanical properties that do not favor breakage at the boundary between the phases. Such breakage would lead to liberation by detachment rather than by simple size reduction. Liberation by detachment does not require such a fine grind (9). Galena in particular readily cleaves to give composite particles during grinding. Fig. 1 shows a microphotograph of a complex sulphide ore from Brunswick Mining and Smelting (BMS) (10) containing sphalerite (brown) and galena (grey) in pyrite (yellow). Notice that the grain size in all the cases is smaller than about 60 μ m. Liberation by size reduction will require grinding to significantly finer than this size. Fig. 2 shows a

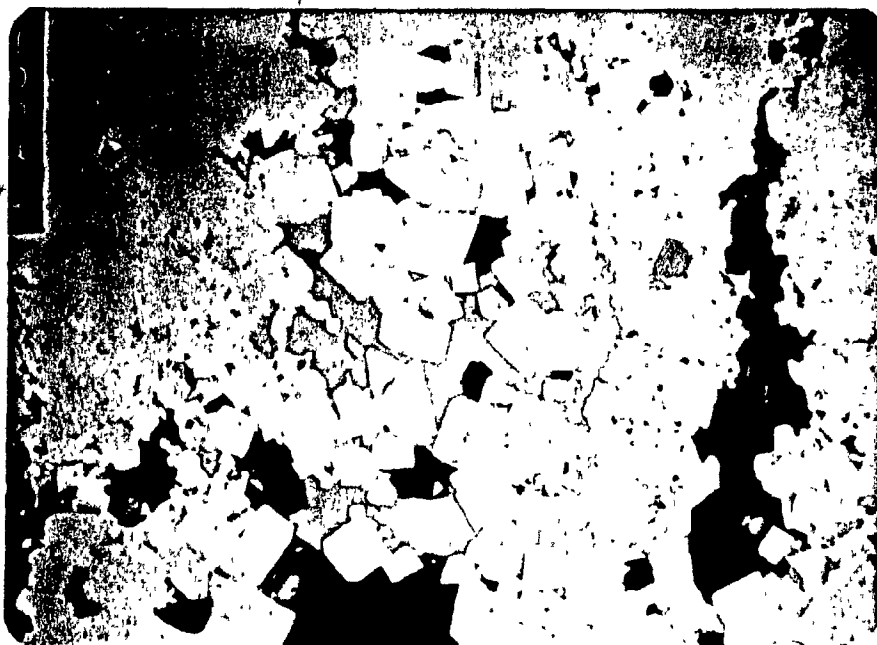


Fig. 1 Microphotograph of a complex sulphide ore from Brunswick Mining and Smelting (BMS), containing sphalerite (brown) and galena (grey) in pyrite (yellow), (10).

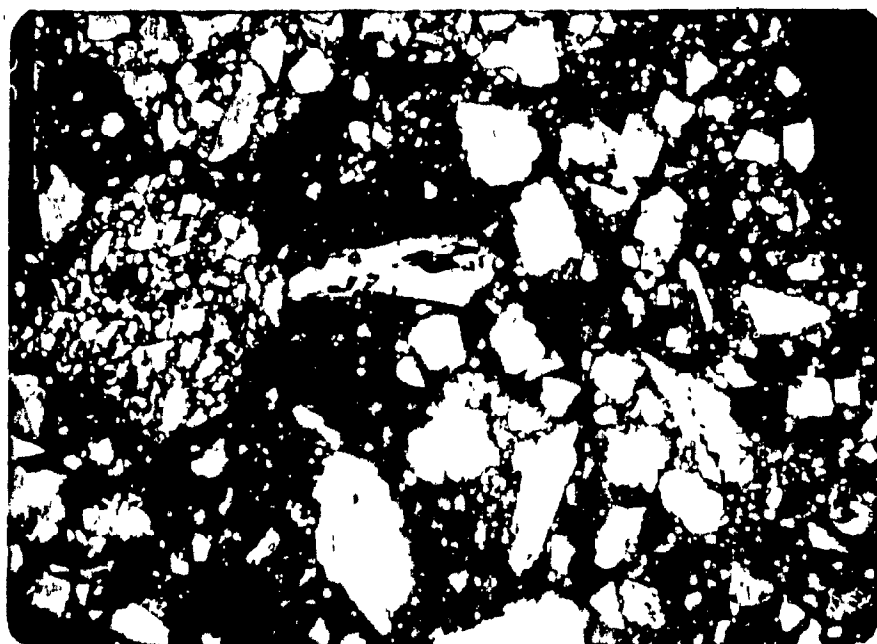


Fig. 2 Microphotograph of a lead concentrate from BMS. Grey particles are galena, yellow ones are pyrite and the brown particles are sphalerite (10).

lead concentrate from BMS (10). Notice that galena (grey), even at this small size ($\sim 10\mu\text{m}$) shows locking with pyrite. The problem of liberation of galena in BMS has been already studied extensively by Petrucek (11) and he found that even with the galena ground to 100% - $44\mu\text{m}$ it was only 37% w/w free; 13% w/w was combined with sphalerite and 50% wt combined with pyrite. Petrucek also confirmed that finer grinding would not significantly increase galena liberation. When galena was ground to 80% to $-25\mu\text{m}$ liberation increased by only about 2%.

Grinding to such fine sizes is energy intensive; indeed, it is possible that there exists a lower size limit to size reduction by conventional means. (12)

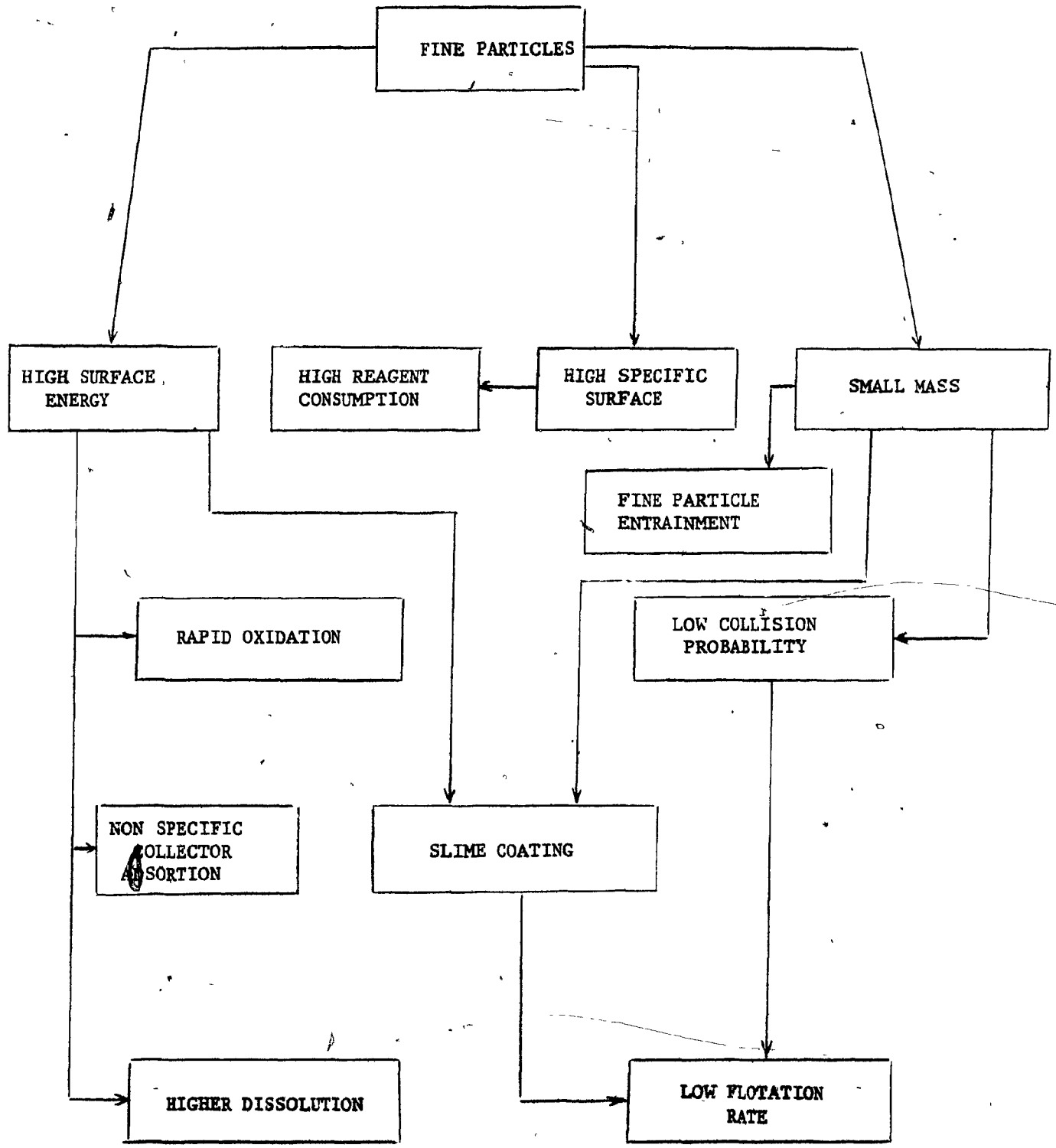
2) Fines Problems in Flotation

In addition to problems in generating fine sizes there is the problem of flotation recovery and selectivity of particles finer than about $10\mu\text{m}$, (13-15).

Fig. 3 shows a relationship between the physical and chemical properties of fine particles and their behavior in flotation. Notice that two main characteristics are dominant as the particle size is reduced: a) the specific surface becomes large and b) the mass of the individual particles becomes very small. These two characteristics give rise to particular problems.

The large specific surface of fine particles leads

Fig. 3. Relationship between the physical and chemical properties of fine particles and their behavior in flotation. (16)

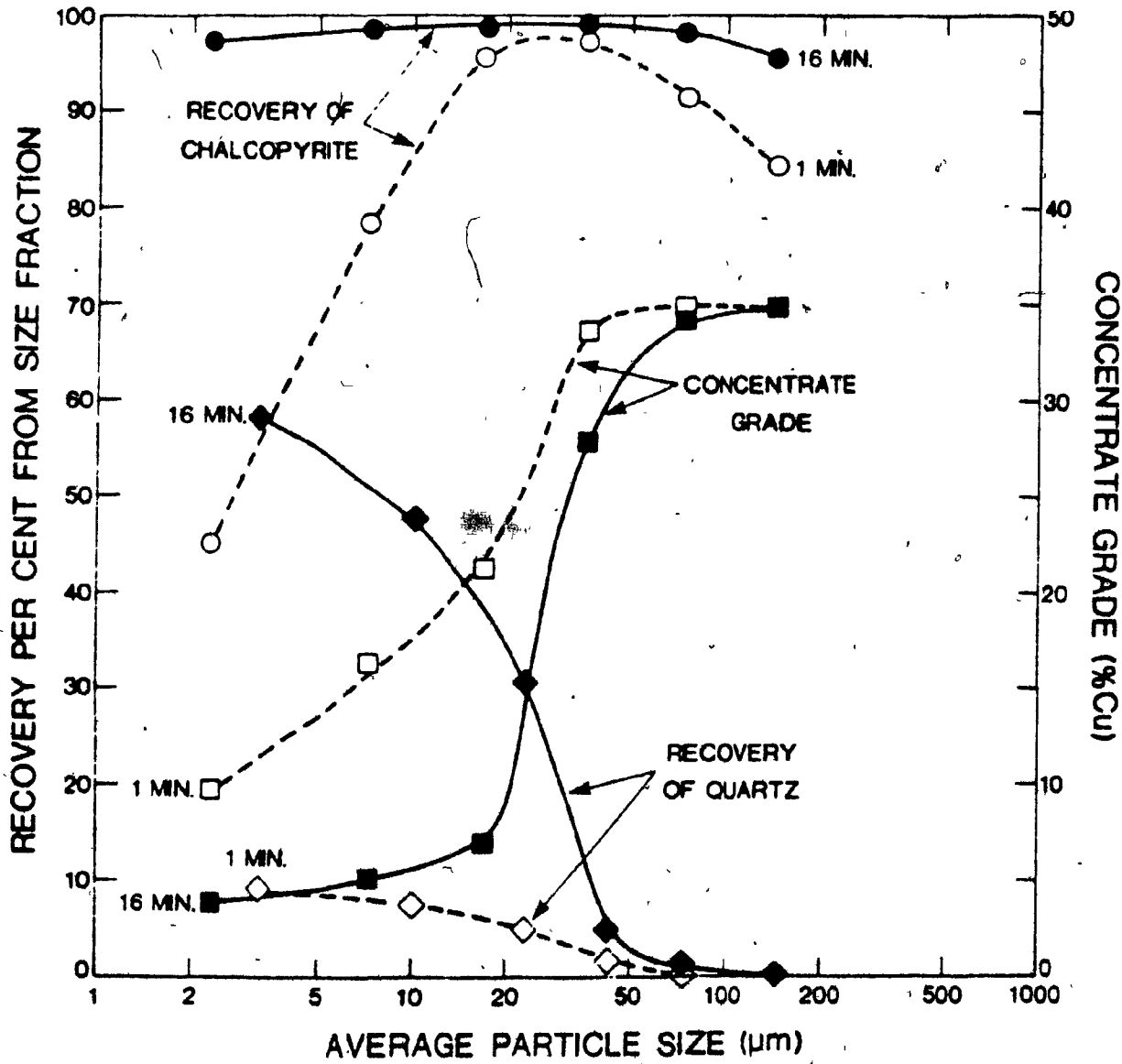


to high adsorption of reagents (determined by the amount adsorbed per unit mass). High adsorption not only leads to increased flotation costs but can also lead to starvation of the coarser particles and subsequently poor coarse flotation.

It has been speculated that surface electro-chemical properties of fine particles are different from coarse particles of the same material. Fine mineral particles conceivably have higher specific surface energy resulting from an increased number of edges, corners and crystallographic imperfections. High specific surface energy of fine particles may influence flotation in many ways; for example: a) increased dissolution making adsorbed layers unstable, and introducing possibly undesirable impurities into solution, affecting collector-mineral interactions, and b) increased tendency of the collectors to adsorb nonspecifically.

Because of the small mass of fine particles mechanical entrainment (i.e. carry-over into the froth with water) can be significant (17). Trahar (17) has indicated that as the particles become very small recovery by mechanical entrainment increases. He has found that the role of entrainment when treating ultrafine particles is often of such a magnitude that the true flotation of fines ceases to be the dominant recovery mechanism. To illustrate the importance of entrainment, Trahar (18) carried out separation tests of chalcopyrite from quartz. Fig. 4 presents the observations. As can be seen, in the first minute the recovery of all chalcopyrite coarser than $10\mu\text{m}$ was


Fig. 4 Effect of entrainment of quartz on grade of chalcopyrite concentrate in a typical batch flotation test at pH 11 without collector, (18).



more than 85% compared with 45% for the $-10\mu\text{m}$ fraction. The recovery of quartz was less than 10% throughout. After a further 15 minutes the recovery of the finest chalcopyrite had risen to 97% but at the same time the recovery of the finest quartz by entrainment had risen to 58%. Thus a high recovery of chalcopyrite in all sizes was attained only at the expense of concentrate grade in the fine sizes. It should be noted that no collector was used in this test, the only reagent additions being pH modifier and frother; it is not possible, therefore, to attribute the low grade in the fine sizes of the concentrate to the non-selective adsorption of collector. The possibility that the frother PPG 400 (polypropylene glycol of an average molecular weight of 400) was responsible for inducing genuine flotation of fine quartz was considered remote.

Another problem of fines in flotation is the decrease in the flotation rate, and this is mainly due to the reduction in collision probability when the size becomes small (19,20).

When flotation feed size range is extensive (i.e. slime + coarse feed), there exists the possibility of slime coating. This refers to the attachment of fine particles to larger particles. Slime coating can be detrimental to flotation in several ways. If the fine particles are the valuable minerals and the coarse particles are the gangue minerals, the grade of the concentrate becomes poor. If the fine particles consist of gangue minerals that coat the coarse particles of the



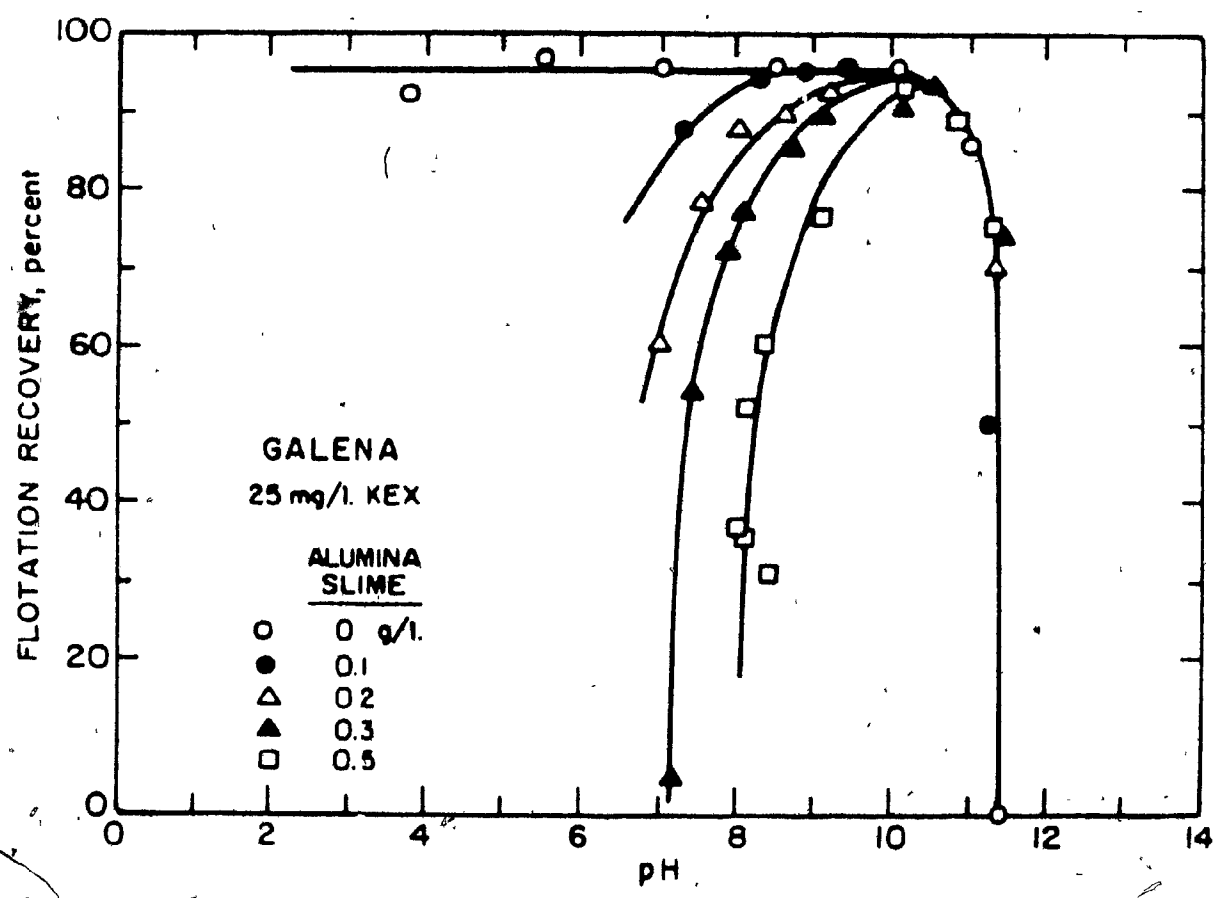
valuable mineral, these particles prevent the attachment of air bubbles and the recovery of valuable mineral may then decrease significantly. Fig. 5 illustrates the influence of alumina slimes on the flotation of galena with potassium ethylxanthate (KEX). Below pH 9, the alumina slimes carry a positive charge whereas above pH 9, they are negatively charged; at all pH's galena is negatively charged. As the amount of slimes in the system increases, the flotation of galena below approximately pH 9 decreases. When the alumina slime becomes negatively charged above pH 9, the tendency to coat the negatively charged galena particles is reduced and the slime coating problem ceases.

3) Selectivity vs. Pyrite

As indicated in the mineralogical section, pyrite is the major gangue.

Selective flotation of sulphide minerals is based primarily on a balance of activation and depression. Pyrite is depressed by sulphite (22), cyanide (23) and hydroxides (23) but these reagents do affect other minerals to some extent. Consequently when pyrite is in excess quantity, the reagent levels required can start to affect the other minerals. This difficulty is compounded by the fact that while coarse sulphide (e.g. +74 μm) selectivity is relatively straightforward, separation becomes more difficult as the size decreases. Circuits can become quite complex in an attempt to maintain recovery and selectivity.

Fig. 5 Influence of alumina slimes on the flotation of galena with potassium ethylxanthate (KEX), (21).



b) Flotation Techniques

Despite all these problems, complex sulphide ores are processed by flotation. There are two techniques:

(i) Sequential Selective Flotation (24,25)

This technique is used to separately obtain concentrates of chalcopyrite, galena and sphalerite, Fig. 6.

(ii) Semi-Bulk Flotation (26-28)

In semi-bulk flotation chalcopyrite and galena are first floated jointly with the depression of sphalerite and pyrite. The Cu-Pb bulk concentrate is subsequently conditioned to depress one or the other of these two minerals, usually galena, Fig. 7. Zinc is selectively floated from the Cu-Pb bulk tails.

When using the above techniques, concentrates are often produced at relatively poor grade and recovery. Typical results are given in Table 1. Clearly, both low grade and low recovery are found. In some ores (e.g. New Brunswick ores) where the mineral association is most intricate and the pyrite is in excess, a very complex circuit has been developed. Fig. 8 presents a generalized flowsheet of the Brunswick Mining and Smelting (BMS) concentrator. The ore is about 9.4% Zn (as sphalerite), 3.9% Pb (as galena), 0.3% Cu (as chalcopyrite) and 2.80 oz/ton Ag (in solid solution with galena and as a tetrahedrite (29)). Notice that besides separate copper, lead and zinc concentrates a lead-zinc bulk concentrate is made and a

Fig. 6 Flowsheet for a sequential selective flotation.

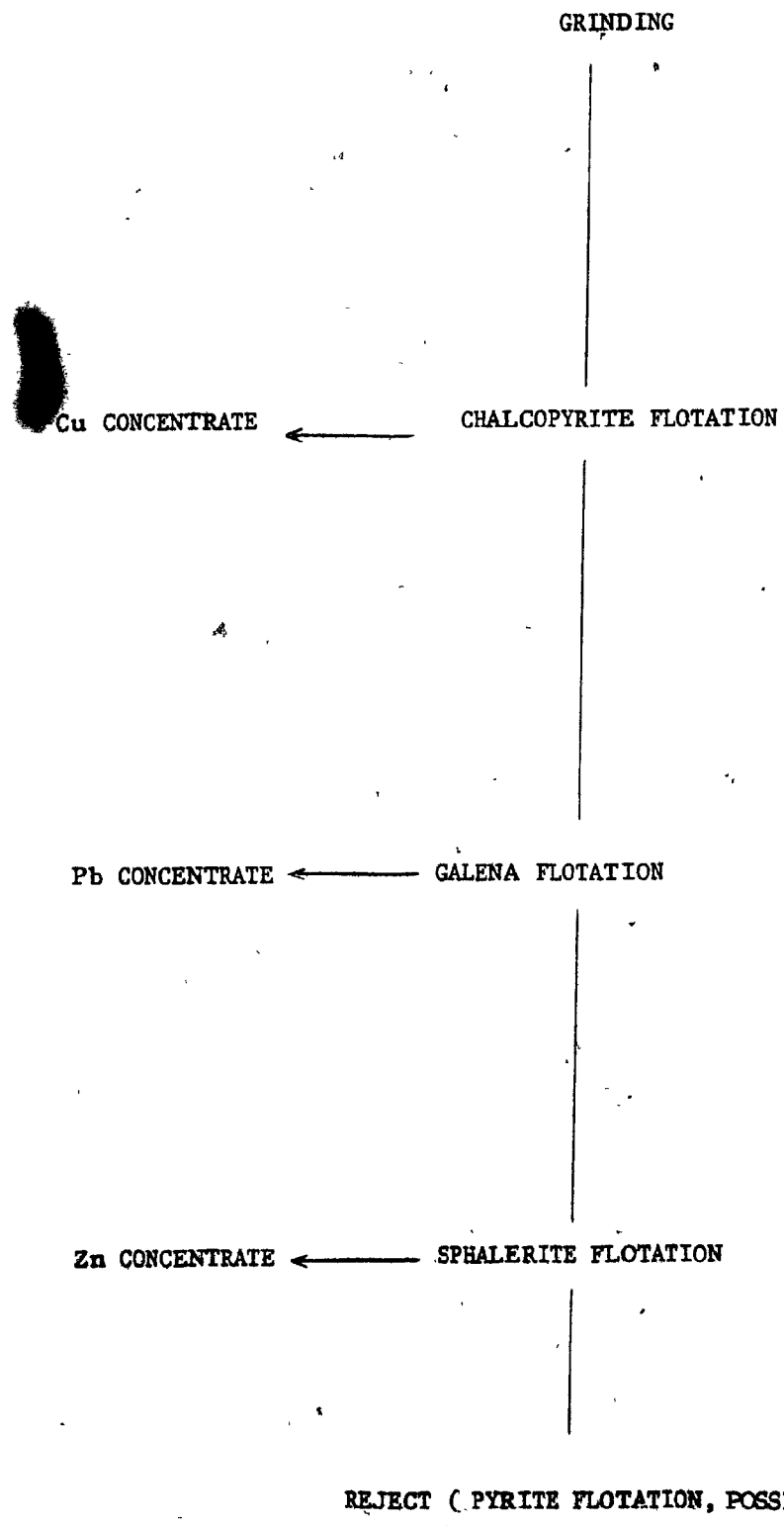


Fig. 7 Flowsheet for semi-bulk flotation.

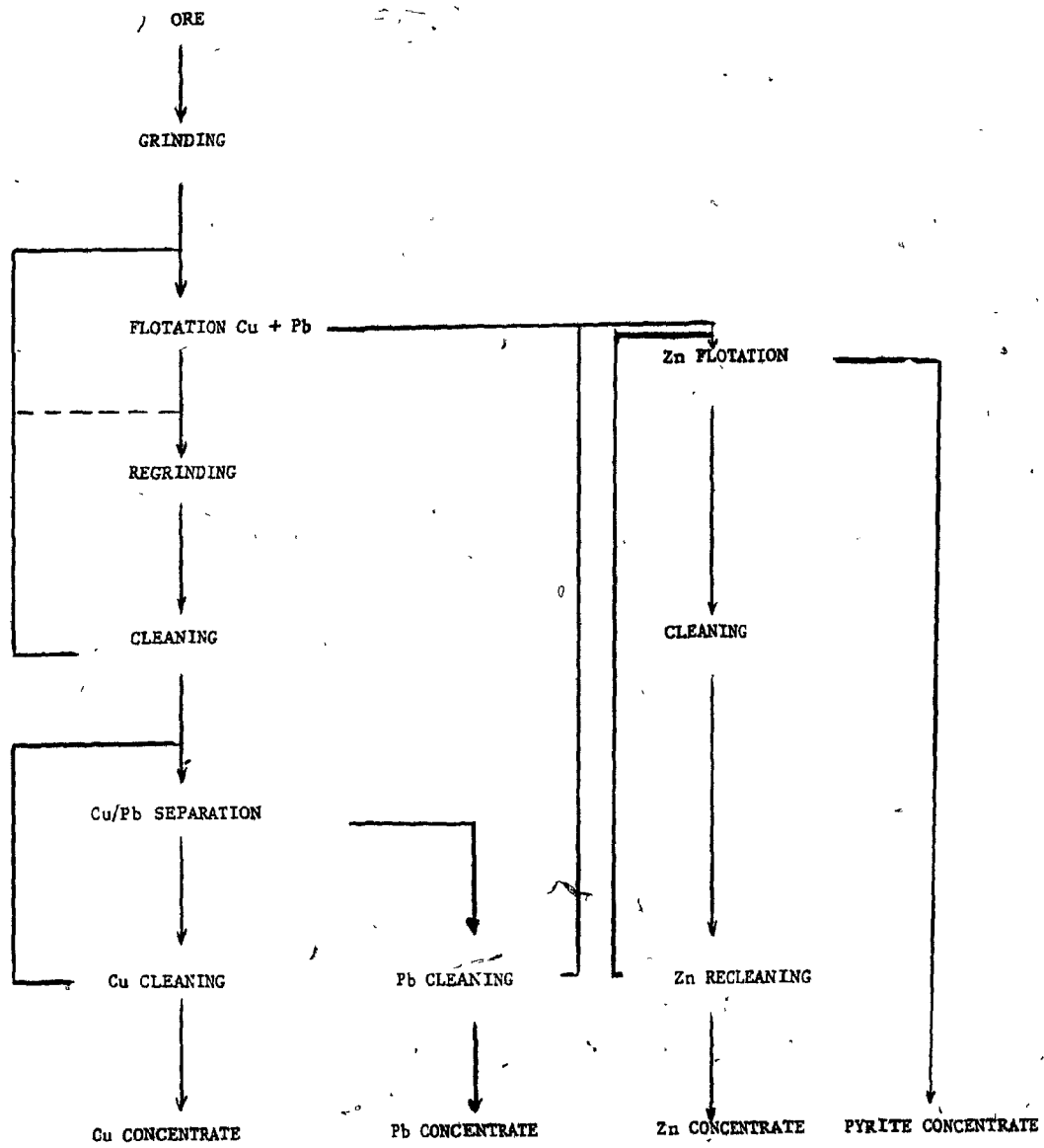
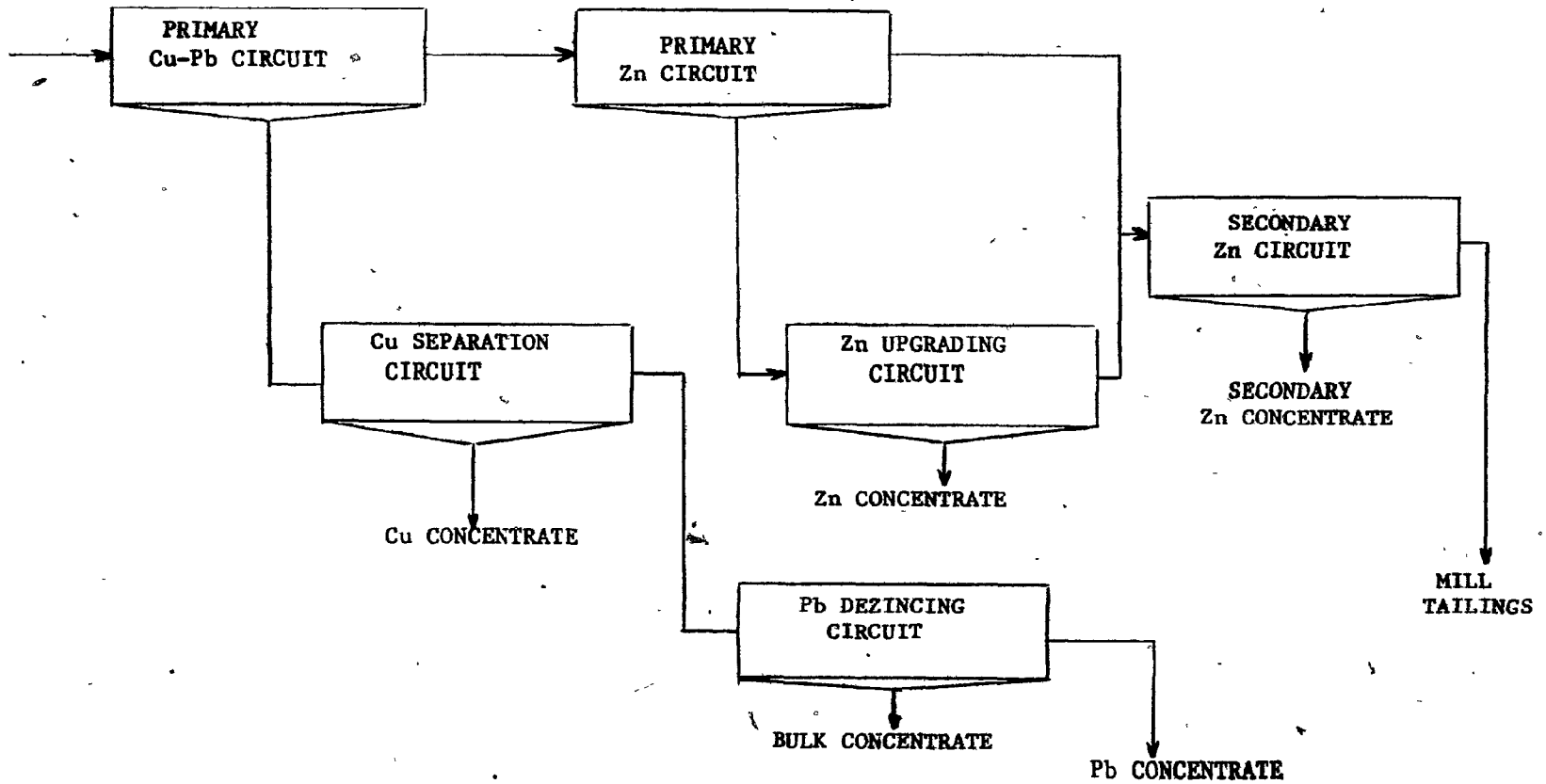


Fig. 8. Generalized flowsheet of Brunswick Mining and Smelting (BMS) flotation circuit.



secondary zinc concentrate.

Table 2 presents the overall lead, zinc and copper recoveries obtained in BMS by this technique. Clearly recoveries are low.

Table 1. Typical Results in Grade and Recovery of Complex Sulphide Ores (30)

Product	Assay (%)			Recovery (%)
	Cu	Pb	Zn	
Copper Concentrate	17-25	3-7	3-11	40-65, Cu
Lead Concentrate	1-4	35-55	3-30	40-60, Pb
Zinc Concentrate	0.5-3	1-5	45-55	70-80, Zn

Faced with these poor recoveries, mineral technologists have been trying to develop alternative process routes. A potential one is to produce a bulk Cu-Zn-Pb-Ag concentrate in order to increase recovery (32-36).

Table 2 gives some examples of the improvement in recovery that can be obtained by bulk flotation in comparison with selective flotation (37). Notice that for BMS, copper recoveries are increased from 50% to 70%, lead from 55% to 87% and zinc from 75% to 95%.

The production of a bulk concentrate has the following advantages:

- (i) Because concentrate grade requirements are less severe with bulk flotation, a higher recovery can be obtained.

Table 2. Comparison of Recoveries Obtained by Selective and Bulk Flotation.

Flotation Technique	Grade (%)			Recovery (%)		
	Cu	Pb	Zn	Cu	Pb	Zn
Aznalcollar (38)						
Selective Flotation	20	50	50	65	40	85
Bulk Concentrate	3.5	6	25	83	55	90
(39)						
Selective Flotation	19	50	50	61	55	72
Bulk Concentrate	1.8	5.8	19.2	80	70	90
New Brunswick (40)						
Selective Flotation				50	55	75
Bulk Concentrate	0.7	10.75	30.0	77	87	95

- (ii) Frequently, the liberation criterion is less strict for bulk flotation than for selective flotation, leading to a coarser grinding size.
- (iii) This technique would be more effective in treating low grade reserves.

The problem now is to extract the metals from the bulk concentrate. Several possibilities are reviewed by Barbery et al. (41). An attractive one is the hydrometallurgical route.

1.1.4 Processing of Bulk Concentrates

Most of the initial efforts on hydrometallurgy were directed to copper concentrates, but are now being extended to complex sulphide bulk concentrates.

The hydrometallurgical processes fall into two main categories, sulphate processes and chloride processes. In the former, H_2SO_4 , is the main leaching reagent and in the later HCl. Several processes have been developed based on these two leaching routes.

Three of the most important sulphate processes are (42): the Sherritt Gordon pressure leach process; the New Brunswick Research and Productivity Council sulphation-roast-leach-electrowin process (the RPC or SRLE process) and Técnicas Reunidas (complex process/Zincex process). Under chloride processes, some of the most important are, CLEAR, Minemet, Zincex, Cymet, Habashi-Mizoguchi and U.S.B.M. Of all the above processes, only one, the CLEAR process of Duval, is in commercial operation; several have been tested on a pilot-plant scale (New Brunswick SRLE, Sherritt Gordon, and Técnicas Reunidas) and the remainder have been developed to the stage of continuous laboratory scale.

A general problem in hydrometallurgical treatment of bulk concentrates is the recovery of lead and silver.

The origin of the problem is that leaching properties for galena are quite different from those for copper and zinc minerals. Successful treatment of lead and silver is essential to the processing of New Brunswick ores because of their relatively high abundance (3-5% Pb, 50-150 ppm Ag).

Three of the proposed hydrometallurgical processes to treat a New Brunswick bulk concentrate are:

- a) The Sherritt Gordon Pressure Leach Process (43,44)
- b) Habashi-Mizoguchi Process (45)
- c) The Sulphation Roast-Leach-Electrowin (RPC or SRLE) process (46).

a) The Sherritt Gordon Pressure Leach Process

The Sherritt Gordon process involves sulphuric acid leaching at a total pressure of 690 kPa and 150°C, using commercially pure oxygen as an oxidant. The zinc is dissolved and most of the copper which are then electrowon by conventional means. The leach residue consists of lead and iron as basic sulphates, elemental sulphur and gangue; it must be further processed to recover by-products of lead sulphate and elemental sulphur. Most of the silver in the concentrate is carried with the lead and iron sulphates, and may also be recovered. A simplified process flow diagram of the Sherritt Gordon process applied to New Brunswick ores is presented in

Fig. 9 SHERRITT GORDON Pressure Leach Process applied to New Brunswick ores. Simplified Process Flow Diagram. (47)

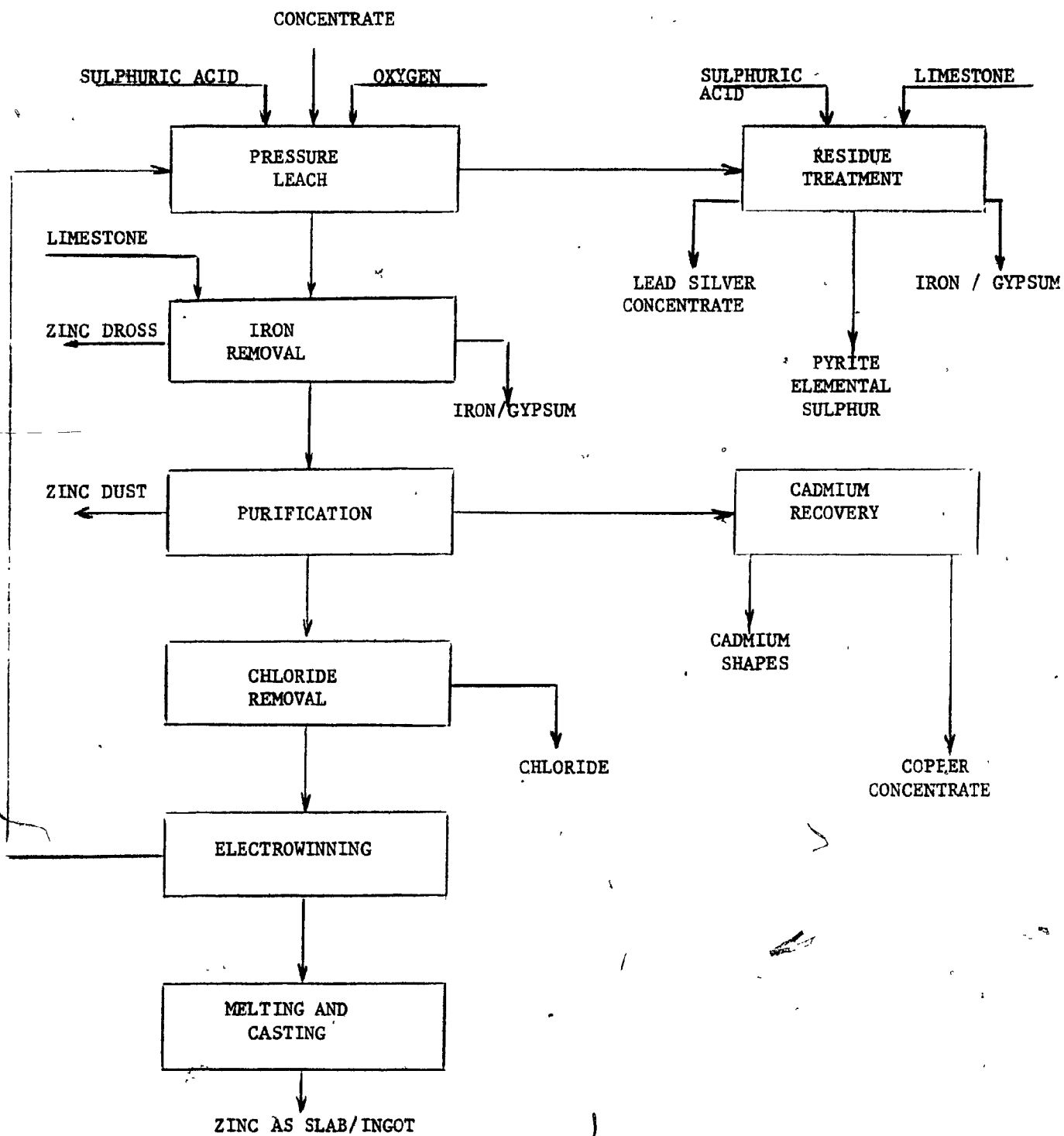


Fig. 9. Table 3 shows typical assays of New Brunswick up-graded tailings and bulk concentrate treated by the Sherritt Gordon process. Recoveries of the order of 96-99% Zn and 57-94% Cu are reported. The lead-silver residue is upgraded by flotation of sulphur and unleached sulphides. In one example the lead-silver concentrate was 19% Pb and 600 ppm Ag starting with an upgraded tailings concentrate (42). From bulk concentrate, this material is supposed to assay about 30% Pb and 700 ppm Ag. Notice that this process is rather effective in the recovery of zinc. Copper apparently can reach recoveries of over 90%.

Table 3 Average Analyses of New Brunswick Concentrates used in Sherritt Gordon Process Test

Concentrate	Chemical Analysis, (% , ppm Ag)				
	Cu	Zn	Pb	Fe	Ag
Upgraded Tailings	0.76	31.0	3.6	21.6	154
Bulk	0.67	29.9	12.4	17.9	398

b) The Mizoguchi-Habashi Process

Another alternative which has been proposed for treatment of New Brunswick Ores is the aqueous oxidation of the bulk concentrate in hydrochloric acid. Table 4 gives the assay of the bulk concentrate used in the testwork. In this

process the leaching of the bulk concentrate is conducted at 1N HCl, 120°C and 1000 kPa partial oxygen pressure, for 90 minutes. Zinc and copper are recovered from the leaching solution and lead and silver from the residue.

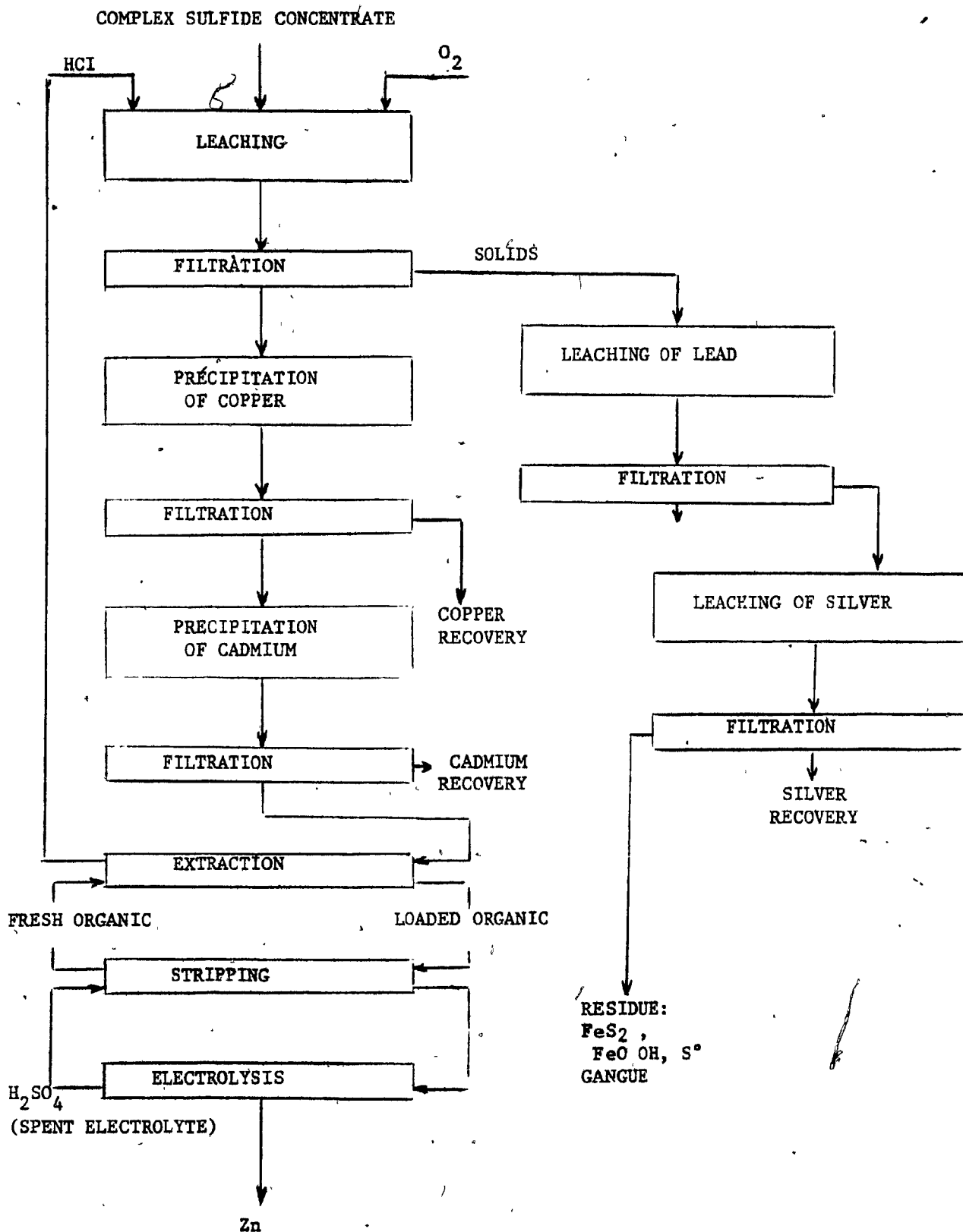
Fig.10 shows a flow sheet of the process. As we can see, the process is rather similar to the Sherritt Gordon process (Fig. 9) in which sulphuric acid is replaced by hydrochloric acid, but since the direct recovery of zinc from a chloride medium is not as technically advanced, zinc was transferred to a sulfate system. The transfer is achieved using an organic solvent, diethylhexyl phosphoric acid. The H_2SO_4 generated during subsequent electrowinning of zinc is used for stripping and the HCl generated during extraction is recycled for leaching. Recoveries of 97% Zn and 95% Cu are reported.

Lead and silver are supposed to be recovered by leaching, with reported recoveries of 83% Pb and 85% Ag, but the details were not given.

Table 4 Assay of the New Brunswick Bulk Concentrate used in the Mizoguchi-Habashi Process

Element	Assay (%)
Zn	26.53
Pb	8.54
Cu	0.84
Cd	0.04
Fe	22.08
S	37.15
Ag	0.023

Fig. 10 Flowsheet of Mizoguchi-Habashi Process. (48)



c) The Sulphation Roast-Leach-Electrowin (RPC or SRLE) Process

The SRLE process developed by The New Brunswick Research and Productivity Council involves a sulphation roast and two leach steps. (Fig. 11)

In the roasting step, copper (as chalcopyrite), Zn (as sphalerite) and lead (as galena) become sulphates and the iron (as pyrite) becomes hematite. The first leach step, called the neutral acid leach (NAL), dissolves the copper and zinc sulphates. The second leach step, called the hot acid leach (HAL), extracts the remaining zinc (mainly as ferrite) and copper (as unroasted chalcopyrite) leaving a considerable amount of iron in solution. After solid-liquid separation, the HAL liquor is recycled to the sulphation roast to fix the iron as hematite and copper and zinc as sulphates. The remaining solid residue (HALR) contains all the lead, silver and iron.

Table 5 presents the operating conditions in the RPC process. Notice that in the NAL step, the pH needed to dissolve copper and zinc sulphates is 3.6-4.0. In contrast, the HAL step needs strong acid conditions (pH = 0.1-0.3) to be able to recover the remaining zinc and copper. Overall, copper and zinc extraction is about 98%. Notice from Fig. 11 and Table 5 that the SRLE process does not report the procedure to recover the lead and silver from the HALR. At present a method to separate lead and silver from the residue has not been fully established.

Fig. 11 The Sulphation Roast-Leach-Electrowinning (RPC or SRLE) Process.

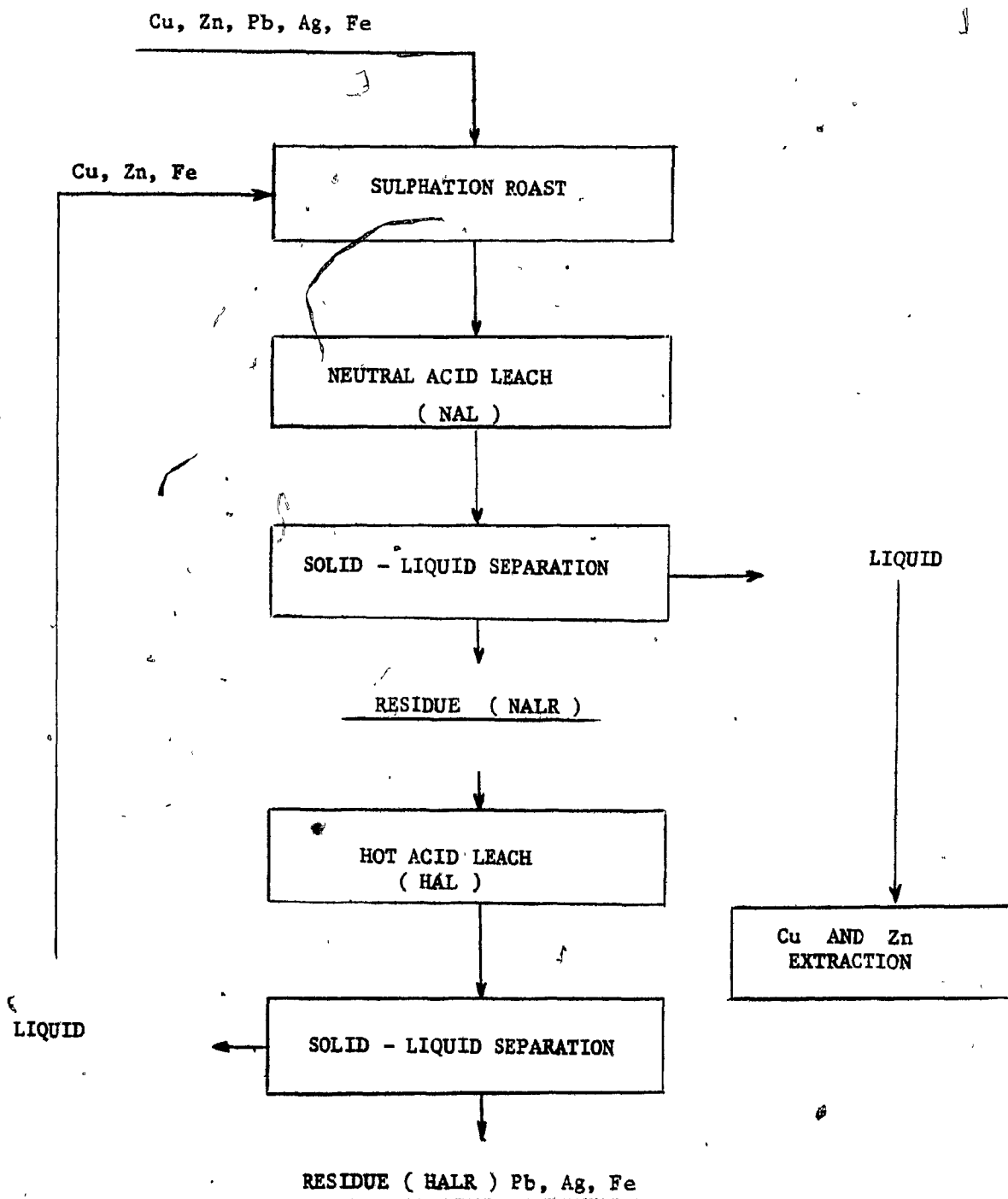


Table 5. Operating Conditions in the SRLE Process

Parameter	Step
	Roasting
Temperature	685±5°C
Retention Time	5.5 hrs.
	Neutral Acid Leach (NAL)
Temperature	55±10°C
Retention Time	1.5 hrs.
pH	3.6-4.0
% Solids in Pulp	20 wt. (%)
	Hot Acid Leach (HAL)
Temperature	95±5°C
Retention Time	2 hrs.
pH	0.1-0.3
% Solids in Pulp	45 wt. (%)

2. STATEMENT OF PROBLEM

The problems associated with the treatment of complex sulphide ores have now been defined. It was shown that an alternative to current practice for increasing metal recoveries is by the production of a bulk concentrate. The subsequent processing of bulk concentrates is rather uncertain when dealing with ores which contain considerable amounts of lead and silver. This is the case for New Brunswick ores in Canada.

One process which has received considerable attention is the SRLE process. One problem is the recovery of the lead and silver from the remaining iron in the HALR.

The object of this investigation is to test a physical separation of lead and silver, from the remaining iron by high gradient magnetic separation (HGMS). Production of a saleable lead-silver concentrate from the HALR would be a factor in making the RPC process a competitive treatment route for complex sulphide ores. In order to evaluate the proposal in a systematic way, a method of attack was established.

2.1 Method of Attack

Samples of calcine from the RPC process were obtained and subjected to the leach steps so that fresh residue samples would be available for high gradient magnetic separation (HGMS) testing. Both NALR and HALR were to be considered for separation.

Separation was to be guided by detailed mineralogical examination of the calcine and residues. Phase identification was to be conducted by X-ray diffraction and optical/electron microscope techniques. Liberation, a key factor in physical separation was to be measured after phase identification.

The potential for magnetic separation was to be tested on the Frantz isodynamic magnetic separator on sized samples (e.g. -25+15 μm) from NALR and HALR.

Dispersion, an important criterion in physical separation of ultrafine particles, was to be achieved before the HGMS tests.

HGMS conditions were to be found using an HGMS recovery model. Magnetic separation tests were to be performed on the Sala HGMS, model 10-15-20 installed at CANMET, Ottawa.

3. CHARACTERISTICS OF THE CALCINE AND LEACH RESIDUES

3.1 The Calcine

3.1.1 Assays of RPC Samples

Fourteen calcine samples were obtained from New Brunswick Research and Productivity Council (RPC). These samples were roasted materials produced from upgraded tailings (30% Zn, 3% Pb) and from a bulk concentrate (30% Zn, 10.75% Pb) (49). All calcines were produced with hot acid leach liquor returned as roaster coolant.

Table 6 gives the assay of each sample. Since there was little difference between samples, they were mixed. Table 7 gives the assay of the representative head sample.

3.1.2 Size and Metal Distribution of Calcine

The size distribution of the calcine was determined using micro sieves. Sizing was performed in an ultra-sonic bath to facilitate sizing to 10 μ m. Acetone was used instead of water to avoid copper and zinc sulphate dissolution.

Table 8 shows the size and metal distribution of the calcine. The results show a uniform distribution of metals among the size fractions.

Table 6. Assay of Calcine Samples

Sample No.	Assay (%)			
	Cu	Zn	Pb	Fe
1	0.63	26.9	6.9	15.5
2	0.62	26.9	6.8	15.8
3	0.62	27.0	6.6	16.3
4	0.63	26.9	6.8	16.3
5	0.64	26.5	7.1	16.3
6	0.61	26.2	7.1	16.1
7	0.63	26.9	6.8	16.3
8	0.62	26.5	6.8	15.4
9	0.61	26.0	6.9	16.1
10	0.61	26.0	6.9	16.3
11	0.58	25.0	6.4	16.4
12	0.61	25.4	6.6	15.9
13	0.60	25.4	6.5	16.0
14	0.61	26.0	6.6	16.1

Table 7. Assay of the Representative Head Sample

Sample	Assay (%)				
	Cu	Zn	Pb	Fe	Ag*
Head	0.57	25.9	6.7	15.2	122

* Ag is reported in ppm.

Table 8. Size and Metal Distribution of the Calcine

Size Fraction Product (μm)	Wt (%)	Assay (%)				Distribution (%)			
		Cu	Zn	Pb	Fe	Cu	Zn	Pb	Fe
+25	52.9	0.57	26.8	6.2	13.3	53.8	55.6	49.0	47.2
-25+15	19.8	0.56	25.5	6.4	15.9	20.0	19.8	18.9	21.1
-15+10	9.3	0.56	24.5	9.2	15.9	9.4	9.0	12.8	9.9
-10	18.0	0.52	22.0	7.2	18.0	16.8	15.6	19.3	21.8
	100.0					100.0	100.0	100.0	100.0
Calc. Feed		0.56	25.4	6.7	14.9				
Assay Feed		0.57	25.9	6.7	15.2				

3.4.3 Mineralogical Examination

To identify all the minerals present in the calcine, X-ray diffraction (XRD) and microscope examination was carried out.

X-Ray Diffraction (XRD)

The powder diffraction technique using the Debye-Scherrer camera was used. Table (9) shows the phases identified. Zinc sulphate is the main component in the calcine.

In Appendix 1 (Table A-1) the d-spacings measured and a comparison with listed values is given.

Microscope Examination

In a Carl-Zeiss microscope with reflected light, unmounted samples of +25 μm , -25 + 15 μm and -15 + 10 μm were

observed under reflected illumination at 100 magnification. The color was the main factor in identification. Zinc sulphate (yellow), lead sulphate (crystalline white), hematite (red), franklinite (or ferrite) (brown-red), quartz (crystal-line colorless) and marmatite (black) were identified, (Table 9). Fig. 12 shows a microphotograph of a -37 + 25 μm calcine fraction. Yellow particles are zinc sulphate, red ones are hematite and the black one in the upper right corner is marmatite.

Mounted samples of + 25 μm , -25 + 15 μm and -15 + 10 μm fractions were studied on a Vickers microscope with reflected light, under polarized conditions. Fig. 13 shows a picture at 440 magnification of the -37 + 25 μm fraction. Since zinc sulphate is the most abundant mineral in the calcine it was easily identified (yellow phase); besides it looks similar to that in unmounted samples, Fig. 12. The other particles in Fig. 13 are: anglesite (crystalline white), hematite (red) and ferrite (red-brown). Identification of these phases was largely as a result of identifying the phases left after the leaching steps. For example, ferrite was clearly identified in the NALR and hematite and anglesite in the HALR. From Fig. 13, the two biggest grains observed are locked particles of hematite-ferrite-anglesite and zinc sulphate-hematite-anglesite.

Table 9 summarizes the results of the mineralogical examination.



Fig. 12 Microphotograph of a $-37 + 25 \mu\text{m}$ calcine fraction. Yellow particles are zinc sulphate, red ones are hematite and the black one in the upper right corner is marmatite.



Fig. 13 Microphotograph of a $-37 + 25 \mu\text{m}$ calcine fraction at 440 magnification with reflected light, under polarized conditions. Zinc sulphate is the yellow phase, anglesite is the crystalline white, hematite is red and ferrite is red-brown.

Table 9. Mineralogical Composition of the Calcine

Name	Formula
Zinc Sulphate	$ZnSO_4$
α -Hematite	Fe_2O_3
Franklinite	$ZnFe_2O_4$
Anglesite	$PbSO_4$
Zinc Oxy-sulphate	$ZnO \cdot 2ZnSO_4$
Copper Sulphate	$CuSO_4$
Quartz	SiO_2
Marmatite	$(Zn,Fe)S$

3.2 Characteristics of the Neutral Acid Leach Residue (NALR).

The neutral acid leach (NAL) step is similar to that in conventional electrolytic zinc plant practice. In the present case dissolution of zinc and copper sulphates and zinc oxysulphate is effected by maintaining the pH at 3.6 to 4.0 for 1.5 hours.

3.2.1 Leach Procedure

The conditions specified by RPC (see Table 5) for the NAL step were followed.

A 2000 ml beaker was used as the reaction vessel. A hot plate with a variable temperature control was used to keep a constant temperature. A variable speed electric stirrer kept the solids well suspended. During the whole test, temperature and pH were carefully controlled.

3.2.2 Metal Distribution in NAL

The metal distribution in the NAL is shown in Table 10.

In this leaching step over 80% of zinc and copper is recovered. Over 99% of lead, silver and iron report to the residue.

About 61% of the calcine is dissolved in the NAL.

Table 10. Metal Distribution in the Neutral Acid Leach (NAL) Step

Product	Wt (%)	Distribution (%)				
		Cu	Zn	Pb	Fe	Ag
Calcine	100.0	100.0	100.0	100.0	100.0	100.0
Filtrate	61.7	82.5	85.3	0.1	0.7	-
NALR	38.3	17.5	14.7	99.9	99.3	100.0
	100.0	100.0	100.0	100.0	100.0	100.0

3.2.3 Size and Metal Distribution of the NALR

The size distribution was again performed by microsieving. The NALR was well dispersed before sizing using a solution of 0.05% calgon, mechanical agitation and 15 minutes in the ultra-sound bath.

Table 11 shows the size and metal distribution of NALR. By comparison with Table 8 the NALR is much finer than the calcine, the per cent passing 10 μ m increasing from 18% to more than 74%. Over 83% of Zn and Pb are in the -10 μ m fraction.

The Zn content is decreased from 25.8 to 9.5%, Cu from 0.57% to 0.29%, Pb is increased from 6.7 to 16% and iron from 15.2 to 40.3%.

Table 11. Size and Metal Distribution of NALR

Product (μm)	Wt (%)	*Assay (%)				Distribution (%)			
		Cu	Zn	Pb	Fe	Cu	Zn	Pb	Fe
+25	4.4	0.38	7.4	6.9	44.7	5.6	3.5	1.9	4.9
-25+15	13.6	0.34	5.8	9.3	48.4	15.3	8.4	8.1	16.4
-15+10	7.3	0.35	6.3	6.3	52.0	8.6	5.0	2.9	9.5
-10	74.7	0.28	10.3	18.3	37.2	70.5	83.1	87.1	69.2
	100.0					100.0	100.0	100.0	100.0
Calc. Feed		0.30	9.3	15.7	40.1				
Assay Feed		0.30	9.7	16.8	40.3				

* Ag assay is 290 ppm.

3.2.4 Mineralogical Examination

Mineralogical examination of NALR was carried out by using XRD, a metallurgical microscope with both, reflected and transmitted illumination and by electron microprobe and the scanning electron microscope (SEM). Where necessary, samples were first split on the Frantz Isodynamic Magnetic Separator (Frantz) to aid identification. Also, comparison with known specimens was used.

X-Ray Diffraction (XRD)

As for the calcine, the powder diffraction technique using the Debye-Scherrer camera was employed. Five compounds

were identified, hematite (Fe_2O_3), ferrite (ZnFe_2O_4), anglesite (PbSO_4), quartz (SiO_2) and sphalerite (ZnS). Further examination on some sphalerite grains by the microprobe indicated marmatite ($(\text{Zn,Fe})\text{S}$) rather than sphalerite. In Appendix 1, Table A-2, the d-spacing measured and a comparison with listed values is given.

Metallurgical Microscope with Reflected Light

Unmounted samples of +25 μm , -25+15 μm and -15 + 10 μm were observed under reflected light at 100 magnification. Hematite, ferrite (franklinite), anglesite, marmatite and quartz were identified. Some locked anglesite-hematite particles ($\text{PbSO}_4\text{-Fe}_2\text{O}_3$) were found. Anglesite particles appeared as if they were agglomerates of small particles, with a rough surface which seemed to trap small hematite grains. Fig. 14 presents a microphotograph with particles of -37+25 μm of the NALR. Red particles are hematite, the white phase is anglesite, the red-brown is ferrite and the black phase is marmatite.

Vickers Microscope with Reflected Light

Mounted samples of +25 μm , -25+15 μm and -15+10 μm fractions were studied on the Vickers Microscope under polarized light. Microphotographs at 440 and 620 magnification are shown in Figs. 15 and 16. The red particles are hematite (most abundant phase), the white phase is anglesite and the red-brown particles are ferrite.



Fig. 14 Microphotograph of $-37 + 25 \mu\text{m}$ particles of NALR. Red particles are hematite, the white phase is anglesite, the red-brown is ferrite and the black phase is marmatite.



Fig. 15 Microphotograph of $-25 + 15 \mu\text{m}$ particles of NALR at 440 magnification with reflected light, under polarized conditions. Red particles are hematite (most abundant phase), the white phase is anglesite and the red-brown particles are ferrite.



Fig. 16 Microphotograph of -25 + 15 μm particles of the NALR at 620 magnification with reflected light, under polarized conditions. Red particles are hematite (most abundant phase), the white phase is anglesite and the red-brown particles are ferrite.

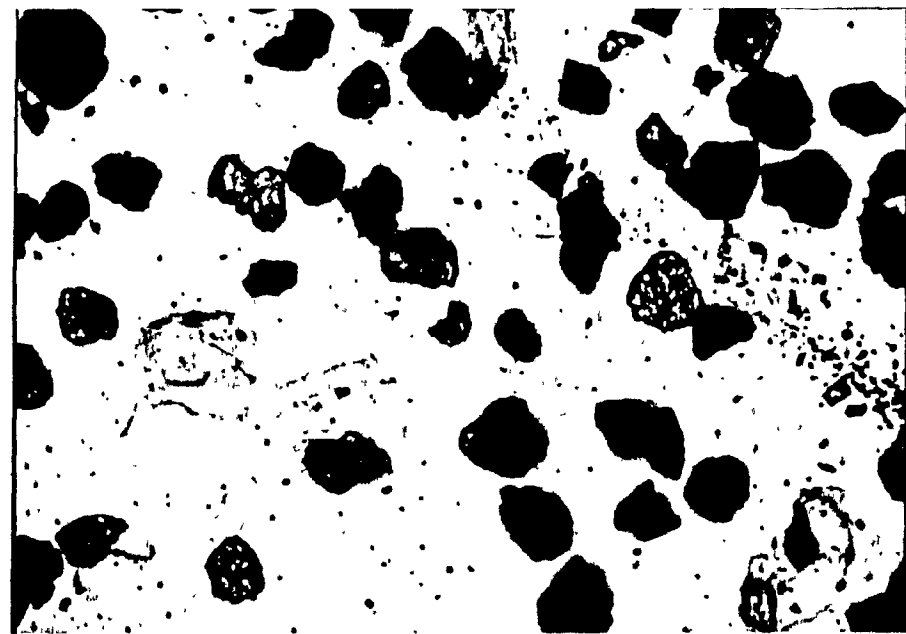


Fig. 17 Microphotograph of -25 + 15 μm particles of the NALR under transmitted light. Anglesite is the white phase, and quartz the colorless. Hematite, ferrite and marmatite are opaque grains.

Carl-Zeiss Microscope with Transmitted Light; Degree of Liberation

Unmounted samples of +25 μ m, -25+15 μ m and -15+10 μ m were immersed in an oil of refractive index 1,516 in order to observe under transmitted light. Fig. 17 shows a microphotograph of the -25+15 μ m fraction. Anglesite is the white phase, and quartz the colorless. Hematite, ferrite and marmatite are opaque grains. From this analysis, liberation of anglesite was determined according to Gaudin's method (9). The degree of liberation is defined as the volume fraction of mineral or phase occurring as free particles in relation to the total volume of that mineral occurring in the free and locked forms. From 300 to 800 particles were counted, which according with Van Der Plas and Tobi (50), Appendix B, gives expected errors from 6 to 1% in the liberation values with a 95 per cent confidence. Appendix B, Table B-2, shows the record sheet used in point counting for each sample.

Table 12 shows the results. At + 25 μ m, the degree of liberation is about 70%. This rises to over 90% at -15+10 μ m. Clearly a substantial fraction of the anglesite is free, suggesting that physical separation is possible.

Electron Microprobe

An electron microprobe examination was carried out on mounted samples of +25 μ m, -25+15 μ m, -15+10 μ m and some isolated samples from the Frantz separator.

Table 12. Liberation Degree in Coarser NALR Sizes

Product (μm)	Degree of liberation (%)	
+25	70	$\pm 6^*$
-25+15	90	± 2
-15+10	94	± 2

* 95% confidence interval

When the beam was focussed on the red particles in Figs. 15 and 16 (i.e. the suspected hematite) the peaks of the spectrum indicated only iron confirming the hematite identification (oxygen cannot be directly detected, but is inferred by difference). Quantification was carried out on several grains, but since the surface of these particles is very rough, a large variation in the intensity occurred and the per cent iron was low, about 50% instead of 70% for hematite.

Following through the other grains (Fig. 16), when the white crystalline particles were analyzed, the spectrum indicated lead and sulphur and some traces of silver. Quantification was again carried out and lead and sulphur compositions corresponding to anglesite were found. Since the amount of silver in the sample is lower than 0.1%, quantification of this element was not carried out. When the red-grey particles, Fig. 15 were analyzed, the spectrum indicated the presence of

iron-zinc and occasionally iron-zinc-copper, suggesting a complex ferrite. Iron-zinc grains were quantified, but again their rough surface disturbed the detected intensity, giving low iron-zinc assays, averaging 43% Fe and 15% Zn.

However, since ferrite is the only mineral which has solely iron and zinc (and oxygen), it can be assumed the particle is ferrite. Further microprobe analysis on ferrites isolated on the Frantz separator (fraction of mags up to 100mA, p.67) found only ferrites of the type iron-zinc-copper, 44% - 10% - 11% respectively. Since this fraction corresponds to the strongest magnetic fraction, it suggests copper makes these ferrites strongly magnetic. Figs. 18 and 19 show microphotographs of this ferrite at 440 and 620 magnification, respectively. The size of the particles is $-25+15\mu\text{m}$. Remember, however, this material represents only about 0.8% of the NALR, Table 19, p. 67.

Some other particles reported a spectrum of silicon, suggesting quartz. Some particles gave copper-iron-sulphur peaks suggesting chalcopyrite. Also traces of aluminium, titanium and tin were detected.

Another phase, which was grey in color and had a smooth surface (Fig. 20) was identified. According to the spectrum this material is zinc-iron-sulphur. Quantification determined a 6:1 iron-zinc ratio; it is clearly a marmatite particle. Microprobe analysis on marmatite isolated on the Frantz separator (fraction of mags 650-850 mA, Table 19, p.67) was carried out.



Fig. 18 Microphotograph of mags fraction up to 100 mA on Frantz, of the NALR. (size of the particles ranges from 25 to 15 μm . The magnification is 440. Red-dark particles are ferrites and red particles, hematite.



Fig. 19 Microphotograph of mags fraction up to 100 mA on Frantz of the NALR. Size of the particles range from 25 to 15 μm . The magnification is 620. Red-dark particles are ferrites and red particles, hematite.



Fig. 20 Microphotograph of mags 650-850 mA fraction in Frantz, of the NALR. (size of the particles ranges from 25 to 15 μm . The magnification is 440). Grey particles are marmatite, red phase, hematite, and the white one is anglesite.

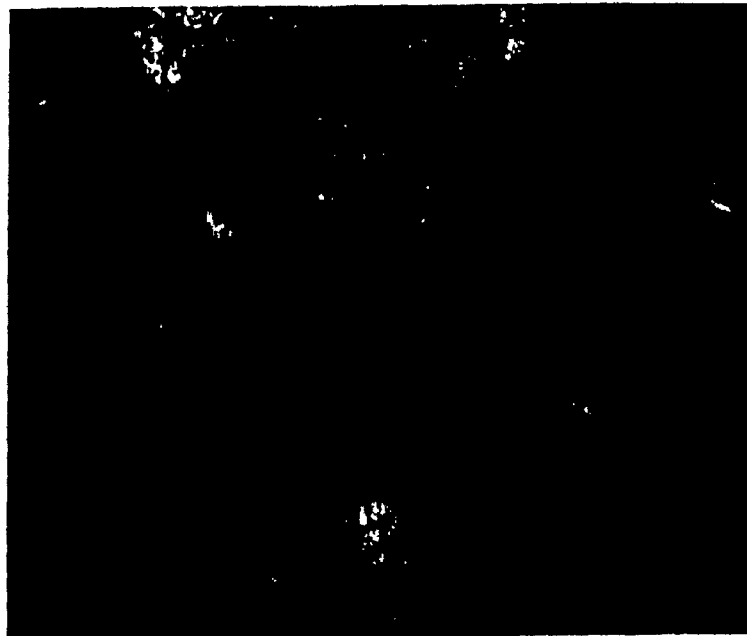


Fig. 21 Microphotograph of mags 650-850 mA fraction on Frantz, of the NALR. (size of the particles ranges from 25 to 15 μm . The magnification is 440). Grey particles are marmatite, red phase, hematite, and the white one is anglesite.

The same 6:1 ratio was found. Figs. 20 and 21 show microphotographs of the isolated marmatites at 440 magnification. The size of the particles is $-25 \pm 15 \mu\text{m}$. Smooth grey particles are marmatite. The red particles are hematite and the red-white ones are locked hematite-anglesite particles.

Scanning Electron Microscopy (SEM)

Fig. 22 shows a microphotograph of a floccule at 10,000 magnification; the size of the floccule is about $8 \mu\text{m}$. Fig. 23 shows a microphotograph of the same sample but now at 40,000 magnification. An EDAX* of the floccule is also given, Fig. 24, reporting mainly iron and zinc peaks and in minor amount, lead. It suggests the floccule is comprised of mainly hematite and ferrite. Notice how fine the individual particles are (less than one micrometre). Clearly it is important to disperse the sample before considering physical separation.

Resumé of Mineralogical Examination

Table 13 summarizes the minerals identified in NALR in decreasing order of estimated content.

The remaining zinc in NALR is as ferrite and marmatite. The remaining copper in the NALR is as chalcopyrite, and with some in a Cu-Zn ferrite.

* Energy Dispersive Analysis of X-rays.

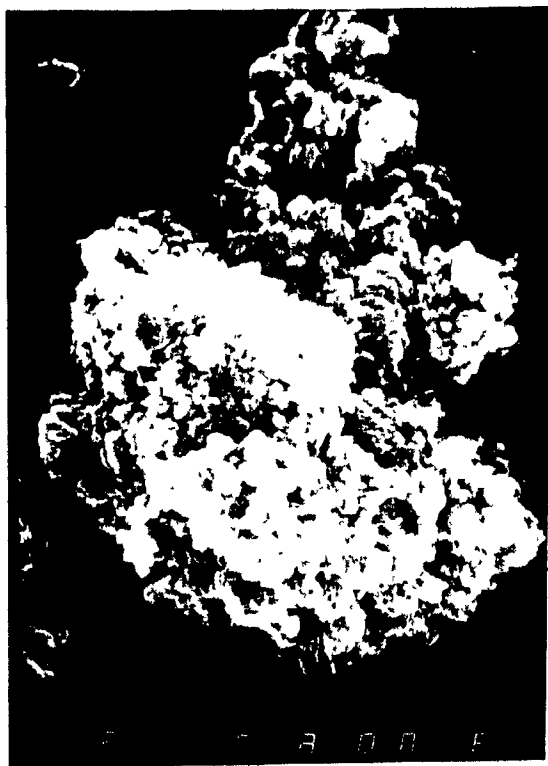


Fig. 22 SEM microphotograph of a floccule of NALR at 10,000 magnification. The size of the floccule is about 8 μm .



Fig. 23 SEM microphotograph of some particles in the NALR at 40,000 magnification. An EDAX on these particles reports mainly iron and zinc peaks and in minor amount, lead.

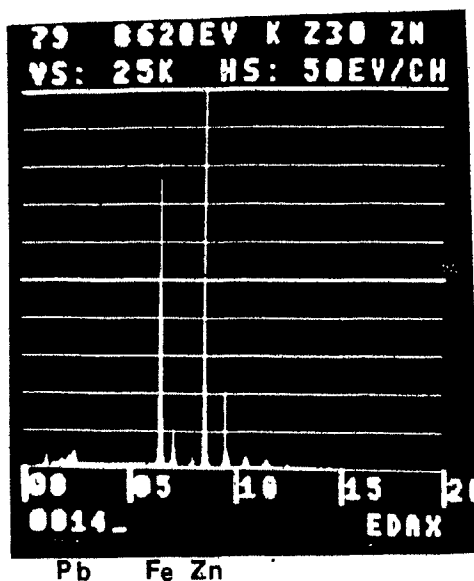


Fig. 24 EDAX of the particles from Fig. 23. Iron and zinc peaks and in minor amount lead, are presented. It suggests the floccule is comprised of mainly hematite and ferrite.

Table 13. Resumé of Mineralogical Identification of NALR

* Name	Formula
Hematite	Fe_2O_3
Anglesite	PbSO_4
Ferrite	ZnFe_2O_4
Marmatite	$(\text{Zn, Fe}) \text{S}$
Quartz	SiO_2
Chalcopyrite	CuFeS_2
Copper Ferrite	$(\text{Cu} \cdot \text{Zn})\text{O} \cdot \text{Fe}_2\text{O}_3$
Aluminum**	Al
Titanium**	Ti
Tin**	Sn
Silver**	Ag

* Names are listed in decreasing order of estimated content.

** Found by electron microprobe.

3.3 CHARACTERISTICS OF THE HOT ACID LEACH RESIDUE (HALR)

In order to recover the remaining zinc (as ferrite and marmatite) and copper (as chalcopyrite) in the NALR, a second leaching step is needed, the hot acid leach (HAL).

3.3.1 Leach Procedure

The conditions specified by RPC were for pH 0.2 for 90 minutes (see Table 5). The same reaction vessel as for the NAL was used.

3.3.2 Metal Distribution in Hot Acid Leach (HAL)

The metal distribution in the HAL together with that in NAL is shown in Table 14. Over 98% of the zinc and copper are recovered in the combination leaches.

In order to recover the zinc and copper in the hot acid leach filtrate (HALF) and to fix the iron, the HALF is returned to the roaster, where zinc and copper become sulphates, and the iron is oxidized to hematite.

Table 14. Metal Distribution in the Hot Acid Leach (HAL) Step

Product	Wt (%)	Distribution (%)				
		Cu	Zn	Pb	Fe	Ag
Calcine	100.0	100.0	100.0	100.0	100.0	100
NALF	61.7	82.5	85.3	0.1	0.7	-
HALF	13.0	15.5	13.6	0.2	34.5	-
HALR	25.3	2.0	1.1	99.7	64.8	100
	100.0	100.0	100.0	100.0	100.0	100

3.3.3 Size and Metal Distributions

The same procedure as for NALR was used in the sizing of HALR. Table 15 shows the size and metal distribution of HALR. Lead in HALR is mainly found in sizes finer than 15 μ m. HALR is about 55% hematite and 35% anglesite with the remainder being predominantly quartz. The zinc assay in HALR is

about 0.8%; copper is less than 0.03% and silver about 420 ppm. Notice that as the size becomes finer, the grade of zinc decreases, ranging from 3.5% Zn(+25 μ m) to 0.490 (-10 μ m). The reason is presumably that the finer ferrite particles are easier to leach.

Table 15. Size and Metal Distribution of HALR

Product	Wt (%)	* Assay (%)			Distribution (%)		
		Zn	Pb	Fe	Zn	Pb	Fe
+25	4.0	3.5	8.9	42.3	17.2	1.5	4.5
-25 + 15	9.7	1.9	13.1	47.0	23.1	5.4	12.1
-15 + 10	13.3	1.3	24.1	38.0	21.3	13.5	13.5
-10	73.0	0.4	25.8	36.0	38.4	79.6	69.9
	100.0				100.0	100.0	100.0
<u>Calculated Feed</u>		0.8	23.6	37.6			
<u>Assay Feed</u>		0.9	24.5	39.5			

*The Cu assay in HALR is - 0.03%

*The As assay in HALR is 420 ppm.

3.3.4 Mineralogical Examination of HALR

A similar mineralogical examination to that on NALR was conducted.

X-Ray Diffraction

Two main compounds (hematite and anglesite) were identified along with quartz (Appendix A, Table A-4).

Metallurgical Microscope with Reflected Light

Unmounted samples of +25 μ m, -25 + 15 μ m, and -15 + 10 μ m were observed under reflected light at 100 magnification. Hematite, anglesite, marmatite and quartz were identified. Some locked anglesite/hematite particles were also found.

Vickers Microscope with Reflected Light

Figs. 25 and 26 show microphotographs of mounted samples of HALR under polarized illumination at 440 and 620 magnification. Red particles are hematite, the white particles anglesite and the grey particle is marmatite.

Carl-Zeiss Microscope with Transmitted Light; Degree of Liberation

Fig. 27 shows a microphotograph of the HALR. The opaque grains are hematite, the crystalline white particles are anglesite and the crystalline colorless particles are quartz.

Table 16 presents the results of the measurement of the degree of liberation. As can be seen, at least in the coarser fractions, there is no further improvement in the liberation of the HALR in comparison with the NALR. Appendix B, Table B-3, shows the record sheet used in point counting for each sample.

Electron Microprobe

The same procedure as in the NALR was applied to the HALR, using the mounted samples in Figs. 25 and 26.

The results were as in the NALR with the only difference being that in the HALR ferrites were not detected and neither



Fig. 25 Microphotograph of $-37 + 25 \mu\text{m}$ particles of the HALR at 440 magnification with reflected light, under polarized conditions. Red particles are hematite, the white particles anglesite and the grey particle is marmatite.



Fig. 26 Microphotograph of $-25 + 15 \mu\text{m}$ particles of the HALR at 620 magnification with reflected light, under polarized conditions. Red particles are hematite, and the white particles, anglesite.

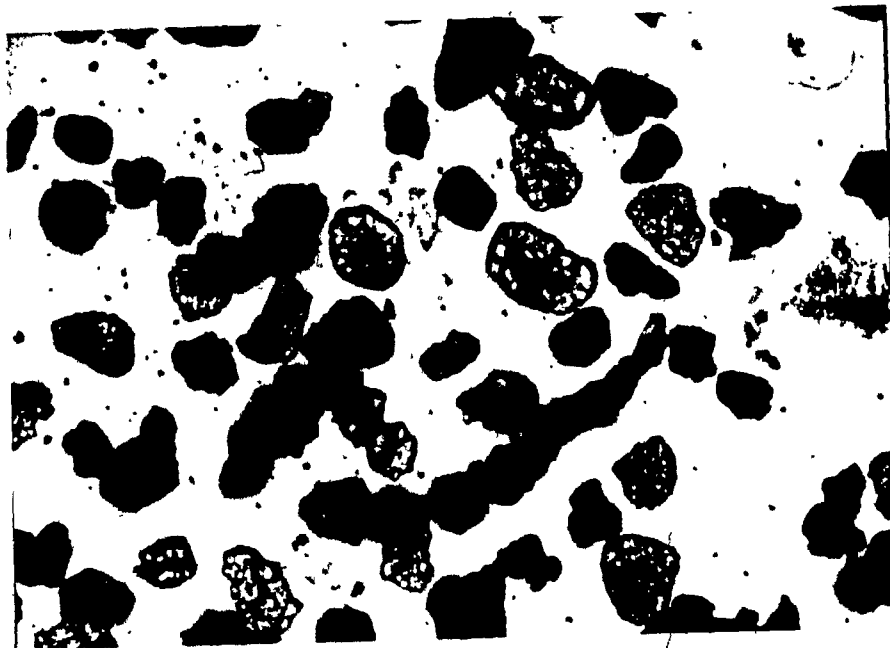


Fig. 27 Microphotograph of $-25 + 15 \mu\text{m}$ particles of the HALR with transmitted light. Crystalline white particles are anglesite, crystalline colorless ones are quartz and the opaque particles are hematite.

Table 16. Liberation Degree in Coarser HALR Sizes

Product (μm)	Degree of liberation (%)
+25	71 \pm 6*
-25 + 15	93 \pm 3
-15 + 10	94 \pm 1

* 95% confidence interval

was chalcopyrite; marmatite was detected only in two grains. This indicates that both ferrites and unroasted sulphides were effectively dissolved and the small amount of zinc remaining in the HALR (0.9%) is as marmatite.

Scanning Electron Microscopy (SEM)

The samples were analysed using a scanning transmission electron microscope (STEM) in the secondary electron mode. This system gives better resolution (30 Å) and increased peaks to background ratio than conventional scanning electron microscopes. This was important in the analysis of the samples under investigation due to the small size of many of the particles.

This microscope was equipped with an energy dispersive analyser which allowed for the analysis of individual particles and the formation of X-ray images for individual elements of interest.

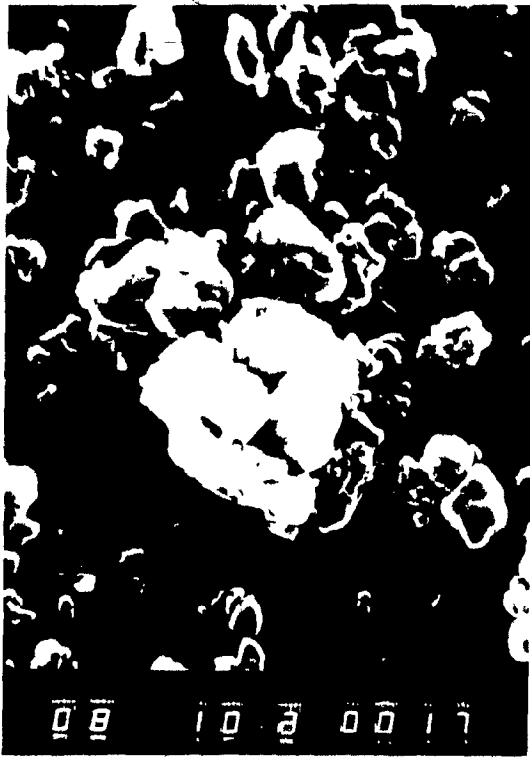
A sample of HALR was examined under the SEM. Sample preparation used the same dispersion conditions as in the HGMS tests (see Chap. 6).

Fig. 28a shows a general view of the sample at 10k magnification. Fig. 28b shows the same view but now with a lead X-ray map in order to identify lead particles. The particles showing the white dots contain lead. The other particles contain the iron. Notice that there are some dots in all parts of the picture including some parts where there are no particles. These are caused by secondary fluorescence due to X-ray scattering. The picture reveals that on average the lead-containing particles are larger than the others. The size of lead particles in this picture ranges from 1-2 μm ; iron particles are from 0.1-0.5 μm .

Fig. 28c shows another view of this sample but now at 20k magnification. Fig. 28d presents the same view but with the lead X-ray map superimposed. Again, the clustering of dots indicates lead. The size of the lead particles is about 2 μm and the iron particles are from 0.1-0.5 μm . Fig. 29a also shows a view of the HALR sample, at 20k magnification. A lead X-ray map of this is shown in Fig. 29b. The size of the two lead particles seen is about 1 and 0.5 μm . The iron particles again range from 0.1-0.5 μm .

From the above Figs., two general observations can be drawn:

a



b



4.2 μm

c



d

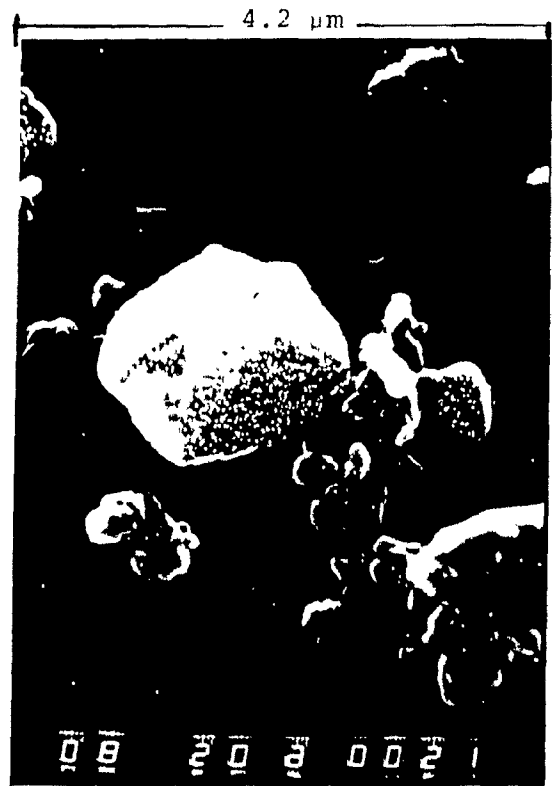


Fig. 28 SEM microphotographs of the HALR. Lead particles (anglesite) are differentiated from iron (hematite), with a lead X-ray map (particles showing the white dots.); right side pictures.

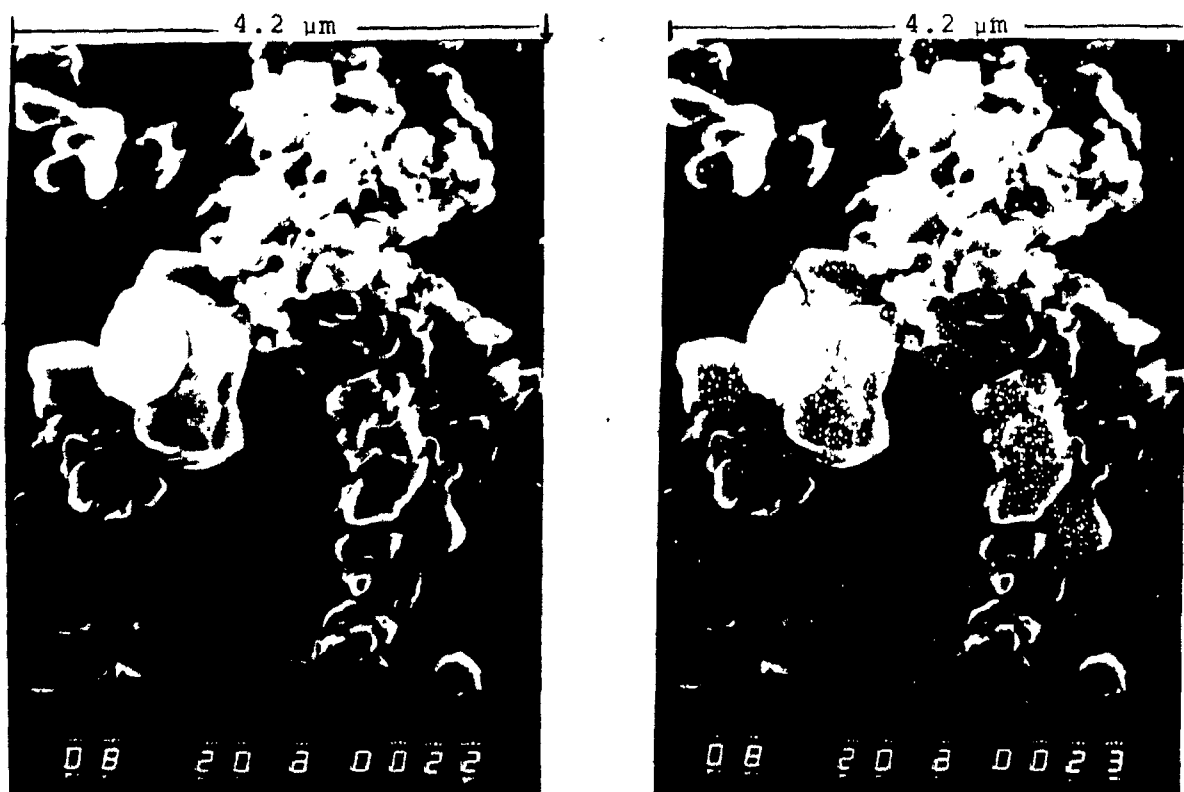


Fig. 29 SEM microphotographs of the HALR. Lead particles (anglesite) are differentiated from iron (hematite), with a lead X-ray map (particles showing the white dots), right side picture.

- a) lead particles are larger than iron.
 b) the lead particles appear to be free.

Resumé of Mineralogical Examination

Table 17 summarizes the minerals identified in the HALR. Again the minerals are listed in decreasing order of estimated concentration.

Table 17. Resumé of Mineralogical Examination of HALR

Name *	Formula
Hematite	Fe_2O_3
Anglesite	PbSO_4
Quartz	SiO_2
Marmatite	$(\text{Zn}, \text{Fe}) \text{S}$
Aluminum **	Al
Titanium **	Ti
Tin **	Sn
Silver **	Ag

* Names are listed in decreasing order of estimated content.

** Found by electron microprobe.

4. ESTIMATING POTENTIAL FOR MAGNETIC SEPARATION

4.1 Magnetic Profile Using a Frantz Isodynamic Magnetic Separator

In order to measure the particle (volume) susceptibility " κ " and also give some idea of the potential of magnetic concentration, a Frantz Isodynamic Magnetic Separator (Frantz) was used. (Fig. 30)

The Frantz, best known for its geological and mineralogical applications in achieving precise separation of minerals of different magnetic susceptibilities (51) - a use also employed here - has also been used to indicate the potential of a mineral mixture to processing by magnetic methods, (52,53).

4.1.1 Description of the Frantz

The Frantz consists of an inclined chute placed between two long pole pieces of a powerful electro-magnet. The dry sample to be separated is fed down the chute parallel to the length of the pole pieces. The electro-magnet and chute are also slightly tilted to one side, causing the particles to flow down one side of the chute when no magnetic field is applied. When current is passed through the electro-magnets a magnetic field is produced between the pole pieces. The diverging shape of the pole creates a field gradient and causes a magnetic force to act on a para magnetic particle in a direction opposite to the gravitational force.

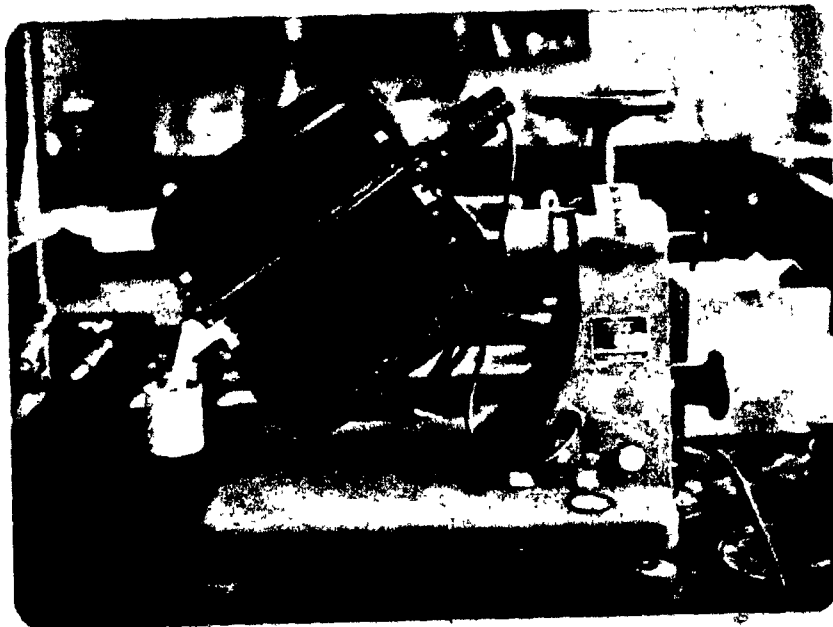


Fig. 30 Photograph of the Frantz Isodynamic Magnetic Separator.

This is illustrated in Fig. 31(54), which shows a cross-section of the chute and pole pieces. A field gradient is produced in the positive X direction, thus producing a magnetic force (F_m) in opposition to the gravity force (F_g).

The main feature of the pole shape, is that a constant product of field and field gradient (and thus a constant F_m) acts on a particle regardless of its position across the chute. Because of the long operating space parallel to the sample flow, the separator provides a long period of magnetic action on the particles rather than a short impulse. The direction of motion of the particles is consequently a resultant of the combined magnetic and gravitational forces.

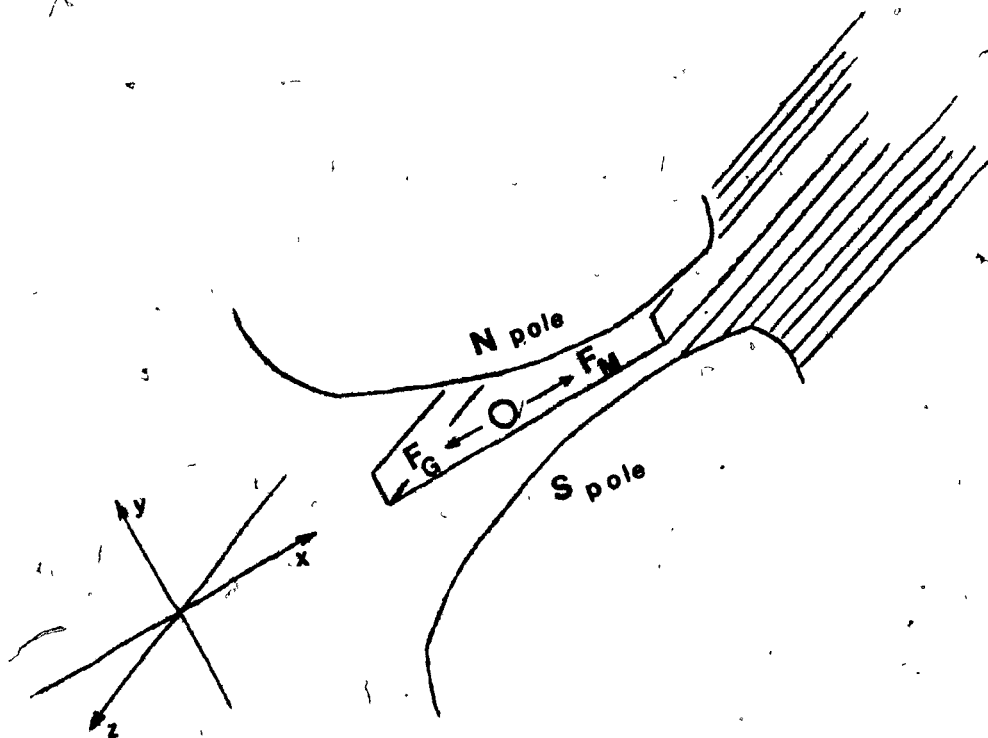
The separation is dependent on the relative F_m to F_g magnitude. Since F_m and F_g are both directly dependent on the cube of particle size, "b", the effect of particle size cancels and the Frantz produces a separation based solely on the mass susceptibility of the particles. The Frantz makes very precise separations between particles of close susceptibility. Half-way down the chute a splitter divides the separated particles into magnetic (mags) and non-magnetic (non-mags) fractions.

* The magnetic force is increased by increasing the current (I) through the electro-magnet, and gravitational force is increased by increasing the side tilt (θ).

4.1.2 Frantz Separator on Synthetic Mixtures

Synthetic hematite/galena mixtures were used to demonstrate

Fig. 31 A force balance of a paramagnetic particle between the pole pieces of the Frantz separator. (54)



the separation on the Frantz.

Galena particles were used instead of anglesite for two reasons:

- (i) Galena, as anglesite, is a dia-magnetic material
- (ii) Pure anglesite of the appropriate size was not available in the laboratory.

Both hematite and galena were natural minerals. The hematite/galena proportion was similar to the hematite/anglesite proportion in the NALR. The values are:

-37 + 25 μ m	85% Fe ₂ O ₃ - 15% PbS
-25 + 15 μ m	80% Fe ₂ O ₃ - 20% PbS
-15 + 10 μ m	72% Fe ₂ O ₃ - 28% PbS

Separation was carried out at 450 mA. Table 18 presents the results. This shows that even with these small particles the Frantz can perform very good separations.

Table 18. Frantz Separations upon Synthetic Mixtures (Fe₂O₃ - PbS). I = 450 mA

Size Range (μ m)	Product	Wt (%)	Assay (%)		Distrib. (%)	
			Pb	Fe	Pb	Fe
-37 + 25	Mag.	84.7	-	69.8	-	99.4
	Non-Mag	15.3	87.8	2.5	100.0	0.6
		100.0			100.0	100.0
-25 + 15	Mag	79.8	-	67.0	-	99.0
	Non-Mag	20.2	85.5	7.5	100.0	1.0
		100.0			100.0	100.0
-15 + 10	Mag	72.4	-	67.0	-	99.2
	Non-Mag	27.6	82.8	1.5	100.0	0.8
		100.0			100.0	100.0

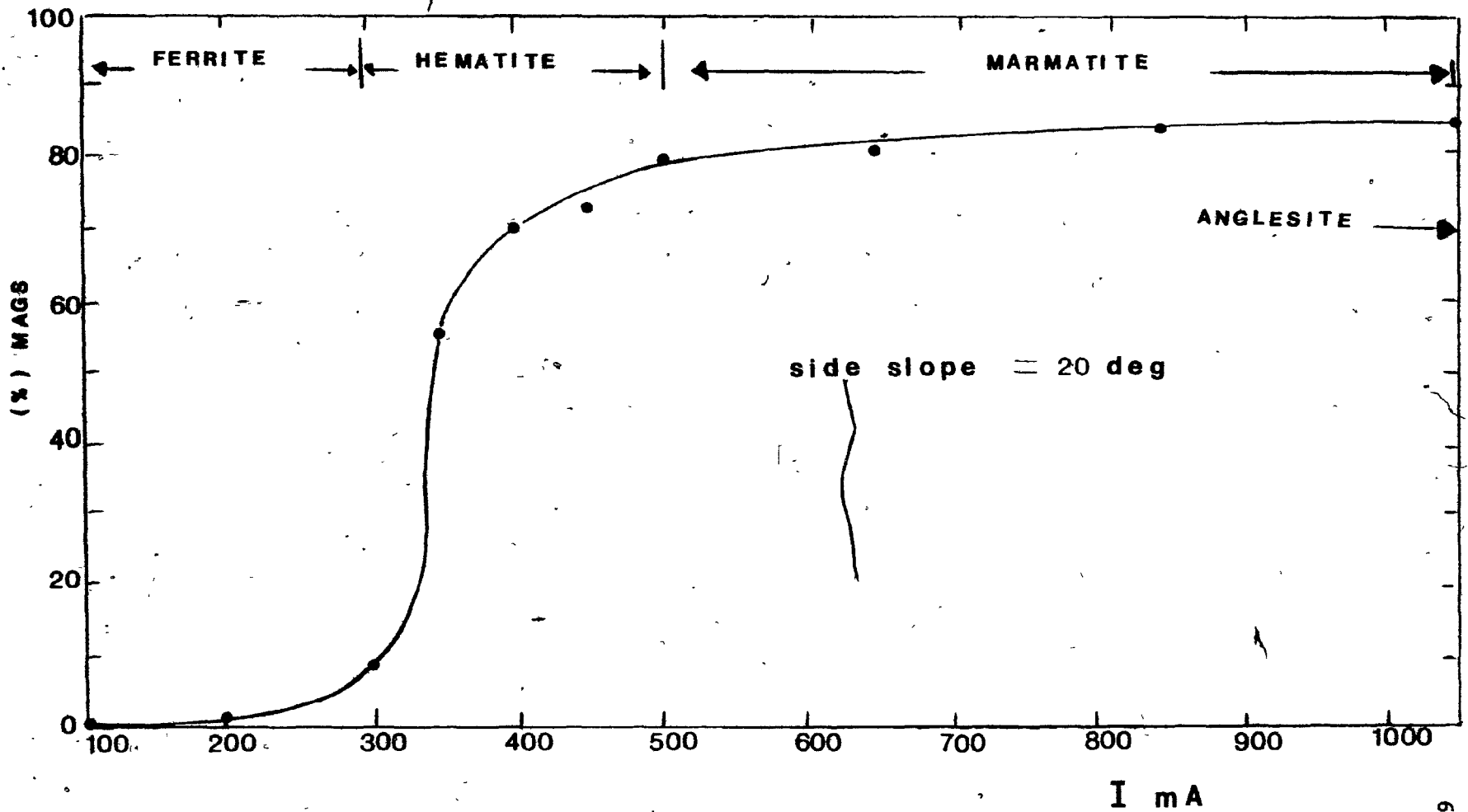
4.1.3 Separation of NALR on Frantz

A sample of $-25 + 15\mu\text{m}$ was passed through the Frantz separator with the non-mags reprocessed at progressively higher currents, to give the magnetic profile. An examination of each fraction with a metallurgical microscope under reflected light at 100 magnification was carried out.

Table 19 shows the results with the graphical presentation of the profile given in Figure 32. The results show how ferrite, hematite and marmatite are removed according with their magnetic susceptibilities to finally leave only anglesite and quartz in the non-mags fraction (at $I > 1050$ mA). From a microscope examination it was possible to observe how some small particles of hematite were encrusted in the rough anglesite surface causing some anglesite to be trapped in the mags fraction.

Figs. 33, 34, 35 and 36 show four different products at $-25 + 15\mu\text{m}$ obtained in the Frantz separation. Fig. 33 corresponds to the mags up to 200 mA. The red grains are hematite, red-dark grains are ferrite and the white-yellow particle which is in the middle is anglesite with two small particles of magnetic material encrusted on it. Fig. 34 corresponds to the magnetic material obtained at 300 to 350 mA. Notice that fewer ferrite particles are found at this current setting. Fig. 35 corresponds to the magnetic fraction obtained at 850 to 1050 mA. The black particles are marmatite. Notice

Fig. 32 Profile of magnetic separation of the NALR, by Frantz separator, -25 + 15 μ m.



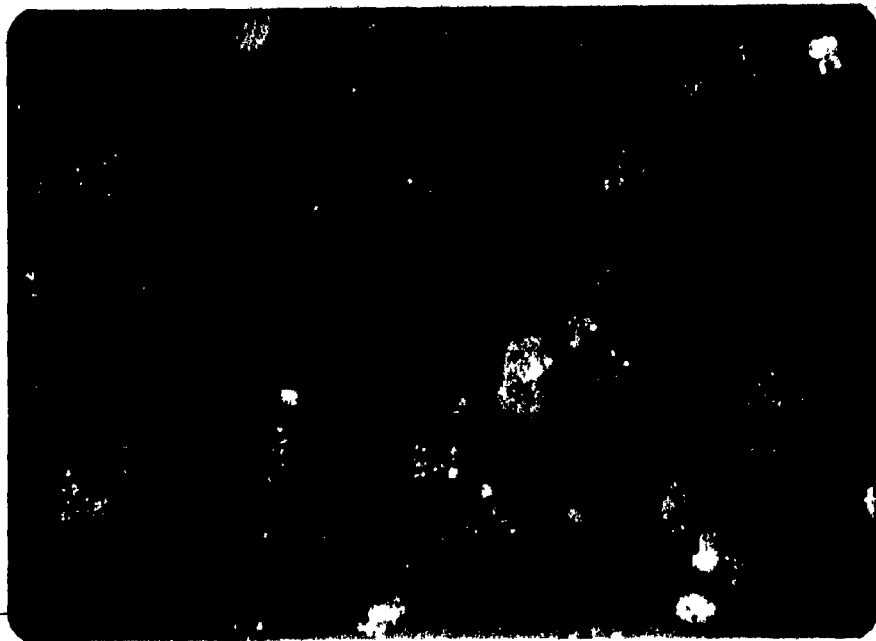


Fig. 33 Microphotograph of mags fraction up to 100 mA in Frantz, of the NALR. The red grains are hematite, dark-red grains are ferrite and the white-yellow particle in the middle is anglesite, with two small particles of magnetic material encrusted on it.

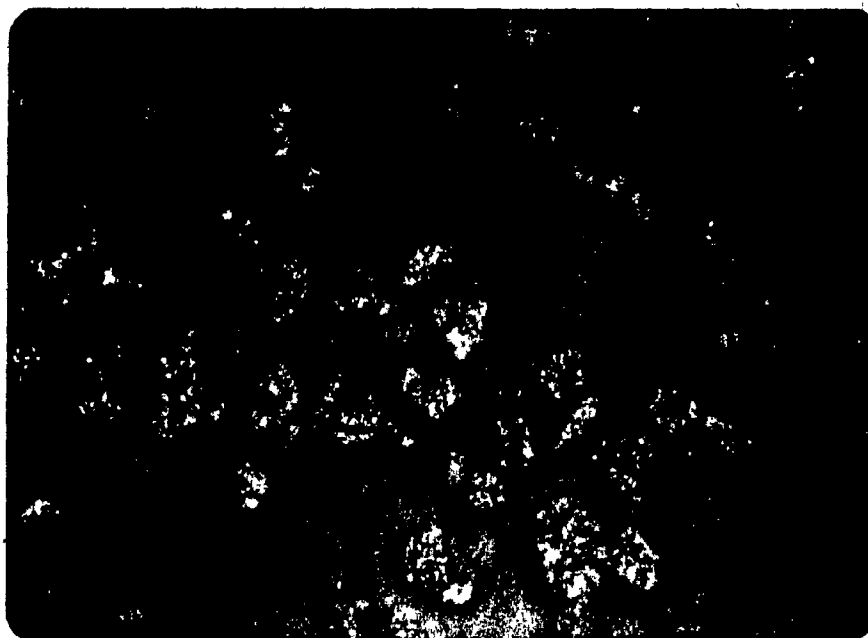


Fig. 34 Microphotograph of the mags fraction at 300 to 350 mA in Frantz, of the NALR. The red grains are hematite, dark-red grains are ferrite and the white yellow particles, anglesite.

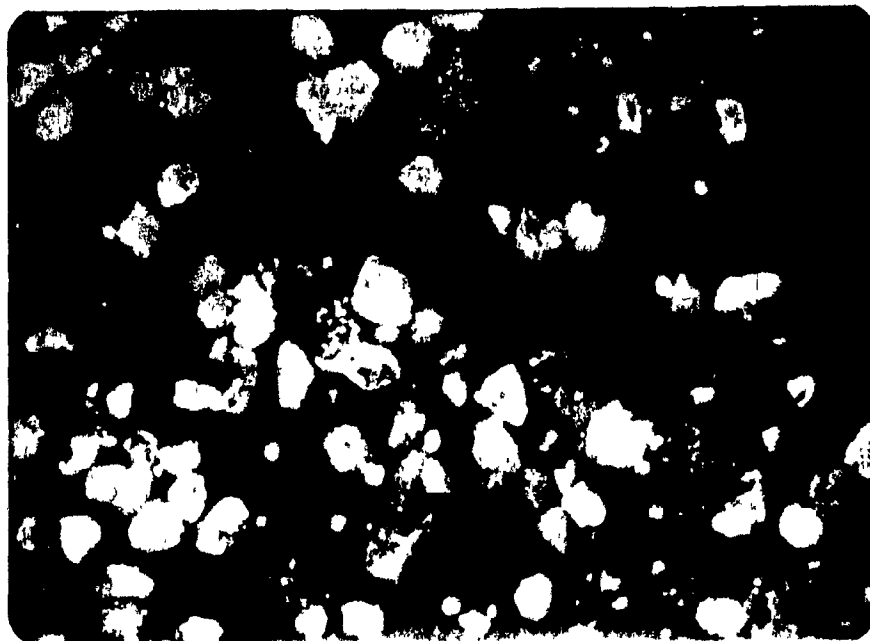


Fig. 35 Microphotograph of the mags fraction at 850 to 1050 mA in Frantz, of the NALR. The black particles are marmatite, white-yellow particles are anglesite and red particles, hematite.

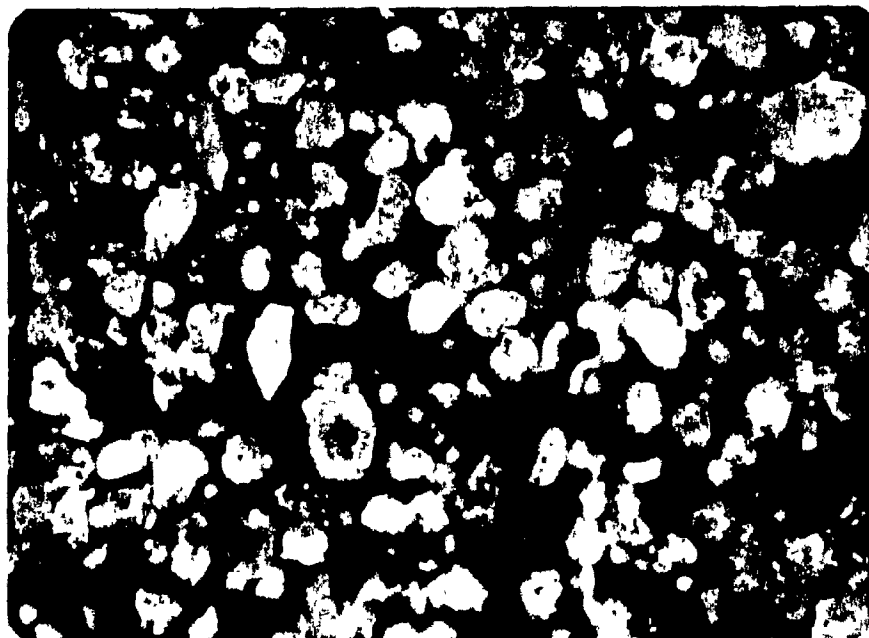


Fig. 36 Microphotograph of the non-mags fraction of the NALR 1050 mA on Frantz. The white-yellow particles are anglesite and black particles are marmatite.

the presence of some locked hematite-anglesite grains.
 Finally, Fig. 36 corresponds to the non-mags fraction (I > 1050 mA) which contains mainly anglesite.

Table 19. Frantz Separator upon NALR

Current (mA)	Wt (%)	Cumulative Mass (%)	Observations
100	0.8	0.8	Ferrite, Hematite (Some grains of locked Anglesite-Ferrite and some Quartz).
200	1.2	2.0	(Same as in 100 mA)
300	7.1	9.1	Ferrite, Hematite
350	55.2	64.3	Hematite, Ferrite (Some Anglesite, Marmatite and Quartz).
400	6.8	71.1	(Same as in 400 mA)
450	2.5	73.6	Hematite, (Hematite + Anglesite), Marmatite, Anglesite with small Hematite grains encrusted on the surface.
500	6.2	79.8	(Same as in 450 mA)
650	0.8	80.6	(Same as in 450 mA)
850	3.1	83.7	Anglesite with encrustation of small Hematite grains. Marmatite.
1050	2.2	85.9	(Same as in 850 mA)
Non-Mag	14.1		Anglesite and Quartz
	100.0		

Table 20 shows the separation achieved at 400 mA. Notice that the zinc splits 65:35 mags to non-mags which is a rough measure of the ferrite to marmatite ratio. About 35% of lead is recovered to mags, but this is believed to be due to the encrustation with hematite noted above.

Table 20. Separation of NALR on Frantz at 400 mA

Size (μm)	I (mA)	Product	Wt (%)	Assay (%)			Distrib. (%)				
				Cu	Zn	Pb	Fe	Cu	Zn	Pb	Fe
-25+15	400	Mag	71.1	0.23	4.4	8.0	57.7	83.0	65.3	37.3	89.2
		Non-Mag	28.9	0.12	5.8	41.0	17.3	17.0	34.7	67.7	10.8
			100.0					100.0	100.0	100.0	100.0

4.1.4 Separation of HALR on Frantz

A sample of -25 + 15 μm was passed through the Frantz separator.

Table 21 and Fig. 37 present the results.

From Table 21, anglesite is concentrated in the non-mags (I > 450 mA). As in the NALR, most of the lead recovered in the mags fraction is because of the rough texture of the anglesite trapping some hematite. By comparison with the profile of magnetic separation for the NALR (Fig. 32) and HALR Fig. 37 shows that ferrite and marmatite have been dissolved in the HAL step.

Fig. 37 Profile of magnetic separation of the HALR, by Frantz separator, -25 + 15 μm fraction.

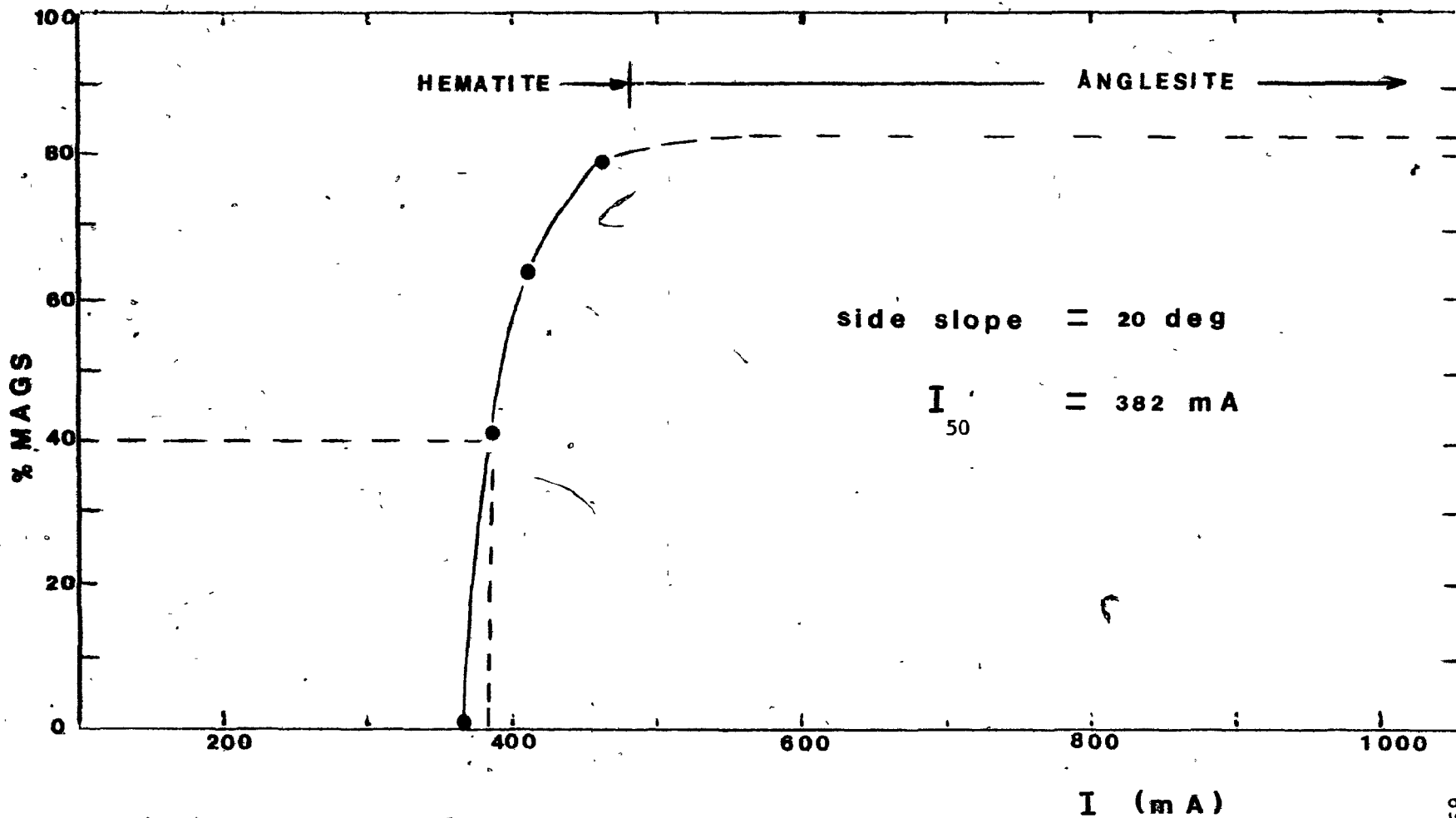


Table 21. Separation of HALR at 450 mA

Size (μm)	I (mA)	Product	Wt (%)	Assay (%)		Dist. (%)	
				Pb	Fe	Pb	Fe
-25+15	450	Mag	74.5	6.5	62.7	37.0	97.4
		Non-Mag	25.5	32.4	5.0	63.0	2.6
			100.0			100.0	100.0
Calculated Feed				13.08	47.0		
Assay Feed				13.11	48.0		

4.1.5 Evaluation of Frantz Results

The Frantz separator results have pointed out that there is potential for magnetic separation on either residue (NALR and HALR). However, the HALR is considered the better candidate for high gradient magnetic separation because:

- a) Separation of NALR will result in about 65% of Zn in the mags (as ferrite) and 35% in the non-mags (as marmatite), necessitating a hot acid leach of both products to maintain high overall zinc recovery. To a lesser extent this is a factor for Cu also, because about 83% is in the mags (as ferrite), and 17% is in the non-mags (as chalcopyrite).
- b) NALR represents 50% more mass than HALR.

5. DISPERSION

When physical separation is to be performed on ultra-fine material, one of the most important parameters is the dispersion. Special attention should be given when ions are present (55). The NALR and HALR will have some residual ions (Zn^{++} , Cu^{++} , Pb^{++} , Fe^{++} , Fe^{+++}) after the solid-liquid separation.

In order to disperse the HALR, the following steps were carried out:

- 1) After leaching, the residue was washed about six times (this number being determined by the pH of the filtration solution) through the filter paper with fresh water, with the purpose of: a) eliminating all the zinc, copper, lead and iron ions present in the residue liquor and, b) increasing the pH to about 6.7-7.0.

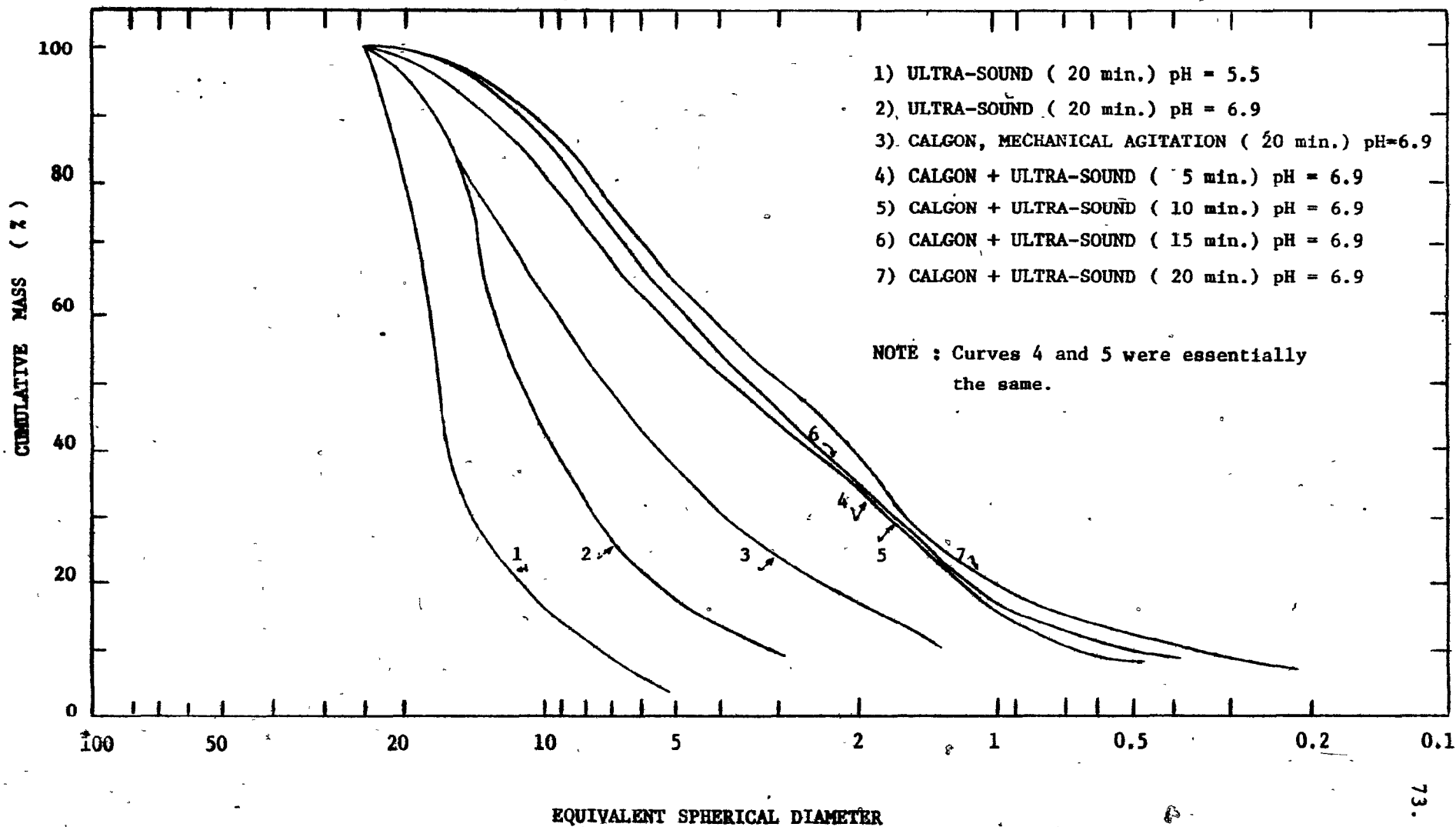
If even after washing, the pH was lower than 6.7, the sample was put in a beaker and agitated with water, then filtered. This gave the desired pH (~ 6.8).

- 2) Dispersion of the sample was achieved using a strong inorganic dispersant, "calgon" (sodium silicate, trisodium phosphate). The dispersion provided by a 0.1% calgon solution was further improved by 20 minutes agitation in an ultrasound bath.

Dispersion was measured on a X-ray sedimentometer, the SediGraph 5000D. This device employs a finely collimated X-ray beam to measure the change with time of particle concentration during settling in a sample cell. The cell also descends relative to the beam consequently reducing the time required for analysis.

Fig. 38 shows the progressive dispersion achieved by various techniques, from untreated residue (curve 1), to treated residue (curves 2 to 7). Using the same ultra-sound dispersion curve 2 shows the benefits of raising the pH to near neutral (pH 6.9); per cent passing 10 μm increased from 18% to 50%. By comparing curve 3 (sample with only calgon) and 7 (sample with calgon and 20 min. of agitation in ultra-sound bath), the amount of material passing 2 μm increased from 20% to 38%. This observation means that dispersion of the sample is being attained. As well it can be observed from Fig. 38 that the ultra-sound on its own cannot supply good dispersion (curve 2). Curve 7 represents the finest dispersion which was achieved. Once the material was dispersed it took at least one day to settle the coarser particles, the remainder took several days. This could pose a problem in subsequent solid/liquid separation. After many trials it was found that Ca^{++} ions, as lime, gave adequate coagulation and settling characteristics.

Fig. 38 Degree of dispersion. Size distribution of the HALR using different dispersion procedures.



6. HIGH GRADIENT MAGNETIC SEPARATION (HGMS)

6.1 Background

Magnetic separation has been used in mineral processing for many years. Until recently, it was primarily used in the concentration of strongly magnetic materials with sizes above 50 micrometres. Since the advent of HGMS, applications have been extended to more weakly magnetic and finer particles. For example, in kaolin processing it is possible to remove weakly magnetic impurities at sizes less than $2\mu\text{m}$ (56) and in steel rolling mills HGMS is used to remove iron oxides ($\sim 20\mu\text{m}$) suspended in water (57). HGMS has potential application in the treatment of taconitic iron ores (58), pyrite removal from coal (59), uranium upgrading, and pyrite and chalcopyrite recovery as impurities from molybdenite concentrates (58).

In HGMS the magnetic trapping force is much greater than in any other magnetic device. These strong trapping forces are created by fine filamentary ferromagnetic matrices perturbing a strong background field and creating high field gradients. Because the force is large, fine and weakly magnetic particles can be trapped on the matrix.

6.2 A Recovery Model for HGMS

Since HGMS is based on reasonably well defined forces (i.e. magnetic, and fluid drag (60)) it has been possible to

predict the performance by mathematical modelling. Nesset and Finch (61) related recovery to a dimensionless group, the loading number N_L . This group represents the ratio of magnetic to fluid shear forces at full load on the upstream side of the wire, where full load means the maximum amount of material that the matrix can hold for a particular set of conditions. The loading number N_L (62), is given in cgs units by:

$$N_L = \frac{2bH_a^2 \kappa A}{\rho_f U_\infty^2 \nu a} \quad \text{dimensionless (1)}$$

where:

b is the particle radius, cm

H_a applied or background field strength, Oe

κ particle (volume) susceptibility, emu/cm^3 - Oe

A perturbation term in magnetic field expression

$$= \frac{2\pi M_w}{H_a}$$

M_w wire (volume) magnetization, emu/cm^3

ρ_f fluid density, g/cm^3

U_∞ fluid velocity, cm/s

ν dynamic viscosity, cm^2/s

a wire radius, cm

*See Appendix D, Table D-2 for S.I. units.

Assuming build up is over the front 90° of the matrix wire, the mass loading γ_m (mass of mags per unit mass of matrix) can be predicted (47), and is represented by eq. (2):

$$Y_m = \frac{\epsilon}{4} \left[\left(\frac{N_L}{2.5} \right)^{4/5} - 1 \right] \frac{\rho_p}{\rho_w} \frac{\text{g particles}}{\text{g wire}} \quad (2)$$

where:

ϵ is packing density (- 0.7)

ρ_p is particle density, g/cm³

ρ_w is wire density, g/cm³

Finally, recovery can be estimated by assuming the matrix loads to 75% of full capacity (63).

$$R(\%) = (0.75 \frac{Y_m}{L}) \times 100 \quad (3)$$

where:

R(%) is recovery in per cent

L is the mass of magnetics in the feed per unit of matrix mass.

Particle Parameters

In order to predict the recovery using the above model, the particle parameters κ and b must be known.

The particle volume susceptibility, " κ ", can be measured from the magnetic profile developed on the Frantz separator, Fig. 32. In the cgs system the appropriate calculation is (64):

$$\kappa = \frac{20 \times 10^{-6} \sin \theta \rho_p}{I_{50}^2}$$

A profile for HALR is shown in Fig. 37. The current I is taken as the current at which 50% reports to magnetics. From Figure 37 for hematite, $I = 0.3825A$ and since $\theta = 20^\circ$ and $\rho_p = 5.25 \text{ g/cm}^3$, $\kappa = 245.44 \times 10^{-6} \text{ emu/cm}^3 - \text{Oe}$

The particle radius, b , was determined from Fig. 38.

The size range can be approximated by selecting the 50% passing size (i.e. ~ 1.45 μ m, in Fig. 38, curve 7) or better, by considering the full size distribution, divided into increments and summing the increment recoveries (53).

Operating Parameters

The fine size implies the need for a steel wool matrix. A medium fine steel wool, as used in kaolin processing with a = 0.0030 cm (2a = 60 μ m), was selected.

Two matrices were made. Matrix A was 30g of steel wool and matrix B was 24g. These masses were packed into a 3.8 x 8 cm section of a 3.8 x 12.5 cm canister. Packing densities were consequently 4.3% and 3.4% v/v respectively. For matrix A 30g of sample was used, and for matrix B, 21g. The objective in working with two matrices was to investigate the possible role of packing density in the efficiency of separation and in physical trapping.

The mass of magnetics in the feed per unit of matrix mass, L, in both cases was the same, it was $L = 30 (0.53/30) = 0.53$ and $L = 21 (0.53/24) = 0.53$, where 0.53 in brackets represents the 53% hematite content in HALR, (Table 22). The magnetic fields considered were high, since the particles were fine and only weakly magnetic. Two magnetic fields were selected: 13,800 Oe and 21,400 Oe. Once the above operating parameters had been selected it was only necessary to set the recovery and back calculate the required flow velocity.

Table 22 summarizes the calculations for two of the runs in which recovery was set at ~ 90% hematite, with fields of 13,800 Oe and 21,400 Oe. Notice that higher flow velocities can be used with the higher magnetic fields, as expected. Experiments were then designed around these flow velocities.

Table 22. Summary of the Calculations to Estimate the Required Flow Velocity.

$$\begin{aligned}
 L &= 0.53 \\
 \rho_p &= 5.25 \text{ g/cm}^3 \\
 \rho_w &= 7.75 \text{ g/cm}^3 \\
 \epsilon &= 0.7 \\
 R(\%) &= 16.8 \left[\frac{N_L}{2.5}^{0.8} - 1 \right] \\
 b &= 0.0001455 \text{ cm} \\
 \kappa &= 245.44 \times 10^{-6} \text{ emu/cm}^3 \text{ - Oe} \\
 a &= 0.0030 \text{ cm} \\
 \rho_f &= 1.0 \text{ g/cm}^3 \\
 v &= 0.01 \text{ cm}^2/\text{S} \\
 N_L &= \frac{8.963 \times 10^{-2} b A Ha^2}{U_\infty^{3/2}} \\
 \text{if } Ha &= 13,800 \text{ Oe} & A &= 0.625 \\
 &Ha = 21,400 \text{ Oe} & A &= 0.420
 \end{aligned}$$

If hematite recovery is set to ~90%, then estimated flow velocities are*

Ha (Oe)	U_∞ (cm/s)
13,800	8.45
21,400	11.40

* using full size distribution.

6.3 Equipment

The equipment used in the investigation was a SALA-HGMS model 10-15-20, installed at the ore processing laboratories CANMET, Ottawa. A schematic diagram of the HGMS and feed system is presented in Fig. 39.

The separator is basically made up of:

- a) A magnet and power supply which provides 8 fields ranging from 980 to 21,400 Oe.
- b) A feed unit which keeps the solids in suspension while they are fed into the system. Also, some inlets are provided in order to flush out all the magnets trapped during the tests.
- c) A canister of 3.8 cm in diameter and 12.5 cm long to hold the matrix.

6.4 Conditions of the Tests

Having calculated the fluid velocity, U_{∞} , for a given field, tests were organized around these flow rates. The test conditions are summarized in Table 23.

6.5 Results

6.5.1 Results of Test Series 1 13,800 Oe - Matrix A

Runs of test series 1 were carried out with an applied field of 13,800 oersted.

Figs. 40 and 41 show the flowsheet followed in run 1,

Fig. 39 Schematic Diagram of HGMS.

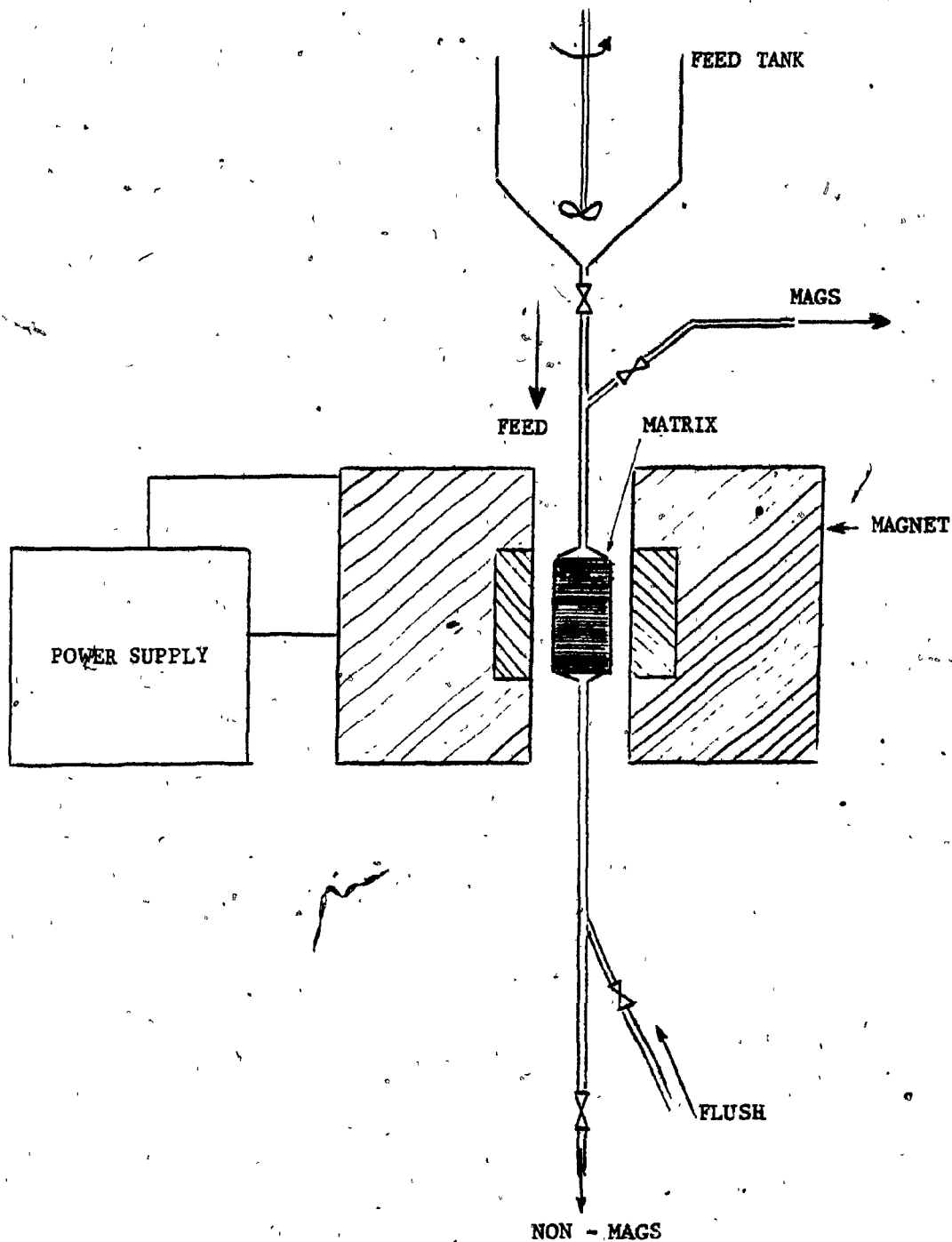


Table 23. Conditions of the HGMS Tests

Series #	Run (Num.)	Sample (g)	† Matrix	Velocity (cm/s)	Field (Oe)
1	1	30	* A	6.51	13,800
	2	30	A	8.45	13,800
	3	30	A	10.29	13,800
2	4	30	A	9.35	21,400
	5	30	A	11.40	21,400
	6	30	A	13.91	21,400
3	7	21	** B	6.51	13,800
	8	21	B	8.45	13,800
	9	21	B	10.29	13,800

† Matrix: Stainless steel wool (wire radius, 30µm)

* A : 30g matrix packed into a canister 3.8 cm in diameter and 8.0 cm long. Packing density = 4.3% v/v basis.

** B : 21g matrix packed into a canister 3.8 cm in diameter and 8.0 cm long. Packing density = 3.4% v/v basis.

and runs 2 and 3 respectively. As can be seen, the settling conditions of the non-mags* for run 1 and for runs 2 and 3 were different. In run 1, the non-mags were allowed to settle for a day and then decanted to obtain two products, one which is the coarser settled material, the Non-Mags** and a slime which is the ultrafine material.

* non-mags, refers to the non-mags product plus slime in run 1.

** Non-Mags refers to the final non-mag product in run 1.

Fig. 40 A schematic representation of the HGMS flowsheet in run #1.

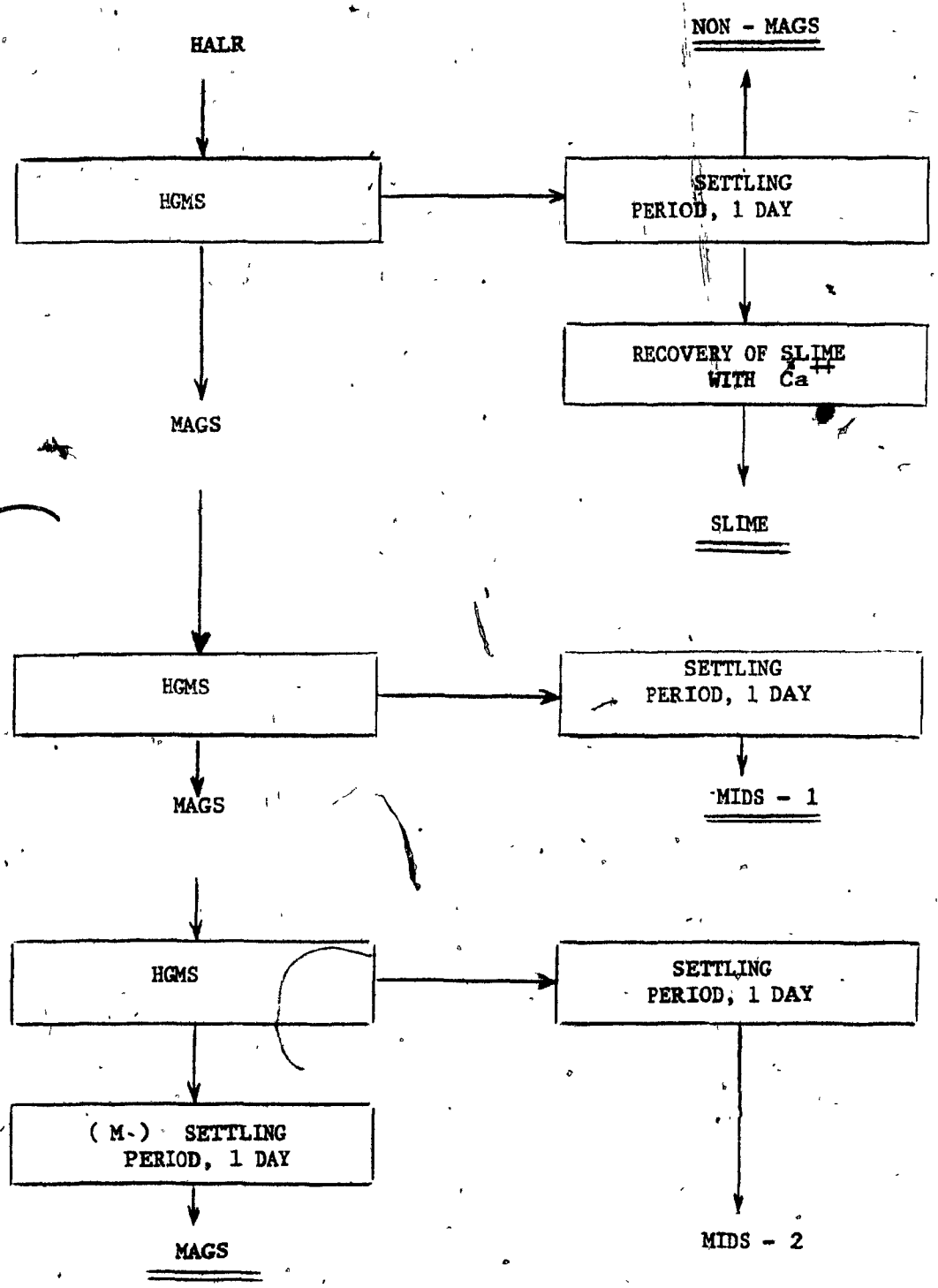
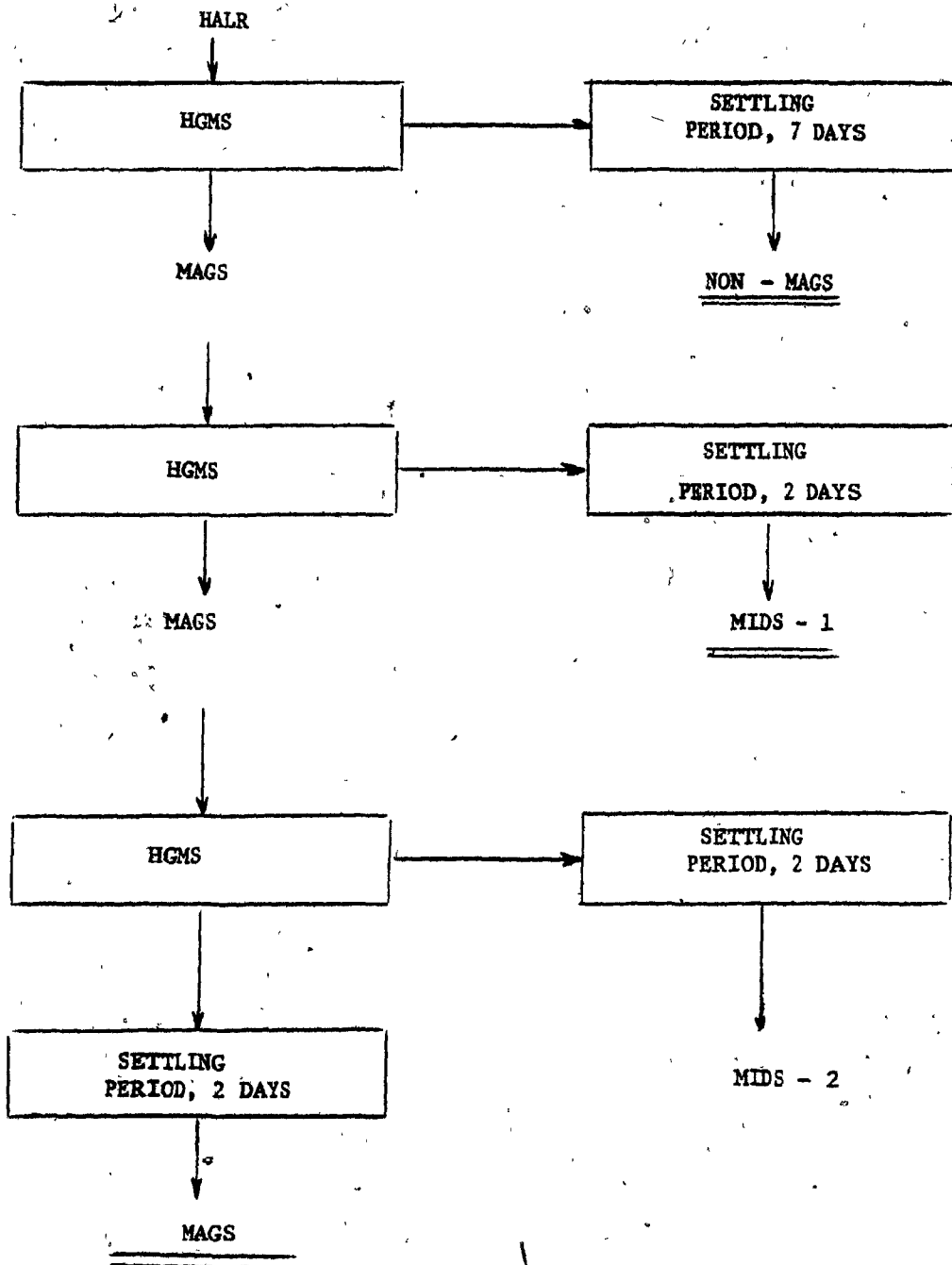


Fig. 41 A schematic representation of the HGMS flowsheet, followed in runs 2 and 3.



The slimes were subsequently settled by adding Ca^{++} (as a solution of lime). In contrast, for runs 2 and 3, the non-mags were allowed to settle for a week. Losses in the first procedure were practically zero and in the latter were less than 5%.

Table 24 shows the fluid velocities in the rougher and two scavenging steps.

Table 25 summarizes the results of runs 1, 2 and 3. Notice that the non-mags of run 1 and non-mags of runs 2 and 3 assay over 40% Pb, with recoveries of more than 70%. The mag products have over 60% Fe with low lead contents. The product mid-2 of runs 2 and 3 has a lead content below the feed value which suggests this second scavenging step is not beneficial. Finally when mid-1, mid-2 and non-mags are combined, a material referred to as lead concentrate is obtained which represents the maximum lead recovery attained. For runs 1, 2 and 3 the lead concentrates range from 38.2% Pb with 87.2% lead recovery to 34.5% Pb with 94.7% lead recovery. Silver recoveries were from about 65% in the non-mags, to 85% in the lead concentrate. Notice from run 2 that silver is mainly found in the non-mags products (mid-1, mid-2, non-mags).

Table 24. Series 1. Fluid Velocities in Rougher and Scavengers

Run #	Fluid Velocities (cm/s)		
	Rougher	Scavenger - 1	Scavenger -2
1	6.51	6.51	7.35
2	8.45	8.45	10.29
3	10.29	10.29	11.83

6.5.2 Results of Test Series 2-21,400 Oe - Matrix A

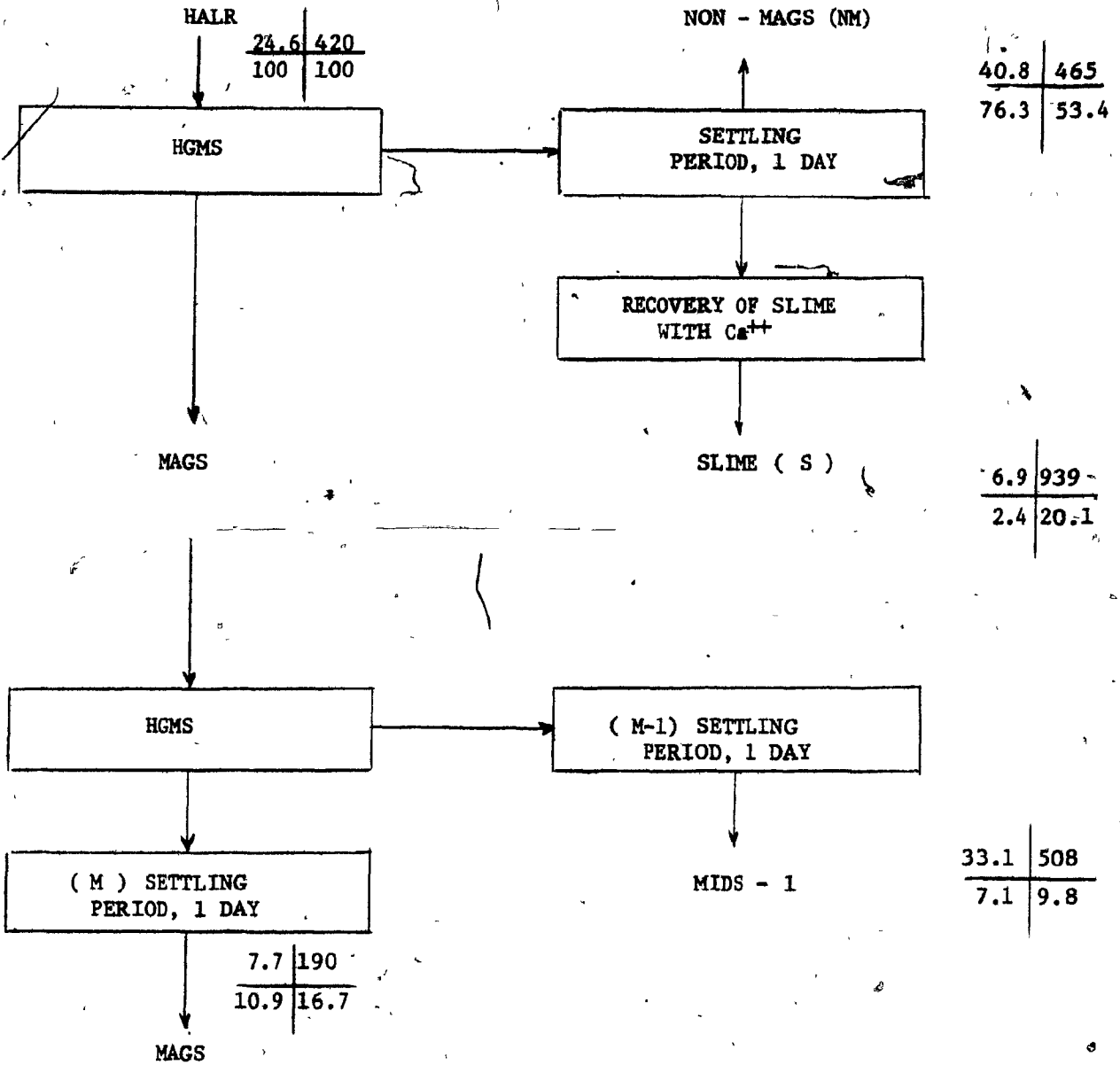
Series 2 was performed with a higher field intensity than series 1. The applied field was 21,400 Oe.

Fig. 42, shows the flowsheet followed in these runs. It is similar to series 1, with one exception, only one scavenging step was used. Fig. 42 also shows the lead and silver distribution in the lead, mags, non-mags, slimes and mid-1, from run #5. Notice that lead is principally recovered in the non-mags; silver also reports to the non-mags but a significant fraction was found in the slimes.

Table 26 shows the fluid velocities used in the roughing and scavenging steps.

Table 27 summarizes the results of runs 4,5, and 6. Notice that overall lead recoveries of series 2 tend to be about 5% less than in series 1, ranging from about 83% to 90%. Silver recoveries were about 83%, 2% less than in series 1. Silver is reported in the non-mags products (mid-1, non-mags and slimes).

Fig. 42 A schematic representation of the HGMS flowsheet followed in series 2 and 3.



% Pb	Ag, ppm
% Pb distrn.	% Ag distrn.

Table 25. HGMS Results of Series 1. - 13,800 Oe Matrix A

Run	Product	Wt (%)	*Assay (%)			Distrib. (%)		
			Pb	Fe	Ag	Pb	Fe	Ag
	MAG	41.4	7.9	61.5		12.8	65.1	
	MID-1	8.0	36.5	25.5		11.4	5.2	
	MID-2	4.3	28.5	34.3		4.8	3.8	
	NON-MAG	36.7	47.0	17.4		67.3	16.3	
	SLIME	9.6	10.1	39.0		3.7	9.6	
		100.0				100.0	100.0	
1	Calculate feed		25.6	39.1				
	Assay feed		24.6	40.2				
	Pb Conc.	58.6	38.2	23.3		87.2	34.9	
	MAG	34.5	5.8	60.5	164	7.9	51.7	15.0
	MID-1	11.5	27.1	33.3	462	12.2	9.5	14.1
	MID-2	6.7	16.3	51.9	350	4.3	8.6	6.2
	NON-MAG	47.3	40.8	25.8	515	75.6	30.2	64.7
		100.0				100.0	100.0	100.0
2	Calculate feed		25.5	40.4	377			
	Assay feed		24.6	38.4	420			
	Pb Conc.	65.5	35.9	30.0	489	92.1	48.5	85.0
	MAG	28.4	4.8	61.6		5.3	45.3	
	MID-1	11.0	22.5	40.6		9.5	11.6	
	MID-2	6.1	13.7	49.3		3.2	7.8	
	NON-MAGS	54.5	39.3	25.0		82.0	35.3	
		100.0				100.0	100.0	
3	Calculate feed		26.1	38.6				
	Assay feed		24.3	38.4				
	Pb Conc.	71.6	34.5	29.5		94.7	54.7	

* Ag is reported in ppm.

Since silver is concentrated in the ultrafine material (slime) we can assume that the silver is not only associated with the lead (see microprobe examination, secs. 3.1.3 and 3.3.4) but is present as free silver of very small size, at least less than 1 micron, (Fig. 47, curve 3).

Table 26. Series 2. Fluid Velocity in Rougher and Scavenger

Run #	Fluid Velocities (cm/s)	
	Rougher	Scavenger
4	9.35	10.29
5	11.40	11.83
6	13.91	13.91

6.5.3 Results of Test Series 3. 13,800 Oe - Matrix B

Series 3 were performed with matrix B. The same magnetic field and flow velocities applied in series 1 were used.

The flow sheet followed in series 3, is the same as that of series 2.

Table 28 gives the flow velocities used in the roughing and scavenging steps.

Table 29 summarizes the results. By comparison with those of series 1, matrix A, tended to give slightly better lead grades (- 2% more) than those of matrix B. Silver recoveries were about the same.

Table 27. HGMS Results of Series 2, 21,400 Oe- Matrix A

Run	Product	Wt. (%)	Assay (%) [*]			Distrib. (%)		
			Pb	Fe	Ag	Pb	Fe	Ag
	MAG	46.5	9.3	59.0		17.1	67.8	
	MID-1	13.5	34.8	29.0		18.9	9.7	
	NON-MAG	31.3	47.8	17.0		60.3	13.2	
	SLIMES	8.7	10.7	43.1		3.7	9.3	
		100.0				100.0	100.0	
4	Calculated feed		24.8	40.4				
	Assay feed		24.6	40.2				
	Pb Conc.	53.5	38.5	24.2		82.9	32.2	
	MAG	36.1	7.7	60.5	190	10.9	55.0	16.7
	MID-1	7.9	33.1	35.8	508	10.4	7.1	9.8
	NON-MAG	47.2	40.8	23.8	465	76.3	28.0	53.4
	SLIMES	8.8	6.9	45.0	939	2.4	9.9	20.1
		100.0				100.0	100.0	100.0
5	Calculated feed		25.2	40.0	411			
	Assay feed		24.6	40.2	420			
	Pb Conc.	63.9	35.2	28.5	536	89.1	45.4	83.3
	MAG	36.4	7.5	61.0		10.4	57.4	
	MID-1	10.4	30.6	30.0		12.1	8.1	
	NON-MAG	49.0	41.0	22.8		76.2	28.9	
	SLIMES	4.9	8.2	44.0		1.3	5.6	
		100.0				100.0	100.0	
6	Calculated feed		24.6	38.6				
	Assay feed		24.6	40.2				
	Pb Conc.	63.6	37.1	25.4		89.6	41.3	

* Ag is reported in ppm.

Table 28. Series 3. Fluid Velocity in Rougher and Scavenger

Run #	Fluid Velocities (cm/s)	
	Rougher	Scavengers
7	6.51	7.35
8	8.45	9.34
9	10.29	11.40

Table 29. HGMS Results of Series 3. 13,800 Oe - Matrix B

Run	Product	Wt (%)	* Assay (%)			Distrib. (%)		
			Pb	Fe	Ag	Pb	Fe	Ag
	MAG	41.4	8.5	60.8		13.7	63.8	
	MID-1	8.1	31.3	30.5		9.9	6.3	
	NON-MAG	38.5	47.8	16.3		71.8	15.9	
	SLIMES	12.0	9.8	46.1		4.6	14.0	
		100.0				100.0	100.0	
7	Calculate feed		25.6	39.5				
	Assay feed		24.6	40.2				
	Pb Conc.	58.6	37.7	24.4		86.3	36.2	
	MAG	35.2	7.7	61.5	220	11.0	55.6	17.2
	MID-1	9.2	28.8	37.1	489	10.7	8.8	10.0
	NON-MAG	41.1	44.2	18.6	515	73.6	19.6	47.1
	SLIMES	14.4	8.0	43.3	810	4.7	16.0	25.7
		100.0				100.0	100.0	100.0
8	Calculated feed		24.7	38.9	449			
	Assay feed		24.6	40.2	420			
	Pb Conc.	64.8	33.90	26.7	574	89.0	43.2	82.8
	MAG	28.6	6.2	64.0		7.2	46.6	
	MID-1	7.8	23.4	40.5		7.4	8.1	
	NON-MAG	54.0	37.2	25.1		81.7	34.5	
	SLIMES	9.6	9.4	44.0		3.7	10.8	
		100.0				100.0	100.0	
9	Calculated feed		24.6	39.3				
	Assay feed		24.6	40.2				
	Pb Conc.	71.4	32.00	29.3		92.8	53.4	

6.5.4 Graphical Summary of Results

Figs. 43, 44 and 45 present graphically the results of the 3 series of magnetic separations.

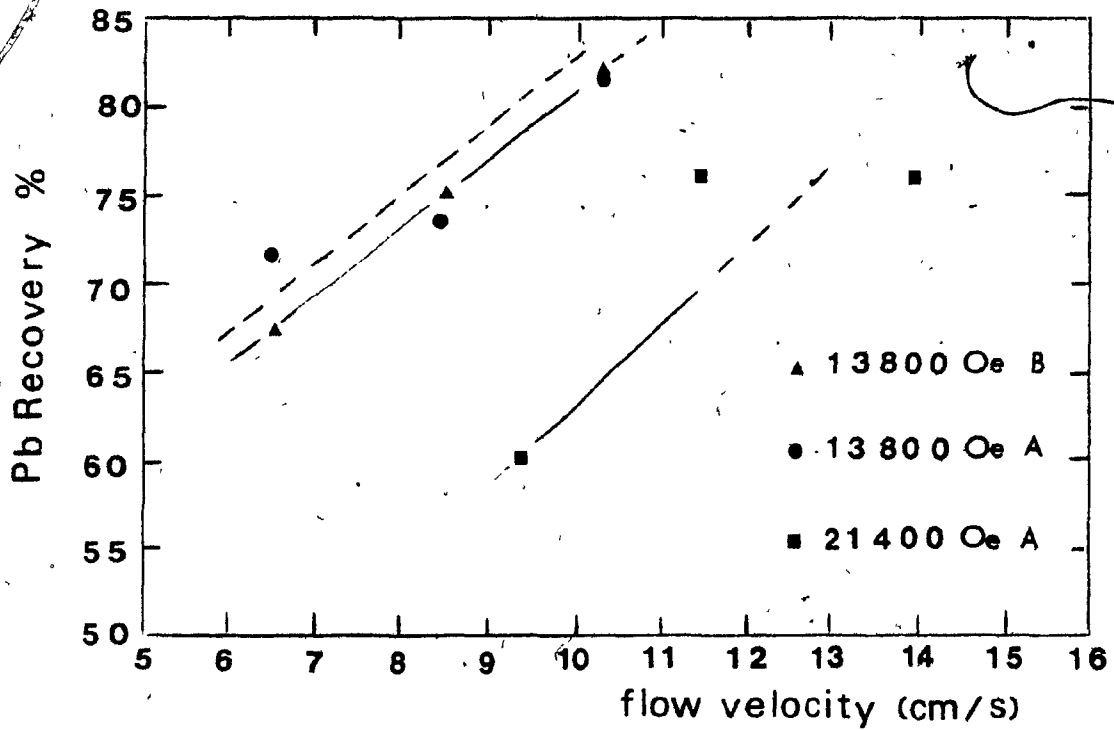
Fig. 43 shows the lead recovery—flow velocity and lead grade—flow velocity relationships, when lead is considered only in the non-mag product, and Fig. 44, when the lead concentrate is considered.

Notice in curves 1 and 2 of both figures that as the flow velocity is increased, lead recovery tends to increase (from about 73% to 84% in Fig. 43 and from about 86% to 95% in Fig. 44), while lead grade decreases (from about 48% to 37% in Fig. 43, and from about 38% to 34% in Fig. 44). When the velocity is increased, the fluid drag force becomes higher and more material reports to the non-mags, especially any anglesite which is physically trapped and the finer hematite grains, for which the trapping force is low. It is possible curve 3 is showing a saturation effect, i.e., maximum recovery, and minimum grade at $U_{\infty} > 14$ cm/s. There is not sufficient data to adequately comment on this.

Fig. 45 shows the cumulative grade-recovery curve obtained from all the test data. Three values were taken from each run. The first value with the highest lead grade is the non-mags, the second one is the non-mags + mid 1 and the third value is the lead concentrate (non-mags + mid 1 + mid 2 in runs 2 and 3, and non-mags + mid-1 + slime in the other

Fig. 43 Lead recovery and grade in the non-mags as a function of the flow velocity. 93.

a) Lead Recovery vs Velocity



b) Lead Grade vs Velocity

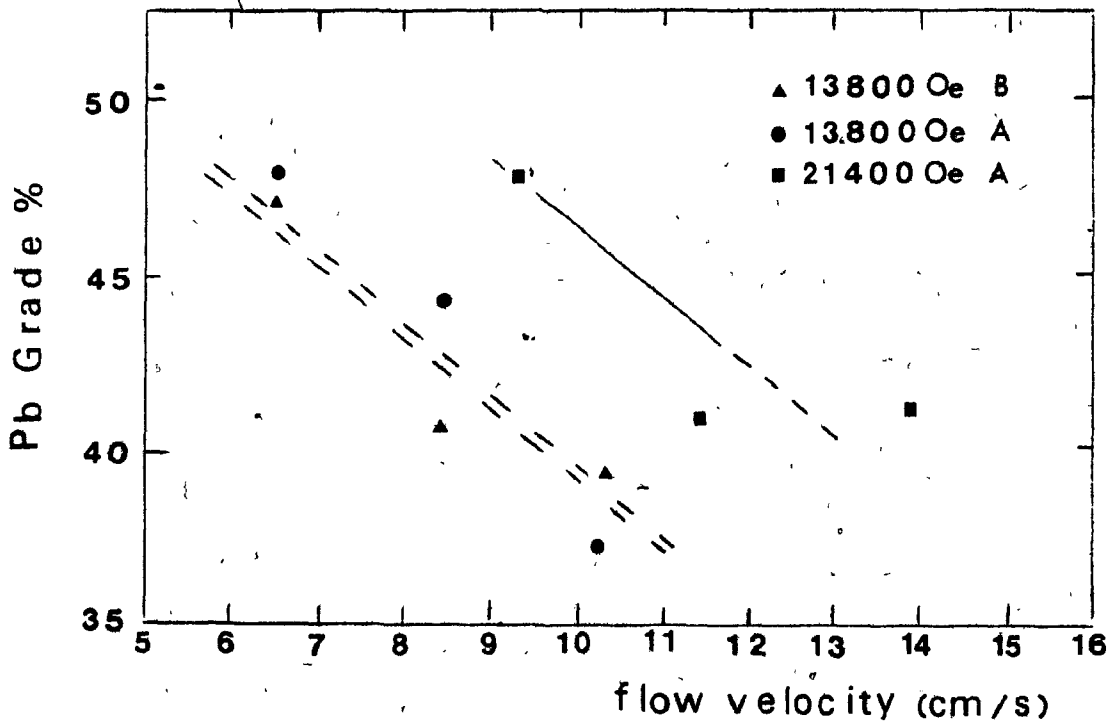
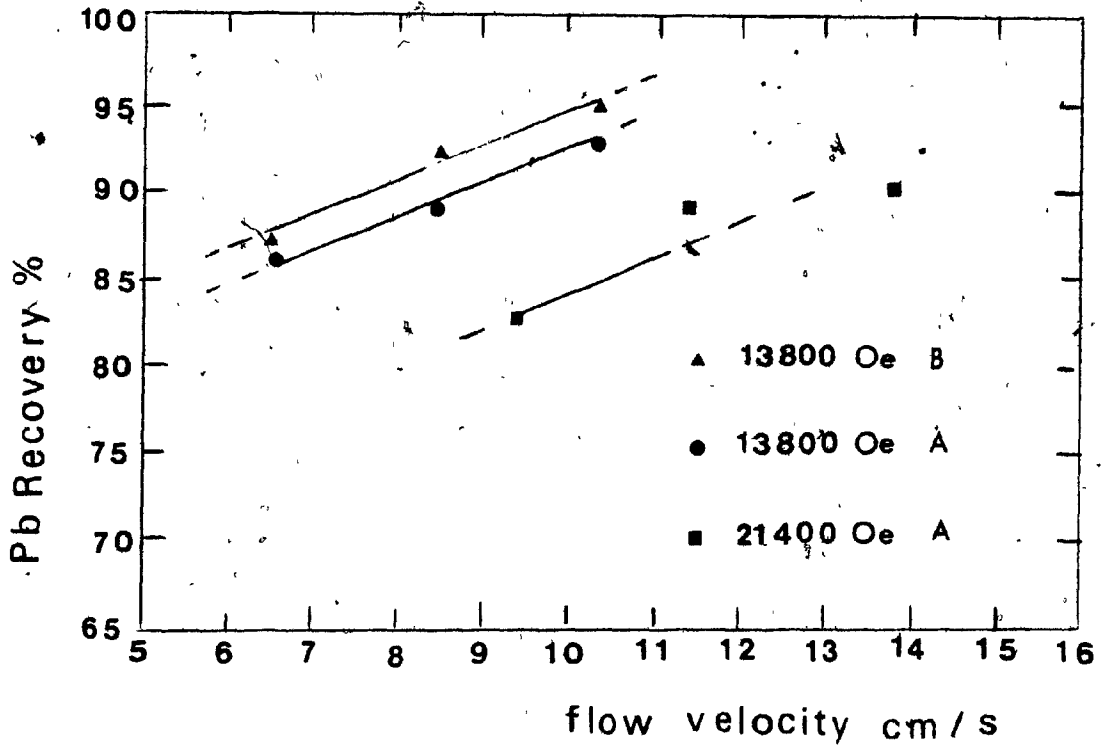


Fig. 44 Lead recovery and grade in the lead concentrate as a function of the flow velocity.

a) Lead Recovery vs Flow Velocity



b) Lead Grade vs Flow Velocity

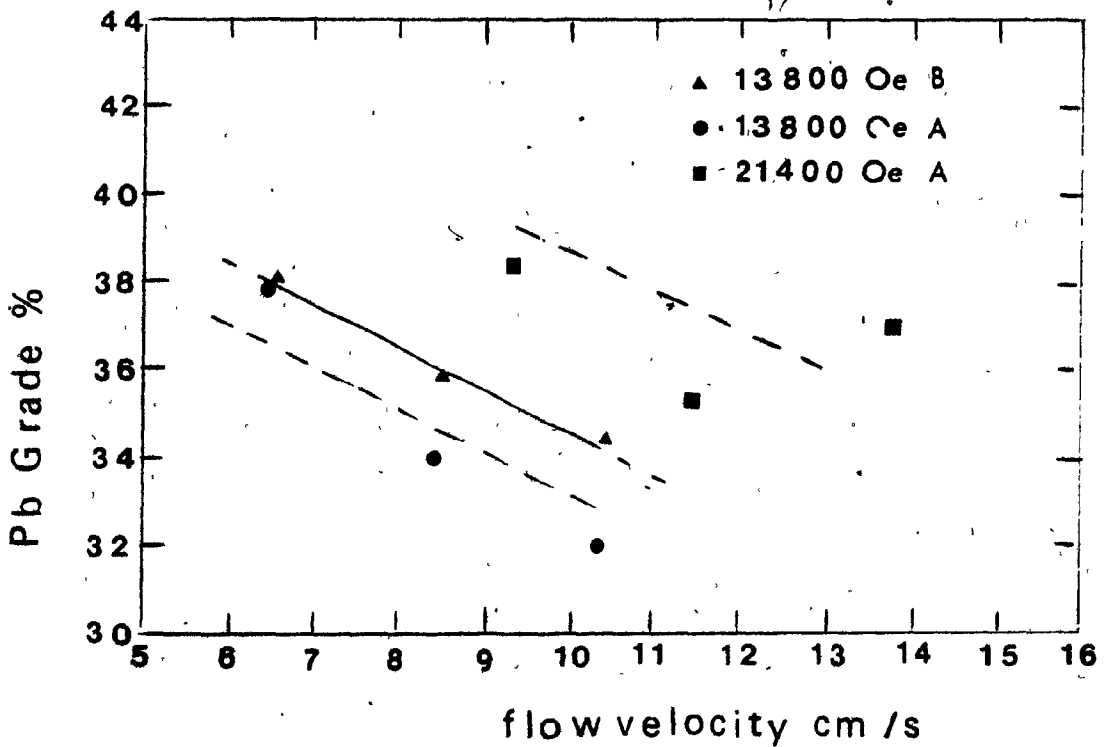
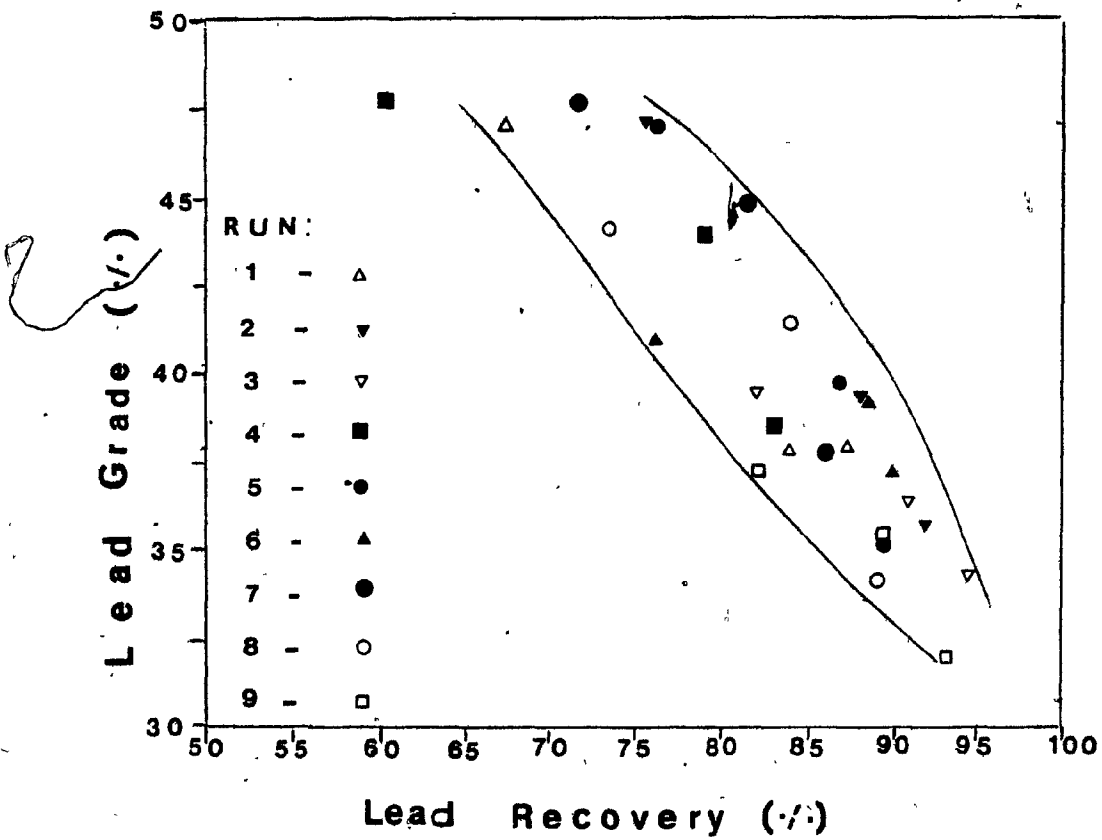


Fig. 45 Grade-Recovery relationship for the lead, constructed from the nine runs.



runs). Fig. 45 allows an estimation of what grades can be obtained for a given recovery or vice versa. Grades of over 46% Pb can be achieved with expected recoveries of less than 77%; over 94% Pb recoveries can be obtained with lead grades of about 34%.

Fig. 46 presents a silver grade-recovery relationship. Notice that grades of over 800 ppm are obtained only from the slimes, but associated recoveries are only of the order of 22%, with practically no lead recovery at all (see run 5, Table 27 and run 8, Table 29). Silver grades of about 560 ppm are obtained with recoveries of ~ 70% from non-mags + slimes, with lead recoveries of ~ 73% (see run 5, Table 27, and run 8, Table 29). Finally silver grades of about 530 ppm are obtained with silver recoveries of ~ 84% in the product referred to as lead concentrate. Lead recoveries in this case are over 90% with about 36% Pb grade.

6.5.5 Size of the Final Products

The size distribution of the mags, non-mags and slimes of run #5 was determined on the Sedigraph. Results are shown in Fig. 47. Notice from Fig. 47 that the mag fraction, curve 1, is the coarsest material, the non-mags, curve 2, is finer and the finest material is the slimes, curve 3 with over 80% $-1 \mu\text{m}$. Knowing that the slimes is high in iron suggests that when the material passes through the matrix the coarser hematite is trapped, while the finer hematite passes through together with the anglesite.

Fig. 46 Grade-recovery relationship for the silver.

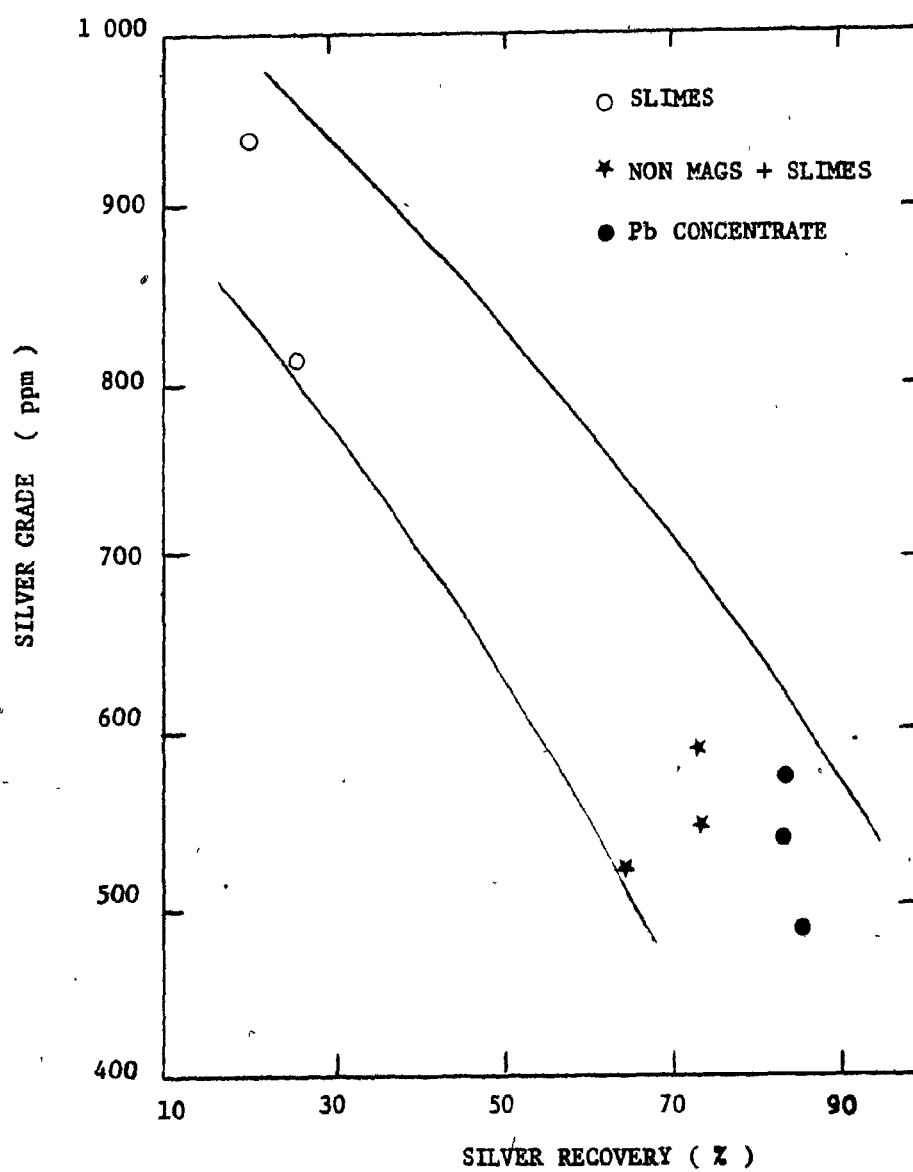
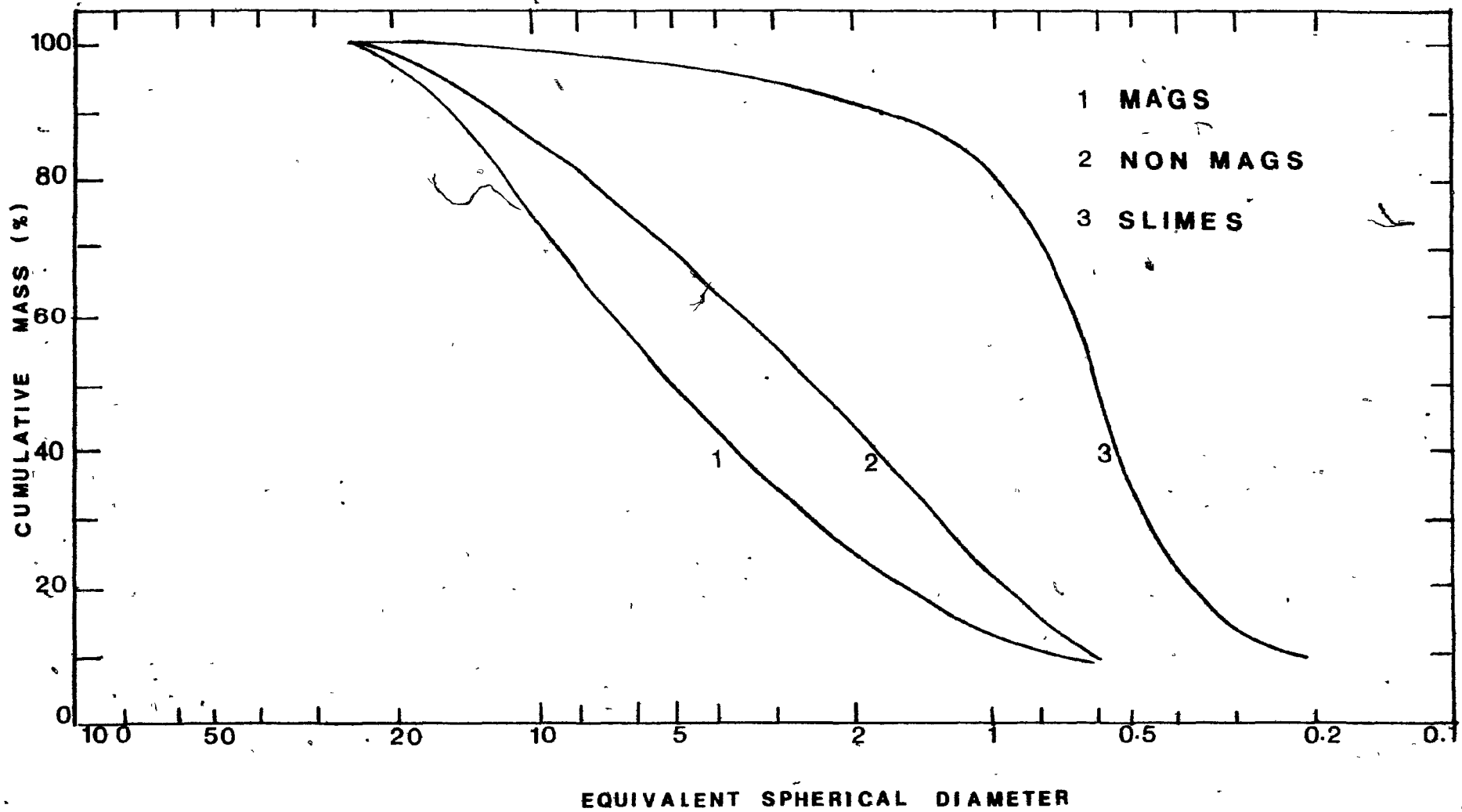


Fig. 47 Particle size of the final products.



6.5.6 Scanning Electron Microscopy (SEM) Examination of the Final HGMS Products

An SEM examination was carried out on run #8, mags, non-mags, mids-1 and slimes. The samples were again well dispersed first. For the slimes, it is possible that dispersion was not attained, since the slimes after HGMS tests were recovered by flocculation with a lime solution.

Figs. 48 and 49 show several views of the mags under the SEM. Figs. 48b, 48d, 49b and 49d show the same views as Figs. 48a, 48c, 49a and 49c, respectively, but with a lead X-ray map in order to identify the lead (anglesite) particles. The size of the lead particles in the Figs. ranges from about 0.5-2 μm ; in general lead particles in the mags ranged from 0.5-3 μm . Iron particles in the pictures are generally less than 2 μm , ranging from 0.1 - 3 μm and they are usually found as aggregates. There appears to be little locking of the lead in the mags.

Fig. 50 shows two views of mids-1. Figs. 50b and 50d show the lead X-ray map of Figs. 50a and 50c respectively. Fig. 50a shows a lead floccule made of particles of about 1 μm and Fig. 50c shows a lead particle of about 2 μm surrounded by iron floccules made of particles finer than 1 μm . In general, lead particles in mids-1 were found to be less than 3 μm . Again, the lead appears to be free.

Figs. 51 and 52 show SEM microphotographs of the non-mags. Figs. 51b, 51d, 52b and 52d show the lead X-ray map

of the Figs. 51a, 51c, 52a and 52c, respectively.

Notice that lead particles are in sizes ranging from 1 to 4 μm ; in general they were found to range from about 1 to 10 μm . In contrast, the iron particles are always finer and forming floccules of particles less than 1 μm . The above observations suggest that lead is found in the non-mags over most of the size range, while iron is always finer than 1 μm .

Fig. 53 shows SEM microphotographs of the slimes. Fig. 53b and 53d show the lead X-ray map of Figs. 53a and 53c respectively. Notice that lead particles are of about 1 μm , and the iron particles are from about 0.1 to 1 μm and often form floccules. This material is probably not as well dispersed due to the previous addition of lime. Even though the slimes contain the highest silver proportion, - 0.08%, it has not proved possible to locate the silver by the SEM. This is compounded by the fact that the particle size is less than 1 μm .

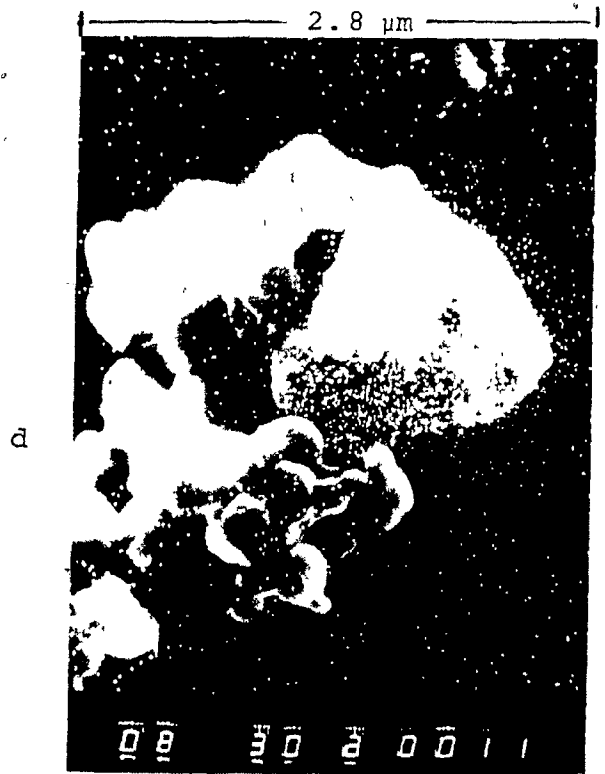
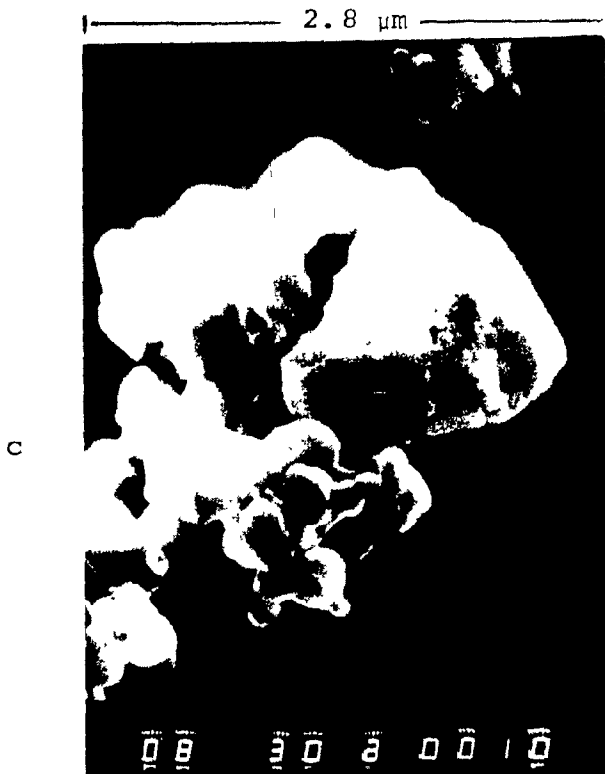
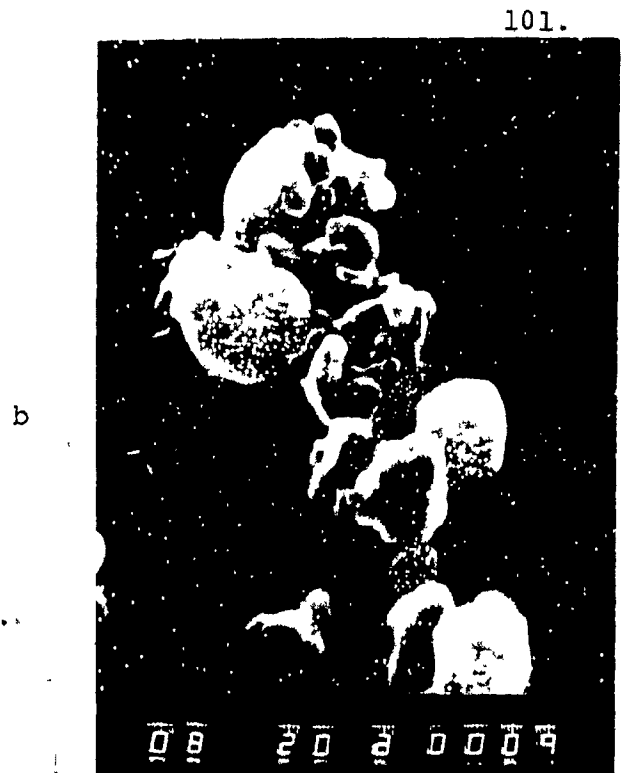


Fig. 48 SEM microphotographs of the mags showing two views of remaining lead. Lead particles are identified with a lead X-ray map (particles showing the white dots.), right side pictures.

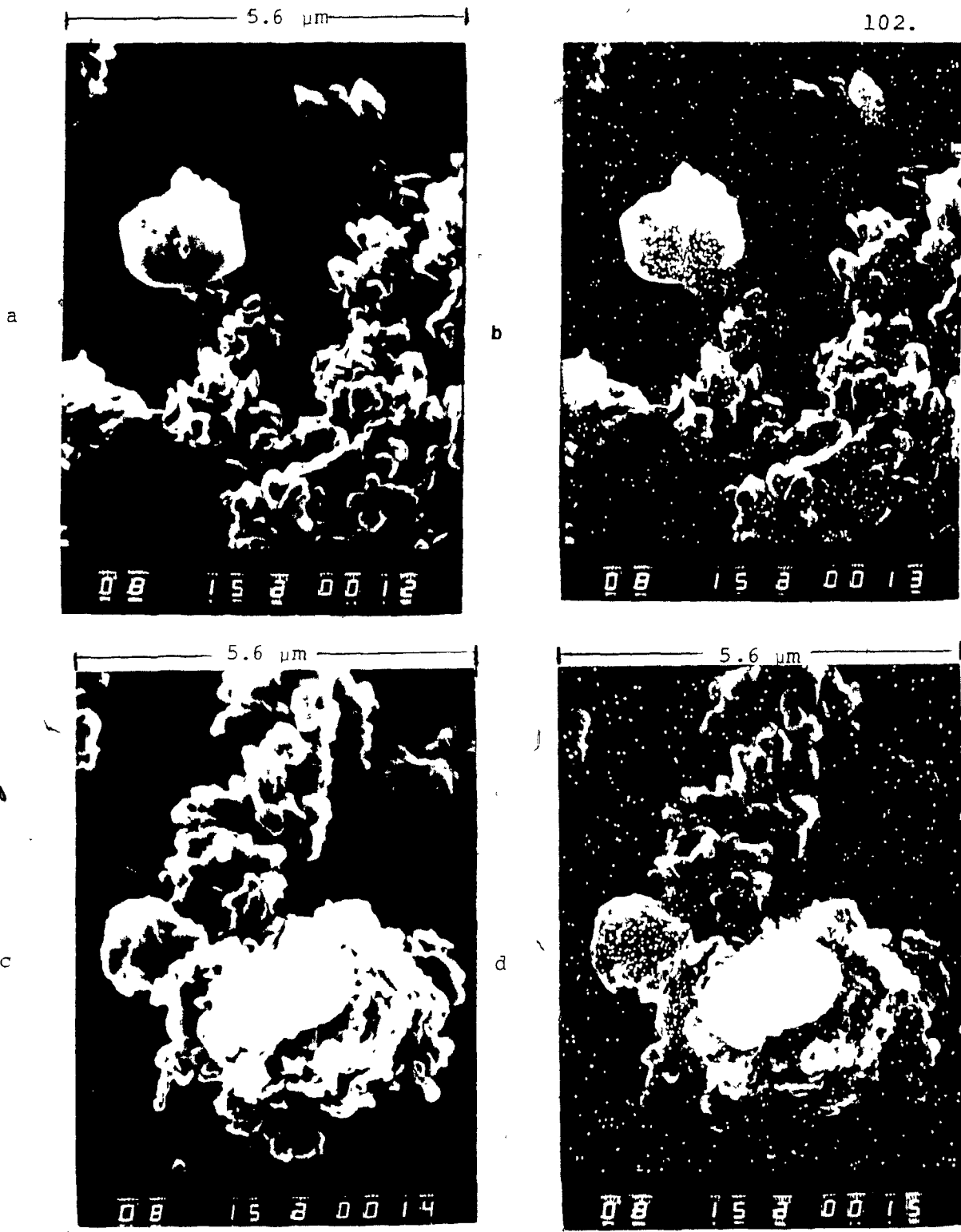


Fig. 49 SEM microphotographs of the mags showing two views of remaining lead. Lead particles are identified with a lead X-ray map (particles showing the white dots.), right side pictures.

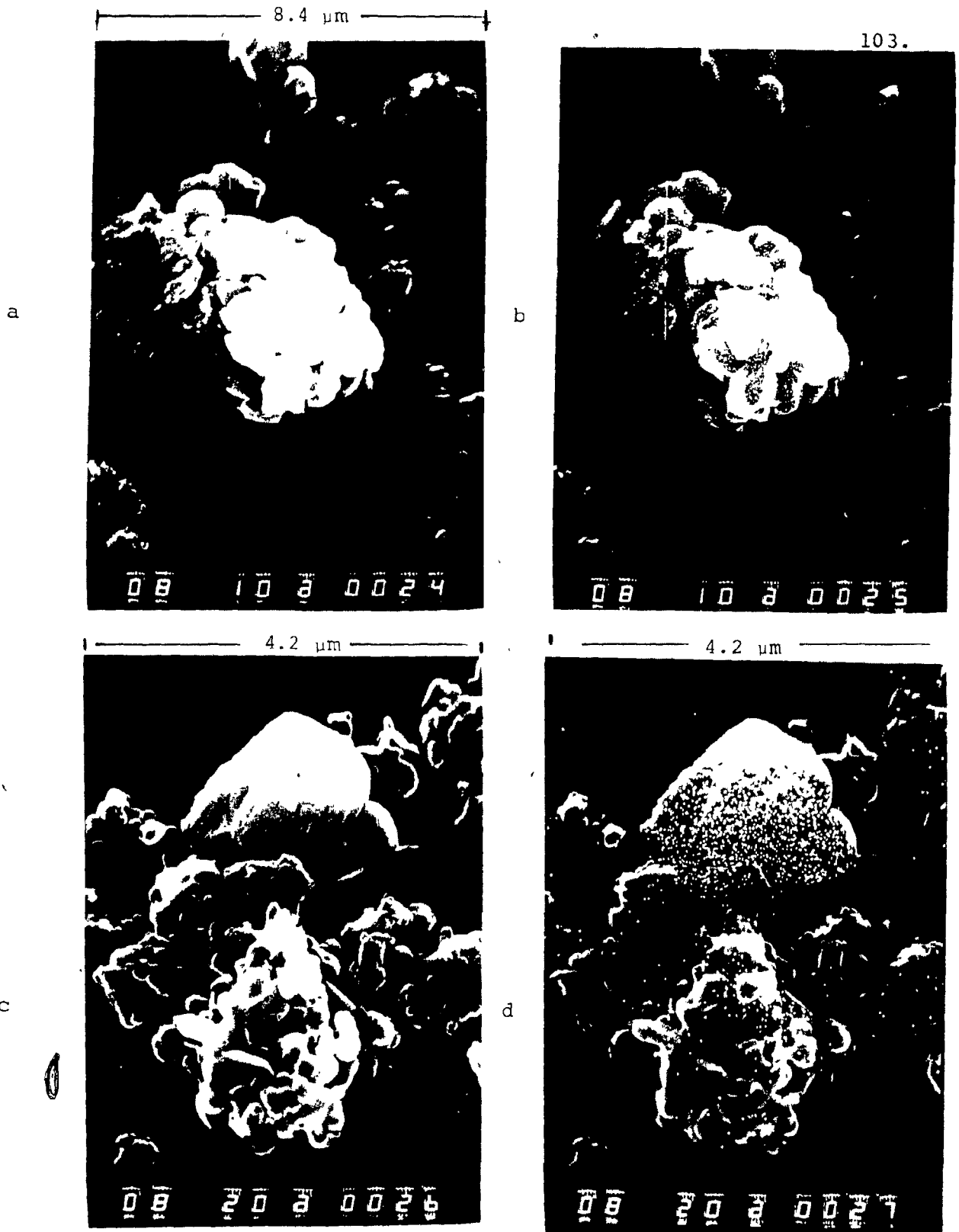


Fig. 50 SEM microphotographs of the mids-1. Lead particles are identified with a lead X-ray map (particles showing the white dots.), right side pictures.

8.4 μm

104.

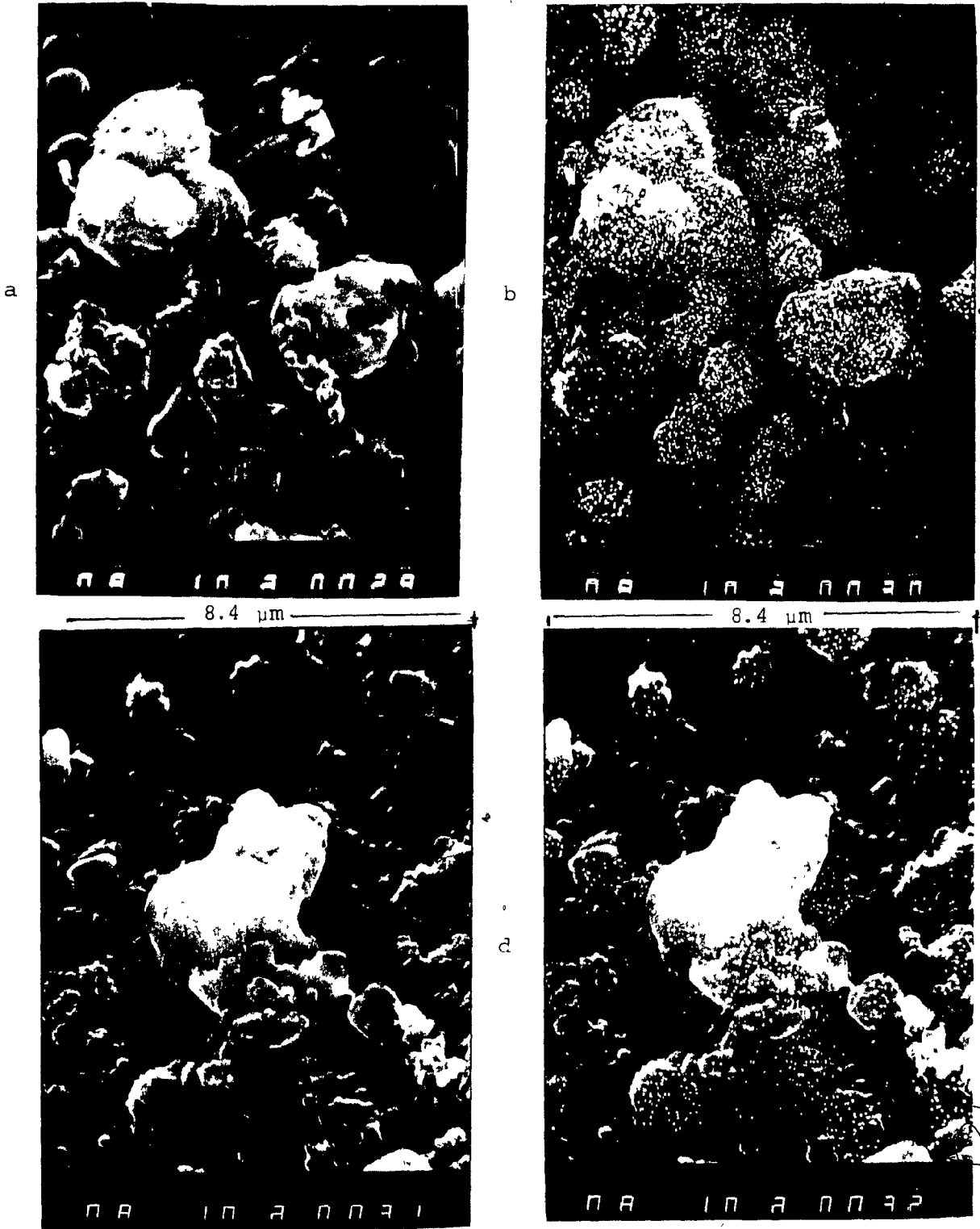


Fig. 51 SEM microphotographs of the non-mags. Lead particles are identified with a lead X-ray map (particles showing the white dots), right side pictures.



Fig. 52 SEM microphotographs of the non-mags. Lead particles are identified with a lead X-ray map (particles showing the white dots.), right side pictures.

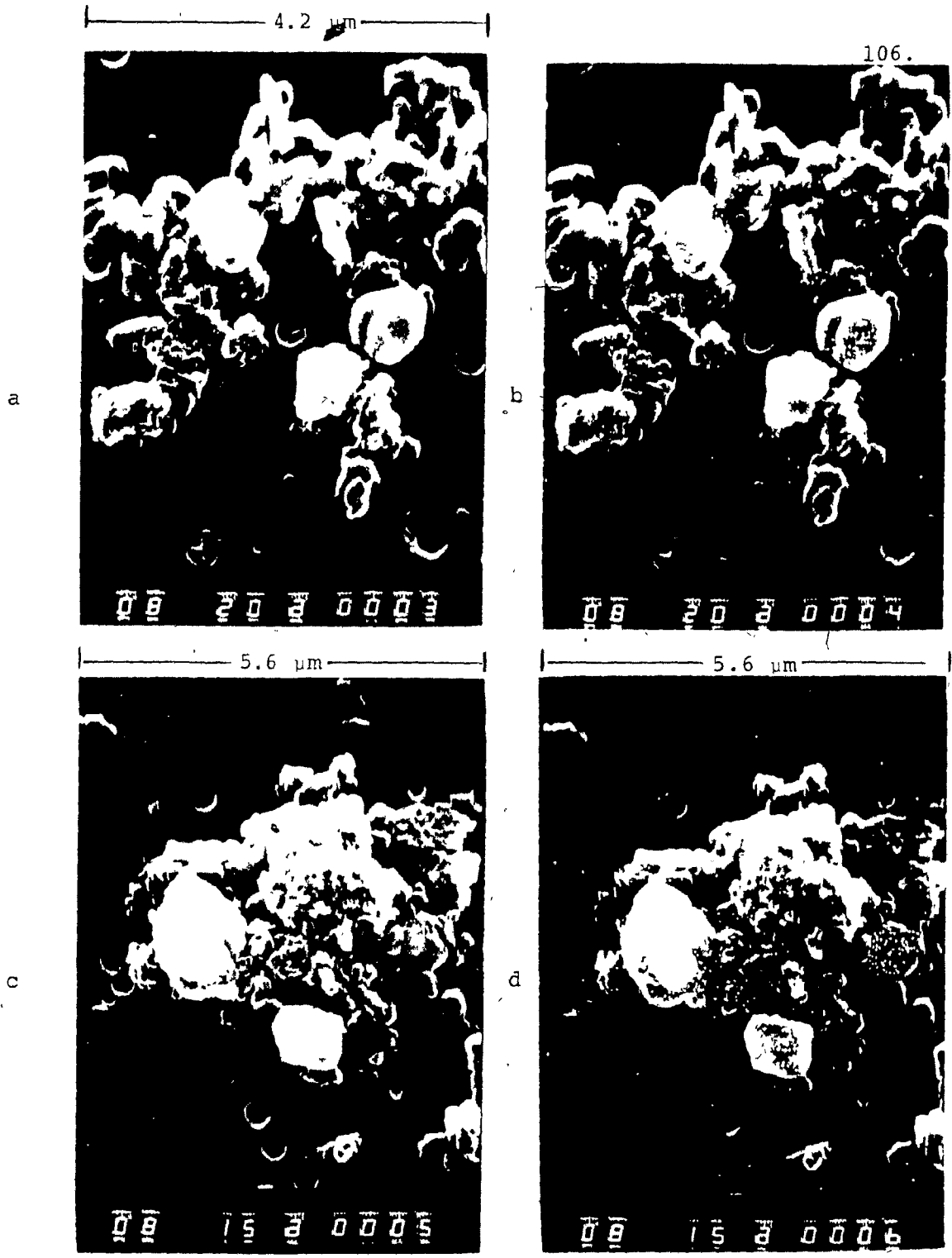


Fig. 53 SEM microphotographs of the slimes. Lead particles are identified with a lead X-ray map (particles showing the white dots), right side pictures.

7. DISCUSSION

7.1 Mineralogical Identification

Electron Microprobe Examination

Electron microprobe examination was used in the identification of both residues, the NALR and the HALR.

There were several advantages to using the microprobe: Some minerals were more clearly distinguished, i.e. ferrite and copper ferrite, marmatite and sphalerite. Silver, which is an important value in the study was found to be associated with the anglesite and not with the hematite. This was valuable information since it is desirable that a combined lead-silver concentrate be produced.

Zinc-iron proportion in the ferrites could be quantified.

Scanning Electron Microscopy (SEM) Examination

SEM examination was carried out on both residues, NALR and HALR, and the final products, mags, mids-1, non-mags and slimes.

Several important features were revealed by the SEM study, particularly on the products of the separation tests.

1) Lead in the mags appeared to be in the range 0.5 - 3 μm and liberated. Thus mechanical entrapment by the steel wool matrix or locking with hematite does not account for the lead

loss. It is speculated that anglesite-hematite agglomerates formed and the resultant agglomerate was magnetically trapped. One possibility is an anglesite grain surrounded by ultrafine hematite. If the anglesite were too large the agglomerate would not become magnetic enough. This may account for lead being at the finer end of the lead size range, which seems to be about 0.5 to 10 μm

2) Lead grade limitations in the non-mags were found to be caused by small iron particles less than 1 μm . The magnetic trapping force, presumably is too small for these particles. A finer matrix, higher fields, lower flow rates and lower feed loadings are the principal options to increase iron recovery below 1 μm .

3) Iron particles finer than 1 μm and frequently as agglomerates larger than 1 μm were located in the mags. Since the magnetic force increases with particle size, agglomeration is initially an attractive way of explaining the trapping of such fine particles. However, the SEM analysis has taken the material out of its processing environment, so it is difficult to determine if agglomeration is a real factor. Whether a deliberate attempt to selectively flocculate the hematite would be beneficial may be worth considering.

Frantz Separator

Since the Frantz separates according to magnetic susceptibility only and can effect separation of minerals of

very close susceptibility this gave several advantages:

- 1) Mineralogical identification was made much easier by working with separate mineral fractions rather than with a wide range. For example, it was possible to isolate the more strongly magnetic ferrites and subsequently show these were Zn-Cu ferrites. Another example was marmatite, when it was isolated from the other minerals, it was readily discriminated from sphalerite.
- 2) The magnetic profile given for the Frantz (Fig. 37) allowed:
 - (i) Estimation of the potential of hematite separation from anglesite by HGMS.
 - (ii) Estimation of the magnetic susceptibility, with which it was possible to solve the HGMS model and select the fluid velocity needed to retain the hematite.

Degree of Liberation

As mentioned in section 1.1.3, lead in the bulk concentrate, according with Petruk, is typically 37% wt free, 13% wt combined with sphalerite and 50% wt combined with pyrite, and is not readily further liberated with grinding. It is worth noting that the roasting-NAL step seems to have increased the degree of liberation from 37% wt to over 94% wt. It is possible that the roasting and leaching is an effective method of achieving liberation. This may warrant further attention.

7.2 MAGNETIC SEPARATION

Estimation of Fluid Velocities, "U"_∞ and Magnetic Recoveries, R (%) in HGMS

Since there are many parameters which control the operation of HGMS, the use of the HGMS model in the investigation was very useful in helping select the initial test conditions. This, it is felt, significantly reduced the number of tests, and consequently the amount of sample needed in the investigation. In the present case this was an especially important factor, since the original calcine was limited to about 3 kg, which after leaching was reduced to about 750 g of HALR.

Table 30 presents the results of the estimation of fluid velocities and a comparison between the measured and predicted recoveries. Notice that measured and predicted recoveries are in good agreement in all cases; this means that the conditions are well selected by the model.

Physical Trapping in HGMS

Physical, or mechanical, trapping by the matrix can be a serious problem. This can arise not only when feed particles are too large (e.g. comparable to the wire diameter) but also when strongly magnetic materials (e.g. ferrites) are not adequately flushed off the matrix and accumulate with repeated cycles. Particle size does not appear to be a factor here, the top size being about 20 μm , or less than one-third of the wire size. In the HALR there are practically no ferrites. This lack of ferrites could be added to the list

Table 30. HGMS. Estimation of fluid velocities U_∞ and a comparison between the measured and predicted recoveries.

$$L = 0.53$$

$$\rho_p = 5.25 \text{ g/cm}^3$$

$$\rho_w = 7.75 \text{ g/cm}^3$$

$$\varepsilon = 0.7$$

$$R (\%) = 16.8 \left[\left(\frac{N_L}{2.5} \right)^{0.8} - 1 \right]$$

$$b = 0.0001455 \text{ cm}$$

$$\kappa = 245.44 \times 10^{-6} \text{ cmu/cm}^3 - \text{Oe}$$

$$a = 0.0030 \text{ cm}$$

$$\rho_f = 1.0 \text{ g/cm}^3$$

$$\mu = 0.01 \text{ cm}^2/\text{s}$$

$$N_L = \frac{8.963 \times 10^{-2} b A H_a^2}{U_\infty^{3/2}}$$

Test	H_a (Oe)	A	U_∞	Recovery of Hematite		
				pred.	(*)	meas.
1	13,800	0.625	6.51	100	96.70	74.1
2	13,800	0.625	8.45	100	91.65	69.9
3	13,800	0.625	10.29	100	87.52	64.7
4	21,400	0.420	9.35	100	93.10	77.5
5	21,400	0.420	11.40	100	91.86	62.0
6	21,400	0.420	13.91	100	87.91	66.7
7	13,800	0.625	6.51	100	96.70	70.1
8	13,800	0.625	8.45	100	91.65	65.5
9	13,800	0.625	10.29	100	83.52	54.7

(*) using full size distribution (curve 6, p. 73).

of reasons for selecting the HALR over the NALR for HGMS.

Separation Results

The lead grade-recovery relationship deduced from the nine runs indicates that grades of over 46% Pb can be achieved with expected recoveries of less than 77%; over 94% Pb recoveries can be obtained with lead grades of about 34%.

Silver grade-recovery relationship indicates that silver grades of about 530 ppm can be obtained with silver recoveries of ~ 84%. The corresponding lead recoveries in this case are of over 90% with about 36% Pb grade.

Further improvements in lead and silver grades and recoveries may be attained when finer (less than $1\ \mu\text{m}$) iron particles can be trapped in the matrix. Principal options to achieve that trapping are higher magnetic fields, lower flow velocities, lower "L" (mass of magnetics in the feed per unit matrix mass) and a finer matrix. In this investigation, higher fields than those in which a good grade and recoveries were attained (13,800 Oe), were tested, 21,400 Oe, but no improvement in grade or recovery was achieved. Several flow velocities were used. It was observed (Figs. 43 and 44) that when flow velocities were reduced in order to achieve higher iron recovery in the mags (and, therefore a higher Pb grade in the non-mags), Pb recovery decreased markedly. This indicates that a strong drag force is needed during the separation to pull out the non-magnetic material.

A lower "L" and a finer matrix are two options that can be considered in further tests. However, the value of "L" should not be very low, since it will mean a considerable loss in the HGMS capacity. The matrix should not be finer than 40 μm in diameter, otherwise physical trapping may become a factor. As mentioned previously, selective flocculation of the hematite may be worth considering.

Silver recovery to the lead concentrate appears quite acceptable, but upgrading is limited to about 530 ppm (for a feed of about 440 ppm). Silver is concentrated in the slimes, however; this suggests that the silver is not only associated with the lead, but is present as a very fine separate phase, probably tetrahedrite as identified in the BMS ore by Patruk (29).

General Observation

As mentioned in the Statement of Problem (Chap.2), the object of this investigation was the production of a saleable lead-silver concentrate from the HALR.

A saleable lead-silver concentrate was attained. The SRLE process in combination with lead/silver recovery by HGMS can render metal extractions of over 98% for copper and zinc, 94% for lead and over 83% for silver.

7.3 ASSAY OF THE SAMPLES

Since the confidence in the assays is an important point in the investigation, samples were sent to the analytical

laboratory, CANMET, Ottawa, in order to compare results. The other purpose of sending samples to CANMET was to determine the silver assays, since facilities were not available at McGill. Only selected samples were sent to CANMET as a precaution. Since the silver is mainly associated with the lead, it was felt that the results from one of the runs of the series would reveal the grades and recoveries to expect.

Table 31 presents a comparison between the zinc, lead and iron assay performed at both places. Silver assays are also included. Notice that there is not a significant difference between the results. Lead assays from CANMET tend to be about 1.5% higher and iron assays about 1.5% lower. Zinc in both cases was the same.

Table 32 presents results from runs 2, 5 and 8 using the CANMET assays. Comparing results of Table 32 with those shown on pp. 87, 89 and 91 for runs 2, 5 and 8 respectively, notice that lead recoveries are the same but lead grade with the CANMET data is about 2% higher.

Table 31. Comparison Between Assays Reported by CANMET and McGill

SAMPLE DESCRIPTION	CANMET				McGILL		
	Zn	Pb	Fe	Ag*	Zn	Pb	Fe
CALCINE	26.78	6.49	15.22	122	25.9	6.7	15.2
NALR	9.85	17.36	41.88	290	9.7	17.3	39.5
HALR	0.93	26.79	41.84	420	0.9	24.6	40.2
MAGS	0.64	6.38	60.5	164		5.8	60.5
MID-1	1.04	28.81	36.11	462		27.1	33.3
Run 2					**		
MID-2	1.29	17.36	47.41	350		16.3	51.9
NON-MAGS	0.54	42.20	24.06	515		40.8	25.8
MAGS	1.17	8.63	56.18	190		7.7	60.5
MID-1	1.51	36.38	27.44	508		33.1	35.8
Run 5					**		
NON-MAGS	0.79	43.09	22.31	465		40.8	23.8
SLIMES	0.41	7.73	44.92	939		6.9	45.0
MAGS	1.07	8.35	60.18	220		7.7	64.5
MID-1	1.68	30.11	33.55	489		28.8	37.1
Run 8					**		
NON-MAGS	0.80	48.01	18.49	515		44.2	18.6
SLIMES	0.45	8.45	41.43	810		8.0	43.3

* Silver assays reported in ppm.

** Zinc assays were not done in any of the runs, at McGill.

Table 32. Results from Runs 2, 5 and 8, Using the CANMET Reported Assays.

Run	Product	Wt (%)	Assay (%)				Distrib. (%)			
			Zn	Pb	Fe	Ag	Zn	Pb	Fe	Ag
2	MAG	34.5	0.64	6.38	62.38	164	32.4	7.8	53.5	15.0
	MID-1	11.5	1.04	28.81	36.11	462	17.5	12.2	10.3	14.1
	MID-2	6.7	1.29	17.36	47.41	350	12.7	4.4	7.9	6.2
	NON-MAGS	47.3	0.54	42.20	24.06	515	37.4	75.6	28.3	64.7
		100.0					100.0	100.0	100.0	100.0
	Calculate feed		0.68	26.42	40.23	377				
	Assay feed		0.93	26.79	41.84	420				
	Pb Conc.	65.5	0.70	37.18	28.70	489	67.6	92.2	46.5	85.0
5	MAGS	36.1	1.17	8.63	56.18	190	44.5	11.5	54.9	16.7
	MID-1	7.9	1.51	36.38	27.44	508	12.5	10.7	5.9	9.8
	NON-MAGS	47.2	0.79	43.09	22.31	465	39.2	75.3	28.5	53.4
	SLIMES	8.8	0.41	7.73	44.92	939	3.8	2.5	10.7	20.1
		100.0					100.0	100.0	100.0	100.0
	Calculate feed		0.95	27.0	36.94	411				
	Assay feed		0.93	26.79	41.84	420				
	Pb Conc.	63.9	0.83	37.39	26.06	536	55.5	88.5	45.1	83.3
8	MAGS	35.2	1.07	8.35	60.18	220	40.7	11.0	56.0	17.2
	MID-1	9.2	1.68	30.11	33.55	489	16.7	10.4	8.2	10.0
	NON-MAGS	41.1	0.80	48.01	18.49	515	35.6	74.0	20.1	47.1
	SLIMES	14.4	0.45	8.45	41.43	810	7.0	4.6	15.7	25.7
		100.00					100.0	100.0	100.0	100.0
	Calculate feed		0.92	26.66	37.84	449				
	Assay feed		0.93	26.79	41.84	420				
	Pb Conc.	64.4	0.85	36.6	25.7	574	59.3	89.0	44.0	82.8

CONCLUSIONS

1. Mineralogical Examination

- All the major phases of the calcine, NALR and HALR were identified.
- Anglesite was shown to be essentially free in the NALR and HALR.

2. HALR vs. NALR

- Results from the Frantz Isodynamic Magnetic Separator revealed that the best material to perform the anglesite/hematite separation was the HALR. In this way, production of two zinc bearing materials would be avoided.
- An HGMS model was used to estimate the initial conditions for magnetic separation.

3. Dispersion and Settling

- Dispersion of the HALR was attained after three steps:
 - a) removal of remaining ions by washing the leach residue with water;
 - b) wetting the sample by means of a dispersant, calgon, and
 - c) twenty minutes of agitation in an ultra-sound bath.
- Settling of solids after HGMS is effected by the addition of Ca^{++} (lime).

4. HGMS Results

- The SRLE process in combination with lead-silver recovery

by HGMS can render metal extractions of over 98% for copper and zinc, 94% for lead and over 83% for silver.

- Grades of over 46% Pb can be attained with recoveries of about 77% Pb and 72% Ag; over 94% Pb and 83% Ag recoveries can be obtained with lead grades of about 34%. Silver grade was relatively constant at 500-550 ppm.
- Lead grades were limited to a high of 48% in the non-mags mainly because of small hematite particles (less than 1 μm) which are not trapped by the HGMS at these flow velocities.
- Removal of slimes from the non-mags can improve the lead grade by about 7% with a 3% decrease in lead recovery; however, about 20% of the silver is in the slimes.
- The origin of lead losses in the mags is suspected to be due to agglomeration of fine lead particles, 1 - 3 μm , with hematite, creating an agglomerate which is magnetically caught.

5. Physical Trapping

- Physical trapping in the matrix (wire diameter of 60 μm and packing density of 4% v/v) is not a problem since the HALR is so fine (100% - 25 μm , 50% - 3 μm and 20% - 1 μm).

6. General

- Hematite removal by HGMS to concentrate lead-silver bearing compounds in the SRLE process is judged technically to be quite successful. An expected result is lead recovery

of 90% with 36% grade and silver recovery of 84% with
530 ppm grade.

8 APPENDIX A. X-RAY IDENTIFICATION

X-ray diffraction of calcine, NALR and HALR: A list of the d-spacing measured and a comparison with listed values is shown. In each case, conditions were: 40 kV, 20 mA, 6 hrs of exposure, with an Fe - tube. Intensities of the lines were estimated by eye.

Table A-1 shows the XRD of calcine. Because of the large number of minerals in the calcine, some "d" values of 2 or 3 minerals appear together. Notice that the measured and listed "d" values for zinc sulphate and zinc oxy-sulphate diverge a little. Possibly, this is due to the poor crystallinity of these compounds.

Table A-2 presents a comparison of measured and listed "d" values of the NALR by XRD. Notice that the α - hematite, anglesite and ferrite measured and listed "d" values correspond closely.

Table A-3 shows a comparison of measured and listed "d" values of the NALR 650 to 850 mA mags fraction on Frantz of the $-25 + 15\mu\text{m}$ size interval (see Table 19). Notice that according with the intensities of the lines, sphalerite and anglesite are the main minerals.

Table A-4 presents a comparison of measured and listed "d" values of the HALR by XRD. Notice that according with the intensities of the lines, hematite and anglesite are the main minerals in the sample.

Table A-1. Calcine. Comparison of Measured and Listed "d" Values in XRD

Measured "d" spacing (Å)	I	Listed "d" Values				
		ZnSO ₄	α - Hematite	Franklinite	Zinc Oxy-Sulphate	Anglesite
4.726	70				4.65	
4.217	30	4.17 ⁽²⁾				4.26 ⁽²⁾
3.784	20					3.813
3.617	5	3.616 ⁽³⁾			3.67 ⁽³⁾	3.622
3.363	100				3.34	3.333 ⁽³⁾
2.948	30			2.984 ⁽²⁾	2.97 ⁽¹⁾	3.000 ⁽¹⁾
2.691	30	2.650 ⁽⁴⁾	2.69 ⁽¹⁾			2.699
2.520	70		2.51 ⁽³⁾	2.543 ⁽¹⁾		
2.395	5	2.383			2.41 ⁽⁴⁾	2.406
2.262	5					2.276
2.189	10					2.193
2.100	5			2.109	2.104	
2.049	8					2.067 ⁽⁴⁾
1.960	5	1.947				1.973
1.834	7	1.832	1.838 ⁽⁴⁾			
1.782	5	1.773				1.793
1.692	13		1.690 ⁽²⁾			
1.652	5					1.656
1.618	13	1.616		1.624 ⁽⁴⁾		1.621
1.489	25	1.491	1.484	1.491 ⁽³⁾		
1.450	8	1.457	1.452			
1.435	5	1.431				1.429
1.349	5		1.349			
1.307	5		1.310			
1.280	8			1.287		
1.215	5		1.213			
1.140	5		1.141			
1.098	15			1.099		
1.077	5		1.076			
1.054	15		1.055			

(1), (2), (3) and (4), represents the main lines.

Table A-2. NALR. Comparison of Measured and listed "d" Values by XRD

Measured "d"		Listed "d" Values		
spacing (Å)	I	Hematite	Franklinite	Anglesite
4.233	80			4.26 ⁽²⁾
3.797	35			3.813
3.652	25	3.66		3.622
3.455	15			3.479
3.335	35			3.333 ⁽³⁾
3.224	30			3.220
2.992	60		2.984 ⁽²⁾	3.001 ⁽¹⁾
2.767	15			2.773
2.692	45	2.69 ⁽¹⁾		
2.537	100	2.51 ⁽³⁾	2.543 ⁽¹⁾	
2.405	15			2.406
2.274	15	2.285		2.276
2.205	15	2.201		
2.155	15			2.164
2.108	15		2.109	
2.066	30	2.070		2.067 ⁽⁴⁾
2.026	25			2.028
1.973	15			1.973
1.911	5			1.905
1.880	5			1.879
1.837	20	1.838 ⁽⁴⁾		
1.785	15			1.793
1.718	15		1.723	1.716
1.692	25	1.690 ⁽²⁾		
1.620	30		1.624 ⁽⁴⁾	
1.569	5			1.571
1.487	50	1.484	1.491 ⁽³⁾	
1.451	15	1.452		
1.438	10			1.429
1.423	5		1.427	
1.400	10			1.406

Table A-2. Continuation. NALR. Comparison of Measured and Listed "d" Values in XRD

Measured "d" spacing (Å)	I	Listed "d" Values		
		α - Hematite	Franklinite	Anglesite
1.348	5	1.349		
1.332	5		1.3348	
1.312	8	1.310		
1.283	20		1.2872	
1.268	7		1.2721	
1.256	5	1.258		
1.227	5	1.226		
1.219	5	1.213	1.2184	
1.188	5	1.189	1.1820	
1.161	15	1.162		
1.140	15	1.141		
1.127	10		1.1280	
1.103	5	1.102		
1.098	25		1.0990	
1.077	15	1.076		
1.055	20	1.055	1.0553	
0.994	15	0.989	0.9949	

(1), (2), (3) and (4) represents the main lines.

Table A-3. NALR. Mags Fraction at 650 to 850 mA on Frantz.
 Comparison of measured and listed "d" values by XRD.
 (See Table 19)

Measured "d"		Listed "d" Values			
spacing (Å)	I	Sphalerite	Anglesite	Hematite	Quartz
4.219	80		4.26 ⁽²⁾		4.26 ⁽²⁾
3.798	35		3.813		
3.630	15		3.622	3.66 ⁽⁴⁾	
3.456	15		3.479		
3.327	23		3.33 ⁽³⁾		
3.216	13	3.20	3.22		3.24 ⁽¹⁾
3.129	100	3.12 ⁽¹⁾			
3.001	35	3.05	3.00 ⁽¹⁾		
2.768	5	2.76	2.773		
2.699	35	2.71	2.699	2.69 ⁽¹⁾	
2.610	5			2.618	
2.511	10	2.52		2.51 ⁽³⁾	
2.396	8		2.406		
2.267	8		2.276	2.285	
2.164	8		2.164		
2.063	28	2.08	2.067 ⁽⁴⁾	2.070	
2.030	20		2.031		
1.970	8	1.977	1.973		1.98
1.908	60	1.904 ⁽²⁾	1.905		
1.872	4	1.871			
1.835	6	1.841		1.838	1.82 ⁽³⁾
1.790	8		1.793		
1.736	5		1.741		
1.697	8			1.69 ⁽²⁾	
1.632	35	1.626 ⁽³⁾		1.634	
1.567	4	1.572			
1.491	10		1.493	1.484	
1.464	3		1.467		

Table A-3. Continuation. NALR. Mags Fraction 650 to 850 mA on Frantz. Comparison of measured and listed "d" values by XRD. (See Table 19)

Measured "d" spacing (Å)	"I"	Listed "d" Values			
		Sphaerite	Anglesite	Hematite	Quartz
1.452	3			1.452	1.453
1.438	3		1.441		
1.425	5		1.429		
1.399	6		1.406		
1.366	8				1.372
1.350	5	1.35		1.349	
1.325	5				
1.283	3				1.288
1.240	20	1.239			
1.220	8			1.226	
1.198	5				1.199
1.162	8			1.162	
1.142	8			1.141	
1.104	25	1.103		1.102	
1.064	8				1.063
1.052	8			1.055	
1.041	15	1.039		1.042	
0.986	8			0.989	
0.977	5				0.978

(1), (2), (3) and (4) represents the main lines.

Table A-4. HALR. Comparison of Measured and Listed "d" Values by XRD

Measured "d" spac- ing (Å)	(I)	Listed "d" Values		
		Hematite	Anglesite	α - Quartz
4.219	80		4.26 ⁽²⁾	4.26 ⁽²⁾
3.785	20		3.813	
3.664	20	3.66 ⁽⁴⁾		
3.455	20		3.479	
3.326	35		3.33 ⁽³⁾	3.34 ⁽¹⁾
3.216	20		3.22	
2.993	35		3.00 ⁽¹⁾	
2.748	10		2.773	
2.692	70	2.69 ⁽¹⁾		
2.609	10		2.618	
2.506	50	2.51 ⁽³⁾		
2.396	10		2.406	
2.263	10	2.285	2.276	2.282
2.194	10		2.193	
2.063	25	2.070	2.067 ⁽⁴⁾	
2.017	20		2.028	
1.967	12		1.973	
1.838	20	1.838		1.82 ⁽³⁾
1.785	10		1.793	
1.738	8		1.741	
1.692	100	1.69 ⁽²⁾		
1.616	10	1.634		
1.564	5		1.571	1.541
1.484	60	1.484		
1.451	30	1.452		
1.397	5			1.382
1.365	10			1.375
1.349	8	1.349		
1.311	6	1.310		
1.262	5	1.258		

Table A-4. Continuation. HALR. Comparison of Measured and Listed "d" values by XRD

Measured "d" spac- ing (Å)	(I)	Listed "d" Values		
		Hematite	Anglesite	α - Quartz
1.216	7	1.213		
1.190	5	1.189		
1.161	15	1.162		
1.140	15	1.141		
1.102	12	1.102		
1.075	10	1.076		
1.065	10			1.0636
1.055	10	1.055		
0.989	5	0.989		
0.975	5			0.9762
0.972	5	0.9715		

(1), (2), (3) and (4) are the main lines)

APPENDIX - B. ESTIMATION OF DEGREE OF LIBERATION

Estimation of Degree of Liberation in NALR and HALR on the + 25 μ m, -25 + 15 μ m and -15 + 10 μ m fractions.

Degree of liberation, "L", as defined by Gaudin, is the volume fraction of mineral or phase occurring as free particles, (A), in relation to the total volume of that mineral occurring in the free (A) and locked forms (B). In the following record sheets the number under "volume of locked anglesite" records the parts per 20 parts of particle volume occupied by the anglesite in the locked particle. B is calculated by summing all these partial volumes and dividing by 20; in other words, B represents the particle equivalents in volume of anglesite. The degree of liberation in per cent, %L, is given by the following expression:

$$\% L = \frac{A}{A + B} \quad (100)$$

where:

A, is the volume of free particles of anglesite.

B, is the particle equivalents in volume of anglesite, as locked grains.

When point counting there is a relationship between the number of points counted and the accuracy of the results. Van Der Plas and Tobi discussed this relationship in terms of the standard deviation. They developed a chart giving the values of 2 σ (~ 95% of confidence) for different values of the estimated

percentage by volume of a mineral and the number of particles counted. Table B-1 shows the error obtained in the present point counting, according with Van Der Plas and Tobi:

Table B-1. Error, with 95% of Confidence, Obtained in Point Counting Technique on the NALR and the HALR.

Product size (μm)	Degree of Liberation	
	NALR	HALR
+ 25	70 \pm 6%	72 \pm 6%
-25 + 15	90 \pm 2%	93 \pm 3%
-15 + 10	94 \pm 2%	95 \pm 1%

Table B-2. Record Sheet Used for Particle Counting in NALR, to measure degree of liberation "L" of the anglesite.

NALR																		
size, μm	Free Anglesite																	
	A = 110																	
+ 25	Volume of Locked Anglesite																	
	10	10	10	18	10	10	7	6	17	15	5	5	14	14	10	2	6	3
	11	3	8	8	4	10	4	8	8	3	14	4	2	10	18	18	10	15
	2	10	4	2	7	6	6	6	8	6	7	10	5	10	5	10	12	15
	8	4	9	12	5	6	6	17	11	10	3	3	6	3	17	7	10	6
	4	15	3	10	3	5	4	2	2	3	3	3	2	4	8	4	18	6
	4	9	15	5	5	2	9	2	10	10	10	14	4	6	10	6	18	6
	10	2	10	6	2	4	18	10	3	10	15							
	B = (920/20) = 46																	
	% L = 70																	
Free Anglesite																		
	A = 290																	
-25 + 15	Locked Anglesite																	
	10	6	5	10	18	18	8	10	10	10	15	15	8	8	2			
	14	10	15	10	10	10	10	10	10	10	10	10	18	8	6			
	10	10	15	6	11	10	10	10	18	14	10	8	9	11	16			
	8	10	10	8	6	5	10	10	10	8	18	6	10					
	B = (621/20) = 31.05																	
	% L = 90																	

Table B-2. Continuation. Record Sheet Used for Particle Counting in NALR, to Measure Degree of Liberation "L" of the Anglesite.

NALR												
size, μm	Free Anglesite											
-15 + 10	10	10	10	10	10	10	10	10	10	10	10	10
	10	10	10	10	10	10	10	10	10	10	10	10
	10	10	10	10	10	10	10	10	10	10	10	10
	10	10	10	10	10	10	10	10	10	10	10	10
	A = 325											
Volume of Locked Anglesite												
	10	10	10	4	10	10	10	10	15	6	10	10
	10	10	10	10	10	10	10	10	12	10	10	8
	8	8	14	10	10	3	3	10	10	10	10	10
	10	10	10	10	10	10	10					
	B = (380/20) = 19											
	% L = 94											

Table B-3. Record Sheet Used for Particle Counting in HALR, to Measure Degree of Liberation, "L" of the Anglesite.

Size, μm		Free Anglesite														
+ 25		 														
		 														
		A = 140														
		Volume of Locked Anglesite														
	12	6	6	10	10	16	18	18	10	10	10	3	15	10		
	5	3	5	10	8	3	10	4	13	12	10	2	17	15		
	18	14	3	15	10	10	16	15	15	3	15	10	10	8		
	7	1	3	6	5	5	10	10	10	5	10	10	3	6		
	3	10	6	18	6	15	15	4	5	12	6	2	6	4		
	14	18	15	13	3	16	18	14	6	3	7	14	18	10		
	18	14	14	3	10	10	15	4	5	10	6	18	18	4		
	6	11	18	3	12	10	4	18	10	8	10	4	3	2		
	15	10														
		B = (1098/20) = 55														
		% L = 72														
Size, μm		Free Anglesite														
-25 + 15		 														
		 														
		A = 373														
		Volume of Locked Anglesite														
	2	6	4	10	4	6	18	10	7	2	6	6	12	14	6	4
	6	2	4	10	2	10	18	10	6	3	10	10	10	6	12	
	10	6	2	12	6	7	7	10	10	8	10	6	8			
	10	8	6	8	10	5	10	8	10	10	10	10	10			
	10	10	8	4	10	10	8	6	10							
		B = (539/20) = 27														
		% L = 93														

Table B-3. Continuation. Record Sheet Used for Particle Counting in HALR, to Measure Degree of Liberation, "L", of the Anglesite.

Size, μm		Free Anglesite									
-15 + 10											
A = 760											
Volume of Locked Anglesite											
	10	10	8	10	10	10	10	10	18	15	10
	12	12	10	10	10	8	10	10	10	10	10
	10	10	10	10	8	10	10	10	10	6	5
	16	10	10	10	10	10	10	10	10	10	10
	10	8	10	10	10	10	10	10	3	10	8
	10	19	10	10	10	10	10	18	10	10	10
	10	10	10	10	10	10	10	10	10	10	10
	10	10	10	10.							
B = (836/20) = 42											
* L = 95											

APPENDIX C. - DISPERSION TESTS

All the dispersion tests were performed on samples essentially free of ions which might interfere with the dispersion. Several dispersants were tested in order to get the best dispersion conditions. The procedure was to take samples of about two grams and repulp them followed by increasing additions of about 250g/t of dispersant with three minutes of agitation. The tests were finished either by adding a large amount of dispersant (more than 2kg/t) or when some dispersion was observed. Degree of dispersion at this stage was estimated only visually.

Table C-1 presents the dispersant used and the results. Notice that the only reagent which gave a good dispersion was the calgon.

Table C-1. Dispersants Tested in NALR and HALR.

Disperant	Observations
Sodium Silicate	Poor
Calgon	Good
Ammonium Lignin Sulphonate	Fairly Good
Palcotan	Fairly Good
Marasperse CB	Fairly Good
Marasperse N	Fairly Good
Stractan	Fairly Good

APPENDIX D. - S.I. UNITS IN MAGNETIC SEPARATION

In the S.I. system, the loading number, given on page 75
as

$$N_L = \frac{2bH_o^2 kA}{\rho_f U_o^3 v^2 a^2} \quad (\text{dimensionless})$$

becomes

$$N_L = \frac{bk_u \epsilon_o^H M_o W}{V_o^3 (\rho_f na)^2} \quad (\text{dimensionless})$$

The susceptibility estimated from the Frantz

$$\kappa = \frac{20 \sin\theta \times 10^{-6} \rho_p}{I^2} \quad (\text{emu/cm}^3 - \text{Oe})$$

becomes:

$$\kappa = \frac{2.5 \sin\theta \times 10^{-7} \rho_p}{I^2} \quad (\text{dimensionless})$$

γ_m and R(%), remain as:

$$\gamma_m = \frac{\epsilon}{4} \left[\left(\frac{N_L}{2.5} \right)^{0.8} - 1 \right] \frac{\rho_p}{\rho_w}$$

$$R(\%) = 0.75 \frac{\gamma_m}{L} \times 100$$

Table D-1 presents the symbols and S.I. units.

Table D-2 shows the calculations to estimate the required flow velocity (p. 137) in S.I. units.

Table D-1. Symbols and SI Units* (65)

a	wire radius, m
b	particle radius, m
I	current on Frantz separator, A
H_0	applied or background field generated in "empty" solenoid, A/m
$\mu_0 H_0$	flux density generated in "empty" solenoid, T
L	feed loading, kg magnetics in feed/kg matrix
** M_w	wire magnetization, A/m
N_L	loading number, dimensionless
R	Recovery, %
V_0	linear velocity (average) through cannister, m/s

Greek

γ_m	mass loading at full capacity, kg captured material/kg matrix.
ϵ	fractional packing density = 0.7
η	viscosity, kg/m.s.
θ	side slope on Frantz, degrees
κ	volume susceptibility, dimensionless
μ	permeability of vacuum ₃ = $4\pi \times 10^{-7}$, T.m/A
ρ_p	particle density, kg/m ³
ρ_f	fluid density, kg/m ³
ρ_w	wire density, kg/m ³

*The following conversions may be useful:

flux density: 1 gauss = 10^{-4} tesla

field intensity: 1 oersted = 79.6 ampere/metre

magnetization: 1 emu/cm³ = 10^3 ampere/metre

susceptibility: 1 emu/cm³ Oe = 12.56 (dimensionless SI).

** M_w can be taken as a constant at 1.35×10^6 A/m, after 1.2 T.

Table D-2. Summary of the Calculations to Estimate the Required Flow Velocity in S.I. Units.

$$L = 0.53$$

$$\rho_p = 5250 \text{ kg/m}^3$$

$$\rho_w = 7750 \text{ kg/m}^3$$

$$\epsilon = 0.7$$

$$R(\%) = 16.8 \left[\left(\frac{N_L}{2.5} \right)^{0.8} - 1 \right]$$

$$b = 1.45 \times 10^{-6} \text{ m}$$

$$\kappa = 3.1 \times 10^{-3}$$

$$a = 3 \times 10^{-5} \text{ m}$$

$$\rho_f \eta = 1 \text{ kg}^2/\text{m}^4 \cdot \text{s}$$

$$N_L = 8.21 \times 10^{-7} \left(\frac{\mu_{O_2} H_{O_2} M_w}{V_o^{3/2}} \right)$$

if $\mu_{O_2} H_{O_2} = 1.38T \therefore M_w = 1.35 \times 10^6 \text{ A/m}$

$\mu_{O_2} H_{O_2} = 2.14T \therefore M_w = 1.35 \times 10^6 \text{ A/m}$

if hematite recovery is set to ~ 90%, then

Estimated Flow Velocities*

$\mu_{O_2} H_{O_2}$ (T)	U_o (cm/s)
1.380	8.45
2.140	11.40

*Using full size distribution which is as before.

REFERENCES

1. Stemerowicz, A.I. and Leigh, G.W.; Flotation Techniques for Producing High Recovery Bulk Zn-Pb-Cu-Ag Concentrate from a New Brunswick Massive Sulphide Ore; CANMET REPORT 79-8, August 1978.
2. Cases, J.M.; Finely Disseminated Complex Sulphide Ores; In Complex Sulphide Ores. Jones, M.J. ed., IMM, London, 1980, pp. 234-247.
3. Ref. 1 p. 2.
4. Strauss, G.K. and Gray, K.G.; Complex Pyritic Ores of the Iberian Peninsula and their Beneficiation, with special reference to Tharsis Company Mines, Spain. In Complex Sulphide Ores. Jones, M.J. ed., IMM, London, 1980, p. 83.
5. Nogueira, E.D., Regite, J.M., Redondo, A.L., Nogueira, G.D., and Zaplana, M., The Complex Process: Non-Ferrous Metals Production from Complex Pyritic Concentrates. In Complex Sulphide Ores, Jones, M.J., ed. IMM, London, 1980 p. 228.
6. Nicolaou, M., Kokonis, D., Geology and Development of Olympias Mine, Eastern Chalkidiki, Macedonia, Greece. In Complex Sulphide Ores, Jones, M.J., ed. IMM, London, 1980 p. 267.
7. Ref. 2, p. 237.
8. Letowski, F. Acid Leaching of Copper Sulphides in Carbonate Bearing Rocks. In Complex Sulphide Ores. Jones, M.J. ed. IMM, London, 1980 pp. 217-226.
9. Gaudin, A.M. Principles of Mineral Dressing, McGraw Hill, 1939, Chap. IV.
10. Petruk, W., Professional Development Seminars at McGill University, April 1980.
11. Petruk, W. and Schnarr, J.R. An Evaluation of the Recovery of Free and Unliberated Mineral Grains, Metals and Trace Elements in the Concentrator of Brunswick Mining and Smelting Corp. Ltd. CANMET Report, MRP/MSL 80-93 (J) pp. 16-17.

12. Austin, L.G. and Bagga, P. An Analysis of Fine Dry Grinding in Ball Mills, Power Technology, 28 (1981) 83-90.
13. Fuerstenau, D.W. Fine Particle Flotation, in Fine Particles Processing, Vol. 1, P. Somasundaran, ed., New York: AIME, 1980, pp. 669-705.
14. Somasundaran, P. Role of Surface Chemistry of Fine Sulphides in their Flotation. In Complex Sulphide Ores, Jones, M.J. ed., IMM, London, 1980, pp. 118-127.
15. Trahar, W.J. A Rational Interpretation of the Role of Particle Size in Flotation. Int. J. Miner. Process. 8:289-327, 1981.
16. Ref. 13, p. 674.
17. Ref. 15, p. 296.
18. Ref. 15, p. 298.
19. Reay, D. and Ratcliff, G.A. Removal of Fine Particles from Water by Dispersed Air Flotation: Effects of Bubble Size and Particle Size on Collection Efficiency. The Can. Jour. of Chem. Engn. Vol. 51, April 1973, pp. 178-185.
20. Flint, L.R. and Howarth, W.J. The Collision Efficiency of Small Particles with Spherical Air Bubbles. Chem. Eng. Sc. 1971, vol. 26, pp. 1155-1168.
21. Gaudin, A.M., Fuerstenau, D.W. and Miaw, H.L. "Slime Coating in Galena Flotation", Transactions, Canadian Institute of Mining and Metallurgy, Vol. 63, 1960, p. 668.
22. Yamamoto, T. Mechanism of Pyrite Depression by Sulphite in the Presence of Sphalerite. Complex Sulphide Ores, Jones, M.J., ed., IMM, London 1980, pp. 71-78.
23. Ball, B. and Rickard, R.S. The Chemistry of Pyrite Flotation and Depression in Flotation: A.M. Gaudin Memorial, Fuerstenau, M.C., ed., New York, AIME, 1976, vol. 1, pp. 458-484.
24. Amsden, M.P. The Ecstall Concentrator. CIM Bull. 67, May 1974, pp. 105-115.

25. Beck, R.D., and Chamart, J.J. The Broken Hill Concentrator of Black Mountain Mineral Development Co. (Pty), Ltd., South Africa. Complex Sulphide Ores, Jones, M.J., ed., IMM, London 1980, pp. 91-95.
26. Roberts, A.N., Burns, C.J. and Cameron, A.W. Metallurgical Development at Woodlawn Mines, Australia. In Complex Sulphide Ores. Jones, M.J., ed., IMM, London 1980, pp. 131-133.
27. Powel, C.R. Asarco Incorporated, Buchans Unit. In Milling Practice in Canada. Pickett, D.E., ed., CIM Special Volume 16, p. 157.
28. Schnarr, J.R. Brunswick Mining and Smelting Corporation. In Milling Practice in Canada. Pickett, D.E., ed., CIM Special Volume 16, pp. 158-161.
29. Ref. 11, pp. 18-22.
30. Barbery, G., Fletcher, A.W. and Sirois, L.L. Exploitation of Complex Sulphide Deposits: A Review of Processing Options from Ore to Metals. In Complex Sulphide Ores, Jones, M.J., ed., IMM, London 1980, p. 138.
31. Petruk, W. and Schnarr, J.R. The Behaviour of Minerals During Flotation of a Base Metal Ore from the Brunswick No. 12 Deposit in Canada. CANMET Division Report MRP/MSL, pp. 81-22.
32. Cambazoglu, M., Ozkol S. Leaching of Cayeli Complex Sulphide Ore by HCl + MgCl₂ Solution; Recovery of Pb, Zn and CuFeS₂ Concentrates in Complex Sulphide Ores, Jones, M.J., ed., IMM, London 1980, pp. 7-11.
33. Carta, M., Marcello, G., Giovanni, R. Beneficiation of a Complex Sulphide Ore by an Integrated Process of Flotation and Bioleaching. In Complex Sulphide Ores. Jones, M.J., ed., IMM, London 1980, pp. 178-185.
34. Ref. 1.
35. Andersen, E., Bøe, G.H., Danielssen, T., Finne, P.M. Production of Base Metals from Complex Sulphide Concentrates by the Ferric Chloride Route in a Small Continuous Pilot Plant. In Complex Sulphide Ores, Jones, M.J., ed., IMM, London 1980, pp. 186-192.
36. Ref. 5, pp. 227-233.

37. Ref. 30, p. 139.
38. Mehlbeer, J. and Melcher, G. A Combined Method for the Treatment and Smelting of Complex Non-Ferrous Metal Ores. In Complex Metallurgy, 78, Jones, M.J., ed., IMM, London 1978, pp, 96-100.
39. Georgeaux, A. et al. Traitement Hydro-métallurgique des Minerais Sulfurés Polymétalliques avec ou sans Concentration Globale Probable. Ind. Minér-minéralurgie 2-77, 1977, pp. 86-93.
40. Ref. 1, p. 7.
41. Ref. 30, pp. 139-147.
42. Ref, 30, p. 145.
43. Bolton, G.L., Zubryckyj, N. and Veltman, H. Pressure Leaching Process for Complex Zinc-Lead Concentrates. Presented at thirteenth International Mineral Processing Congress, Warsaw, Poland, June 1979, pp. 993-1023.
44. Doyle, B.N., Masters, I.M., Webster, I.C., and Veltman, H. Acid Pressure Leaching Zinc Concentrates Produces By-Product Elemental Sulphur. Presented at Eleventh Commonwealth Mining and Metallurgical Congress, Hong Kong, 1978, pp. 645-653.
45. Mizoguchi, T. and Habashi, F. The Aqueous Oxidation of Complex Sulfide Concentrates in Hydrochloric Acid. International Journal of Mineral Processing 8, 1981, pp. 177-193.
46. R.P.C. Report, MDP/78/1.
47. Ref. 43, p. 1011.
48. Ref. 45, p. 190.
49. Letter from Dr. Salter.
50. Van Der Plas, L. and Tobi, A.C. A Chart Judging the Reliability of Point Counting Results. American Journal of Science. Vol. 263, pp. 87-90.
51. Hess, H.H. Notes on Operation of Frantz Isodynamic Magnetic Separator, S.G. Frantz Co.

52. Gaudin, A.M., and Spedden, H.R. "Magnetic Separation of Sulphide Minerals", Pub. No. 1549, AIME, 1943.
53. Dobby, G., Nasset, J., and Finch, J.A. Mineral Recovery by High Gradient Magnetic Separation, Canadian Metallurgical Quarterly, Vol. 18, 1979, pp. 293-301.
54. Dobby, G.S. "High Gradient Magnetic Capture of Mineral Particles", M. Eng. Thesis, McGill University, 1977. p. 52.
55. Kuznetsov, V.P., Volova, M.L., Lyubimova, E.I., Shishkova, L.M., Lifirenko, V.E. and Sokolov, Yu. 'Beneficiation of Finely Dispersed Ores by Selective Flocculation at High Salt Concentrations'. Presented at the Thirteenth International Mineral Processing Congress, Warsaw, Poland, June 1979, Vol. 2, Part A, p. 370.
56. Iannicelli, J. High Intensity High Gradient Magnetic Separation. "Beneficiation of Mineral Fines, Problems and Research Needs", An NSF workshop Report Edited by P. Somasundaran and N. Arbiter, p. 381.
57. Petrakis, L., Ahner, P.F. and Kiviat, F.E., High Gradient Magnetic Separations of Fine Particles from Industrial Streams. "Fine Particles Processing", Vol. 2, Edited by P. Somasundaran, 1980. p. 1264.
58. Arvidson, B.R. Metallurgical and Economic Advantages of High Gradient Magnetic Separators, XII. Int. Min. Proc. Congress, São Paulo, Brazil, Sept. 1977.
59. Maxwell, E., and Kelland, D.R. IEEE Trans. Mag., Vol. MAG-14, No. 5, Sept. 1978, p. 482.
60. Nasset, J.E., Todd, I., Hollingworth, M., and Finch, J.A. A Loading Equation for High Gradient Magnetic Separation, IEEE Transactions on Magnetics, Vol. MAG-16, No. 5, Sept. 1980, pp. 833-835.
61. Nasset, J.E., and Finch, J.A. A Loading Equation for High Gradient Magnetic Separators and Application in Identifying the Fine Size Limit of Recovery. "Fine Particles Processing", Somasundaran Ed., AIME, 1980, Vol. 2, pp. 1217-1241.
62. Ref. 60, p. 833.
63. Nasset, J.E. M. Eng. Thesis, A Static Model of High Gradient Magnetic Separation, McGill University, 1980.
64. Ref. 53, p. 295.

65. Finch, J.A, and Leroux, M. A Guide to High Gradient Magnetic Separation. To be published in the Int. J. Min. Proc.